1965

Superconducting coils for shielding in space

George Anthony Englesson
Iowa State University

66–2957

ENGLESSON, George Anthony, 1929–

SUPERCONDUCTING COILS FOR SHIELDING IN SPACE.

Iowa State University of Science and Technology
Ph.D., 1965
Engineering, general

University Microfilms, Inc., Ann Arbor, Michigan

SUPERCONDUCTING COILS FOR SHIELDING IN SPACE

by

George Anthony Englesson

A Dissertation Submitted to the
Graduate Faculty in Partial Fulfillment of
The Requirements for the Degree of
DOCTOR OF PHILOSOPHY

Major Subject: Nuclear Engineering

Approved:

Signature was redacted for privacy.
In Charge of Major Work

Signature was redacted for privacy.
Head of Major Department

Signature was redacted for privacy.
Dean of Graduate College

Iowa State University
Of Science and Technology
Ames, Iowa

1965

TABLE OF CONTENTS

INTRODUCTION

The Nature of the Problem

Two uncontrolled sources of particle radiation will influence manned space flight; our galaxy, the source of cosmic radiation, and our sun, the source of solar cosmic radiation. Nuclear or thermonuclear sources may provide additional sources. At any given time the radiation environment may consist of these primary particles enhanced by secondary particles generated by primaries impinging on the space vehicle or other objects in space.

Cosmic radiation consists of nuclear particles and photons characterized by a maximum energy as great as 10^{20} ev. The particles are believed to be 80 percent protons, 19 percent alpha particles and the rest electrons and stripped atomic nuclei. The hard component of this radiation is so penetrating that shielding of it will be out of the question for some time to come. Fortunately the flux density is low enough that the accrued dose will be approximately 10 rem per year. Intensity measurements of a number of investigators have been used to plot the integral energy spectra of the components of the primary cosmic radiation shown in Figure 1 (27).

Solar cosmic radiation is a spectrum of radiation of solar origin associated with chromospheric flares. The energy spectra of solar particles are much steeper than those of cosmic rays and seldom exceed energies of 25 Bev. The compo-

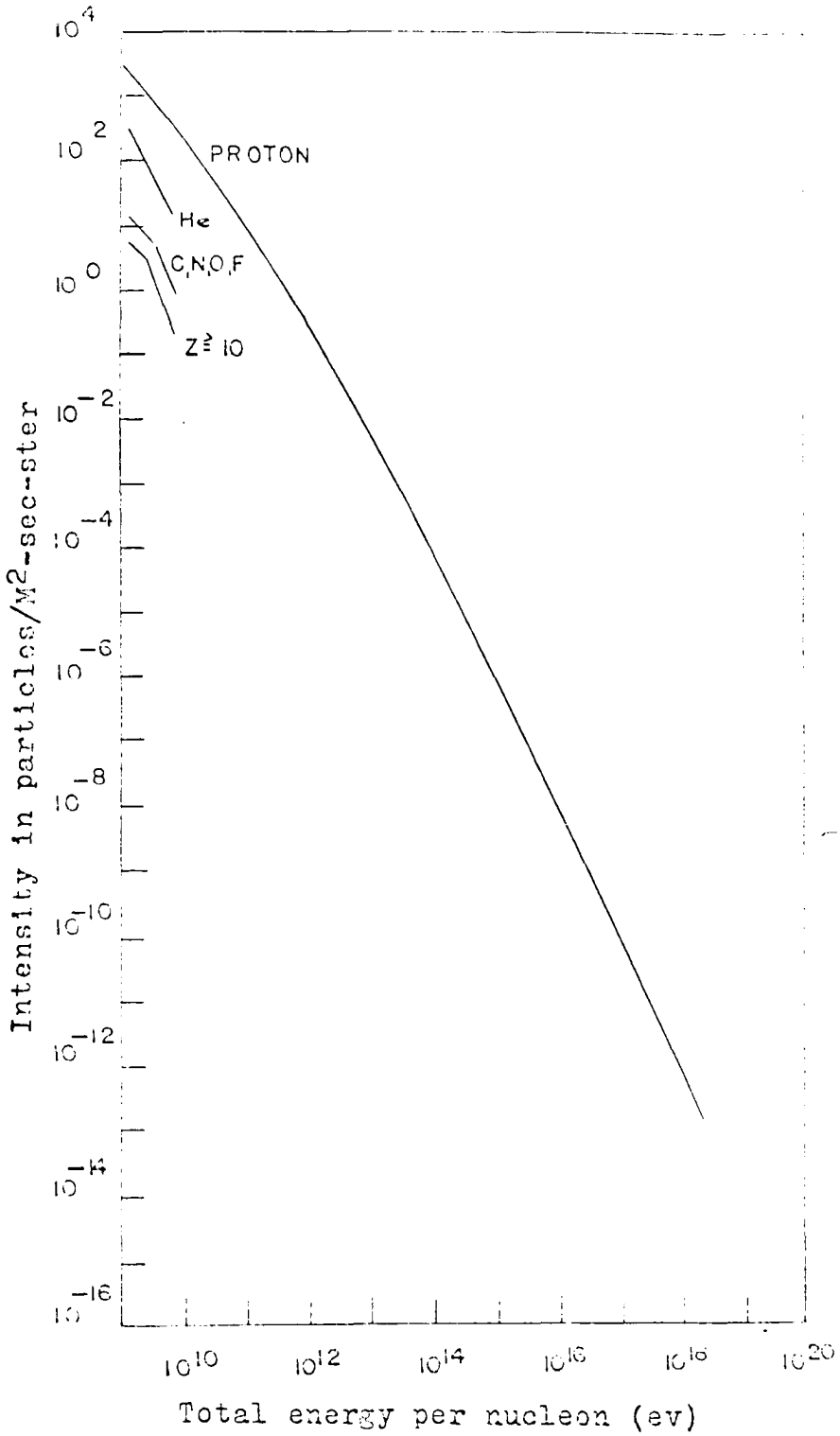

Figure 1. The integral energy spectra of components of the primary cosmic radiation

sition reflects closely that of the solar surface: i.e. more than 90 percent protons, and the rest primarily alpha particles. In recent years solar flares have been investigated in which the primary components have been electrons; however, these are always low energy events.

The characteristics of the solar proton events can be summarized as follows:

1. Solar flare activity varies with sunspot activity in an eleven-year cycle.

2. These events are quite frequent. The year 1960 is considered near the peak of a cycle. During that year there were thirty-four major solar flares classified 3 or 3^+; that is, the disturbance was visible over a fraction of the solar disk area equal to or greater than 0.0003.

3. Not all flares result in a detectable increase in low-energy cosmic rays at the earth. There are approximately 0.2 events detected at earth for each flare of 2^+, 3, or 3^+ importance.

4. The delay time between the observation of the flare and the time particles appear at earth varies from event to event, but usually is one to two hours.

5. The buildup of energy is also variable, but typically the maximum is reached in 15 minutes to a few hours after the first activity is detected at the earth. Buildup times are typically longer for lower energy particles.

6. After buildup, there is a highly-fluctuating transition period a few hours long.

7. After transition, decay begins and typically the flux decays as the square of the time, usually in 10 to 40 hours.

The solar events are usually divided into high and low energy events depending on the average energy of the emitted protons. High-energy events contain an appreciable number of particles of energy above 0.5 Bev per nucleon.

The most intense high energy event observed to date occurred on 23 February 1956. It had a peak intensity of 1.6×10^5 protons/cm^2-sec for proton energies greater than 1000 Mev. The integral proton energy spectra at maximum intensity is shown in Figure 2 (37).

The most intense low-energy event observed to date occurred on 14 July 1959. It had a peak intensity of 2×10^6 protons/cm^2-sec for proton energies greater than 10 Mev. The integral proton spectrum at maximum intensity is shown in Figure 3 (34).

The primary process by which high-energy charged particles lose energy in matter is by collision with atomic electrons. This type of energy interchange is well understood, and curves can be drawn showing range (in g/cm^2) of a proton of a given energy in any particular material. Figure 4 shows range-energy information for H_2, H_2O, C, air, Al, stainless steel and Pb. Hydrogen is the best material on a weight

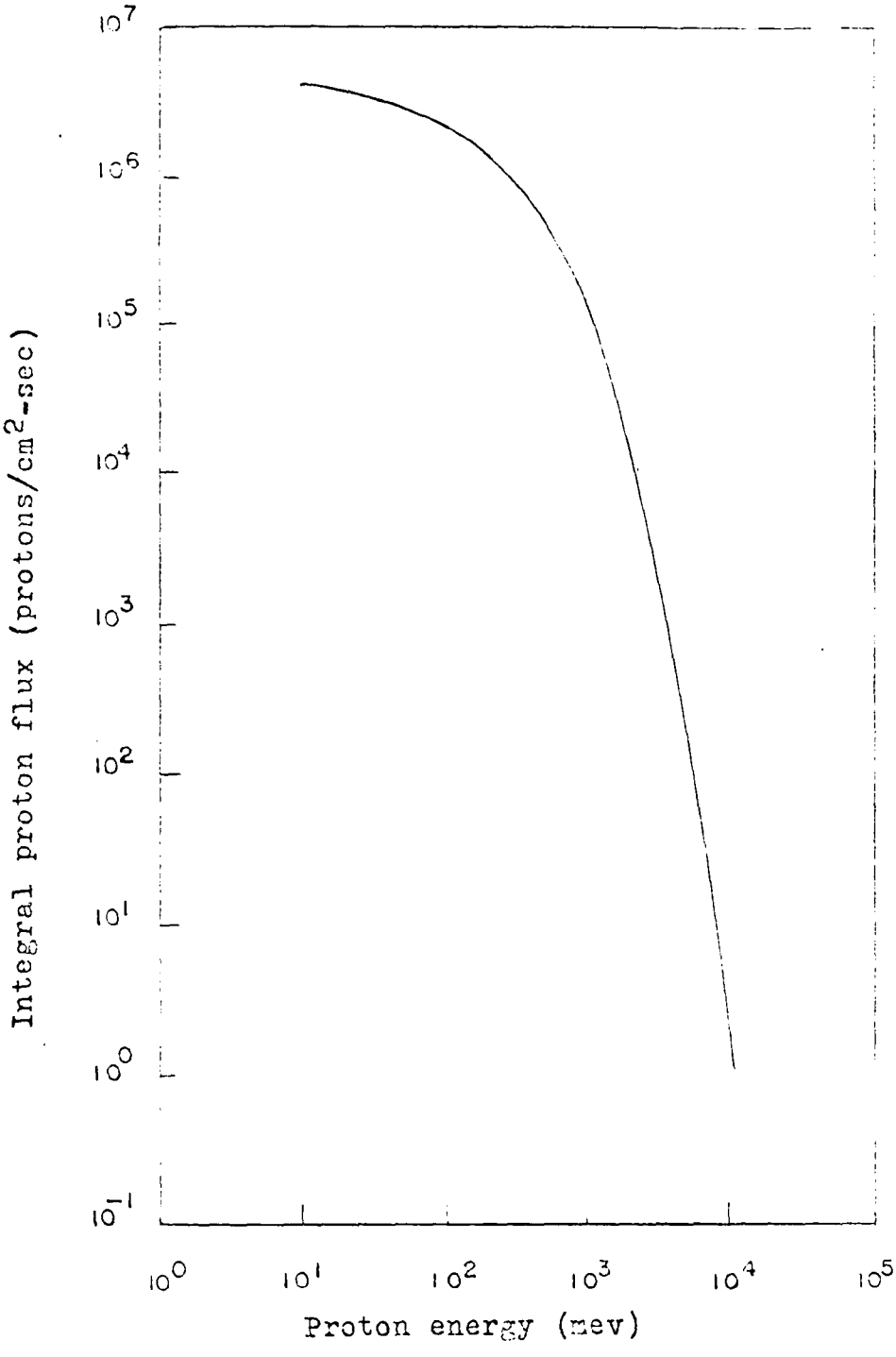

Figure 2. Integral energy spectrum of the solar flare on 23 February 1956

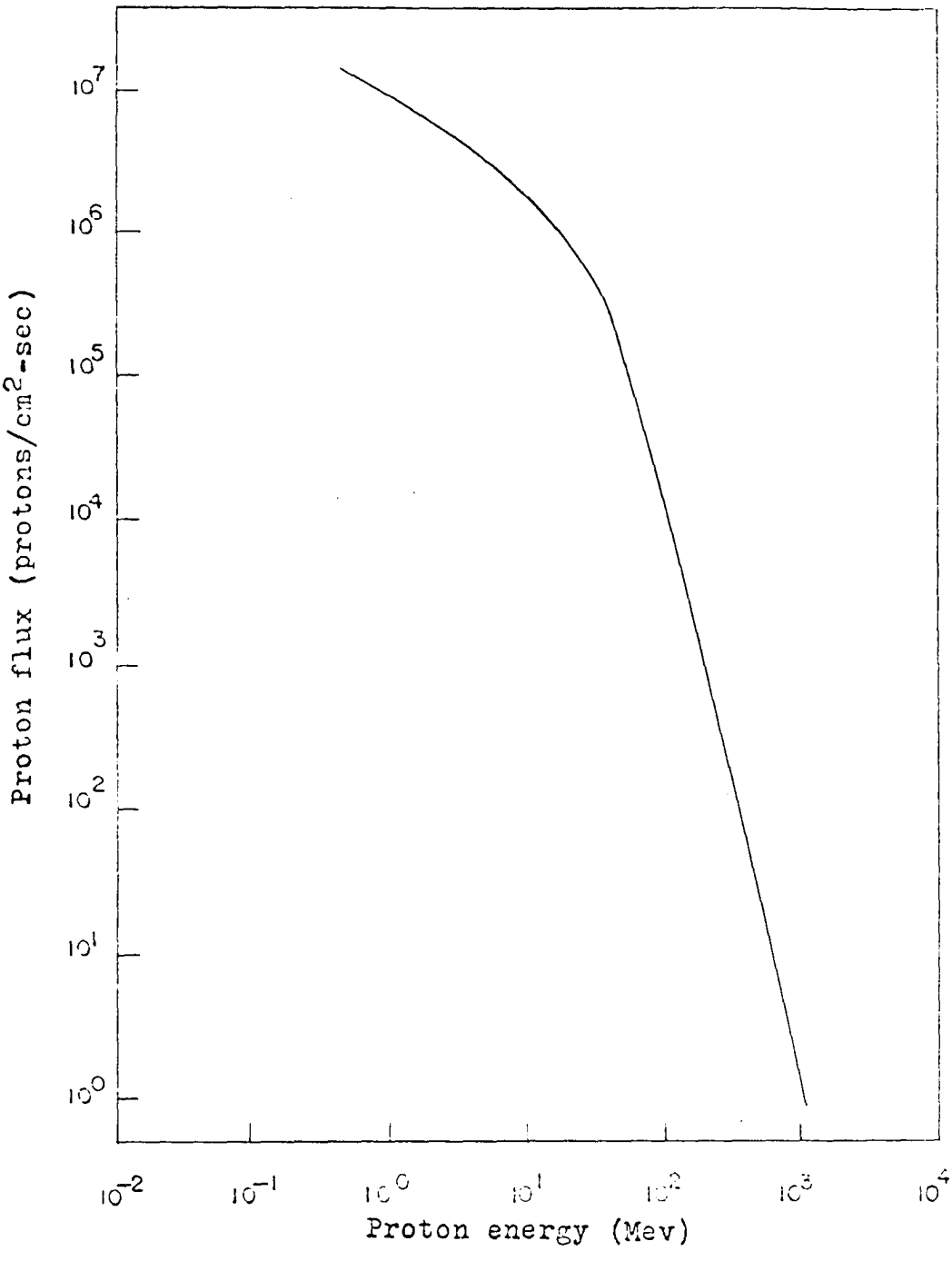

Figure 3. Energy spectrum of the solar flare on 14 July 1959

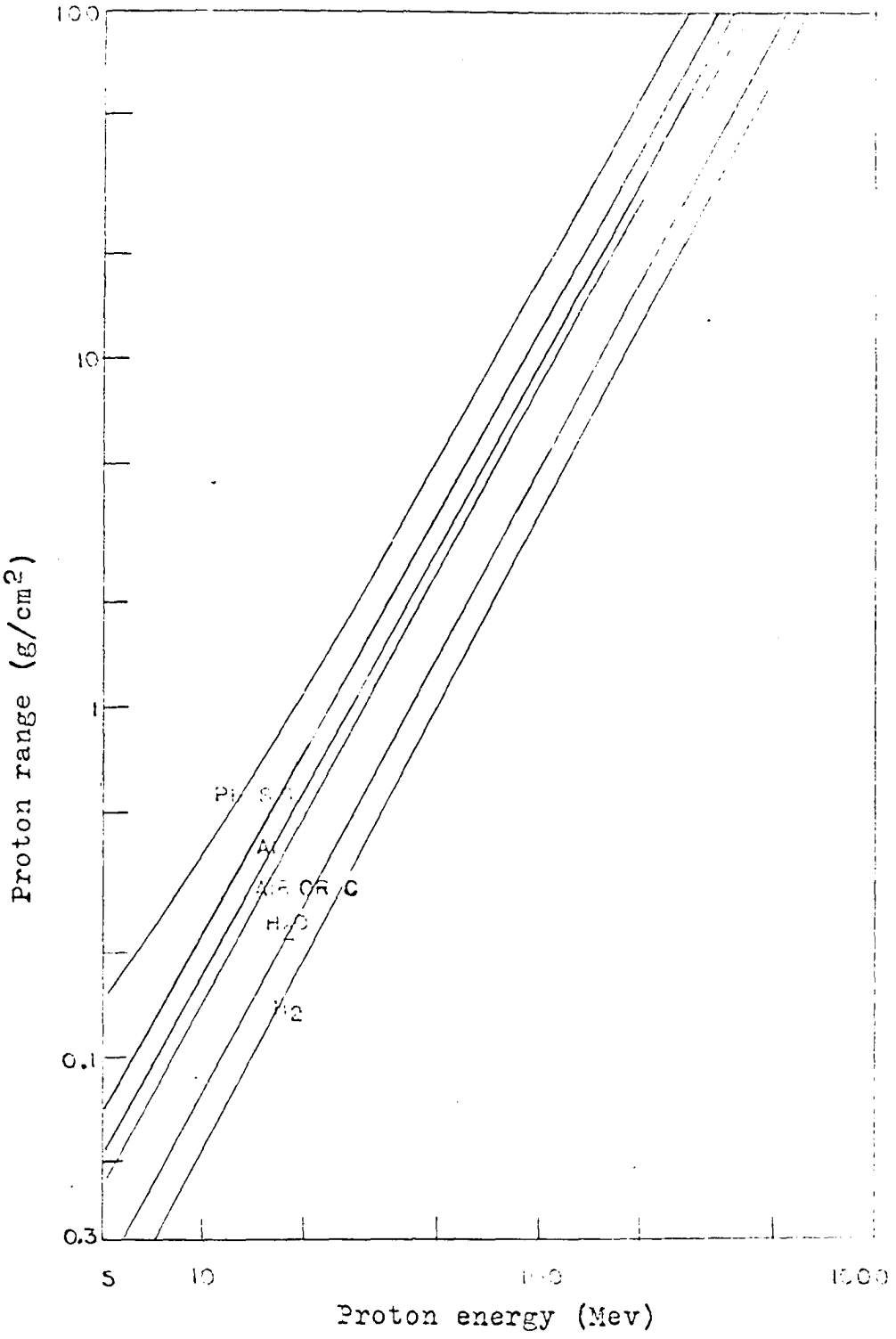

Figure 4. Range energy relation for protons in several materials

basis, but is unsuitable for shielding purposes due to its great bulk even in liquid form. Consequently water or carbon is almost always suggested as proton shields.

The ranges shown in Figure 4 neglect nuclear interactions. At high energies these nuclear processes become relatively important; for example, 2 Bev protons are attenuated approximately 15 percent in intensity in a 1-inch thick lead absorber while losing less than three percent of their energy by ionization. When an energetic proton undergoes a short range interaction with a nucleus, nucleons are "knocked out" instantaneously. This process of instantaneous nucleon emission is called the intranuclear cascade. After the cascade, the nucleus is left in an excited state and usually de-excites, in a process called evaporation. This results in the delayed emission of neutrons, protons, and occasionally, heavy fragments. Neutrons will provide the most penetrating component of these secondary particles; however, the production of any of the secondaries can produce a significant portion of the total dose absorbed by a space traveler.

Secondary neutrons, produced by nuclear interaction of galactic and solar cosmic rays with the top of the atmosphere, are considered to be the principal source of protons and electrons trapped in the magnetic field of the earth. The neutrons decay in the mode

$$n \rightarrow p + e + \bar{\nu} \qquad (1)$$

with a half life of about 12 minutes. Some of the neutrons

travel outward from the earth and may decay within the magnetosphere. The decay products may be injected into the field in such a way that the proton and the electron will be trapped in a magnetic mirror system.

The proton spectrum at the lower edge of the inner Van Allen belt has been reproduced in Figure 5. The spectrum and intensity of the proton flux is stable except for periods immediately after solar storms. After a storm the intensity may rise to several times the pre-storm value, but decays again to the equilibrium value. The Van Allen belt electrons cannot penetrate material thicker than 0.2 g/cm^2. However the shielding of these electrons results in the production of much more penetrating bremsstrahlung.

The radiation belts are permanent in time and place; galactic cosmic radiation, although influenced by the solar magnetic field, also presents a permanent spectrum; solar flares, although associated with sun spot activity, are not permanent and are not predictable. It is possible, however, to predict times when there is little possibility of a flare. These predictions have reached a state of the art such that eight-day periods of no solar flare activity have been correctly predicted. A successful prediction scheme of this type would permit missions of the order of one to two weeks to be undertaken with reasonable probabilities of success. It must be emphasized that it really is a question of probability and solar flare prediction is analogous to weather prediction.

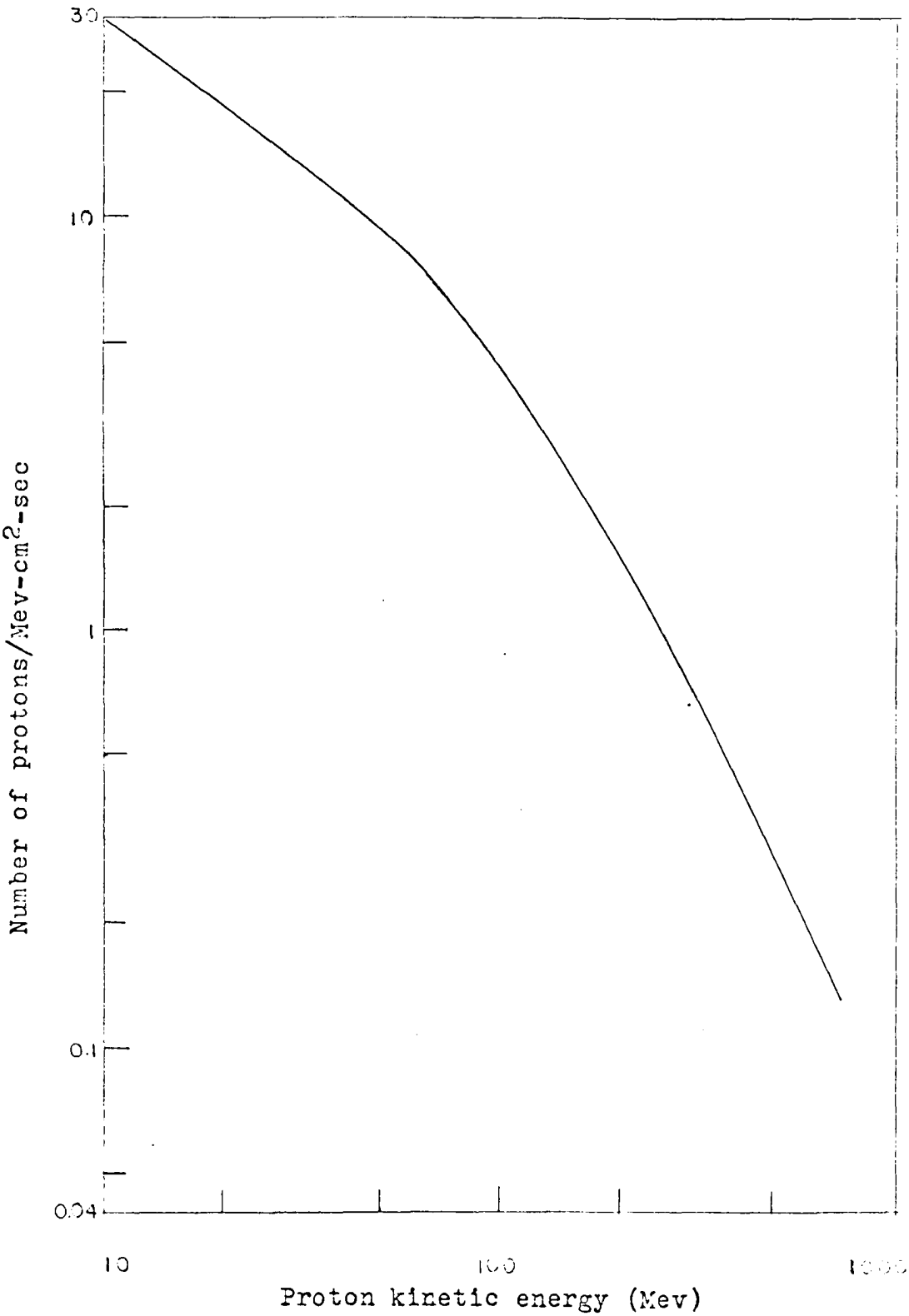

Figure 5. Proton spectrum in the inner zone of the Van Allen belt

As an example, one prediction scheme discussed predicts 139 periods of seven days duration which might be considered safe in the years 1956-1961 (27). A major flare occurred during seven of these periods.

As mission requirements grow longer, two effects become increasingly important; first, as the quality of prediction deteriorates, the risk of encountering a large flare grows. Secondly a sufficiently long term prediction will be indistinguishable from a purely random calculation based only on the knowledge of the overall frequencies of occurrence. Thus, a point will be reached where a forecast will at all times state with some confidence that during some specified interval one or more large solar flares will certainly occur.

Since 1942, only seven flares of the largest class (class 4) have been observed. The occurrence of these flares does not seem to be associated with the 11-year solar cycle. Furthermore since the frequency of occurrence is of the order of 0.3 per year, it will be many years before a good statistical analysis can be made. Since it would be difficult to contemplate leaving on a mission with less than a 90 percent chance of avoiding such a flare, shielding adequate for protection from the largest flare known will have to be carried for mission times longer than three months (29). Such shielding will have to be capable of stopping protons with energies of the order of 1 Bev.

For trips to the inner planets, travel times of the order

of 18 to 36 months are contemplated. As a result, the dosage behind the required shield will have to be calculated on the basis of the probability of one or more class 4 flares, continuous cosmic flare exposure, plus a wide variety of small flares. Thus, the class 4 solar flare is established as the principal hazard of manned space exploration.

Space Dosimetry

In 1950 the International Commission on Radiological Units recommended that the dose of any ionizing radiation in relation to its biological or related effects be expressed "in terms of the quantity of energy absorbed per unit mass (ergs per gram) of irradiated material at the place of interest." The most widely used unit of radiation is the roentgen (r), which is defined as "that quantity of X of γ radiation such that the associated corpuscular emission per standard cubic centimeter of air produces, in air, ions carrying 1 esu of quantity of electricity of either sign." This means that one r produced 1.61×10^{12} ion pairs per gram of air, which corresponds to the absorption of 84 ergs per gram of air or 93 ergs per gram of water. Water and muscle tissue have about the same density, number of electrons per gram, and effective atomic numbers; thus, a unit of dose equivalent to 93 ergs absorbed per gram of tissue is called roentgen-equivalent-physical (rep). A third identification of dose, the rad, is defined as equal to the absorption of 100 ergs of energy from

any type of ionizing radiation by 1 gm of any material.

Different types of ionizing radiation may deposit the same amount of energy in a material yet have quite different effects. For this reason, a quantity called relative biological effectiveness (RBE) is defined

$$\text{RBE} = \frac{\text{Physical dose of 200 Kev X-rays to produce an effect}}{\text{Physical dose of comparison radiation to produce same effect}} . \qquad (2)$$

A unit which provides a standard criterion of biological injury when applied to different radiations is the rem (roentgen equivalent man) defined

$$\text{rem} = \text{RBE} \times \text{dose in rads (13).} \qquad (3)$$

Rad and rem will be used in this paper.

Energy is imparted to matter by ionization. The energy can be transferred directly by charged particles or indirectly by neutrons and photons. Energy is also imparted by nuclear interaction. These processes create secondary particles which may escape the volume chosen for the dose determination. Thus the energy absorbed will be the difference between the energy imparted by the primary particles and the energy carried out by the secondaries.

It is proposed that space dosimetry have the capability of achieving four objectives (27).

1. Warning of any ionizing radiation environment encountered.

2. Forecasting the extent of a possible hazard.

3. Determination of the surface-dose rate, surface dose, and depth dose distribution for each astronaut whether he is (a) outside the vehicle, (b) inside the vehicle, or (c) protected by any special shielding.

4. Determine the biological response of an astronaut to the specific radiation environment.

One of the most difficult problems of space dosimetry will be to determine the relative biological effect (RBE) to be used to translate earth-radiation response data obtained on animals to predict the biological response of man to space radiation. Low dose rates for long periods of time, fractionation of total dose, and the unsuitability of a group average response to the small number of astronauts will further complicate a difficult problem.

To give a rough idea of the effects of large doses on human beings, the three tables which follow were taken from the Radiological Health Handbook (37).

Table 1. Probable early effects of acute radiation doses over whole body to man

Acute Doses	Probable effect
0-25r	No obvious injury (possible cataracts)
25-50r	Possible blood changes but no serious injury
50-100r	Blood-cell changes, some injury, no disability
100-200r	Injury, possible disability
200-400r	Injury and disability certain, death possible
400r	Fatal to 50 percent
600r	Fatal

Table 2. Estimated doses for varying degrees of injury to man

Dose rate	Period of time	Effect
500 r/day	2 days	Mortality close to 100 percent
100 r/day	Until death	Mean survival time 15 days, 100 percent death in 30 days
60r/day	10 days	Mortality high with crippling disability
30r/day	10 days	Disability moderate
10r/day	365 days	Some deaths
1.5r/day	Few months	No change in efficiency

Table 3. Estimate of effective dose and lethality of various dose rates to man

Day	Dose rate r/day	Accumulated dose (r)	Effective accumulated dose (r)	Estimated mean survival time (days)	Estimated percent deaths in 30 days
1	200	200	200	--	30
3		600	542	20	60
5		1000	819	15	85
10		2000	1326	10	100
1	100	100	100	--	8
3		300	271	--	35
5		500	409	15	50
10		1000	663	15	75
1	50	50	50	--	0
3		150	135	--	15
5		250	204	30	25
10		500	330	30	40
15		1500	395	30	50

Technique of Calculating Absorbed Dose

As a proton (300 Mev > E > 1 Mev) passes through a given material, the predominant mode of energy transfer is by inelastic collisions with atomic electrons. Not all of the energy transfer results in ionization. An important fraction results in excitation, without ionization, of atoms in the absorber. For a particle of any spin having rest mass M, charge Ze and velocity V ($=\beta c$), the energy dE transferred as excitation and ionization along an element of path ds to a homogeneous absorbing medium containing N atoms/cm^3, each of atomic number Z, is well approximated by (11)

$$\frac{dE}{ds} = \frac{4\pi e^4 Z^2}{m_o V^2} NZ \left[\ln \frac{2m_o V^2}{I(1-\beta^2)} - \beta^2 \right] . \qquad (4)$$

The geometric-mean excitation and ionization potential I of the absorbing atoms is a constant whose value must be determined experimentally for each element. For water, the value is somewhere between 66 and 68 ev.

At energies greater than 300 Mev, nuclear reactions producing secondary particles become predominant. The number of secondaries and their energies depend on the energy of the incident proton and the atomic number of the nucleus. The probability that these short range interactions occur is given in a close approximation, by the geometric cross section of the nucleus

$$\sigma = \pi (1.22 A^{1/3})^2 \times 10^{-26} \ (cm^2) \qquad (5)$$

where

A = the number of nucleons in the nucleus

σ = microscopic cross section (cm^2).

The coefficient 1.22 is slightly dependent on the incident proton energy. It gradually increases as the value of the proton energy decreases and reaches 1.4 for 50 Mev protons. Near 25 Mev the cross section rapidly decreases due to coulombic repulsion between the proton and the nucleus.

Table 4 gives energy transfer rates by ionization and by absorption for a few selected energies (27).

Table 4. Energy transfer rate by ionization and absorption for protons in water

Proton energy (Mev)	Approximate dE/ds per proton (rad/cm^2) Ionization	Absorption	Total	Surface source for 1 rad. ($protons/cm^2$)
40	24.2×10^{-8}	1.4×10^{-8}	25.6×10^{-8}	3.91×10^{6}
60	17.6	1.5	19.1	5.24
80	14.0	1.6	15.6	6.41
100	11.9	1.8	13.7	7.30
200	7.3	3.1	10.4	9.62
300	5.7	4.9	10.6	9.43
500	4.4	8.3	12.7	7.87
800	3.8	14.3	18.1	5.52
1000	3.6	19.7	23.3	4.29

Neutrons are produced by proton interaction with the vehicle and in the astronaut as parts of the intranuclear cascade and the evaporation process. The neutron energy spectrum is quite steep and has the form

$$N(E)dE \sim E \exp(-E/\tau)dE \qquad (6)$$

where N(E) is the neutron density at kinetic energy E, and τ is a characteristic of the evaporation neutrons called nuclear temperature. The magnitude of τ is a function of proton energy and atomic number of the targets. For example with atomic number 20, τ varies from 3.7 to 6 Mev for incident protons having energies between 50 to 2000 Mev. For atomic number 5, τ varies from 6 to 7 Mev for the same spread in energy.

The main mechanism for energy loss by neutrons in tissue with energies between 0.5 and 10 Mev is by elastic collisions with hydrogen; below 0.5 Mev by absorption producing (n,p) reactions in nitrogen and (n,γ) with hydrogen; above 10 Mev the neutron and proton reaction cross sections are similar; therefore spallation can be expected.

Table 5 shows the average energy transferred by multiple collision for neutrons in tissue (27).

Table 5. Average energy transfer by multiple collision for neutrons in tissue

Neutron energy (Mev)	Number of neutrons/cm^2 equivalent to a dose of 1 rad in the first gram of tissue
0.005	16.7×10^8
0.5	4.35
1.0	2.63
2.5	1.92
5.0	1.35
10.0	1.52

Above the energy where coulomb repulsion is important, proton and neutron reaction probabilities are comparable. The energy transfer, dE/ds per neutron, is given in close approximation by the column labeled absorption in Table 4 for neutrons of energy greater than 25 Mev.

The excited nuclei from the cascade and from the evaporation process decay by emitting charged particles, neutrons, electrons, and X and Y radiation. The interaction of electrons with electrons, electrons with the electric field of the nuclei, photons with orbital electrons, and photons with nuclei all produce additional sources for the absorbed dose. The class 4 solar proton flare has been established as the principal hazard to manned space, therefore although these secondary sources could be important it will be assumed that the primary component of the dose will come from the protons and the secondary neutrons.

The procedure used in calculating dose is straightforward. After the heterogeneous radiation field is determined, the total energy absorbed is obtained by adding the energy absorbed from each energy group of each type present. If the spectrum N(E) of each type, i, is known, the dose may be calculated from

$$D = \sum_{i} \int_{o}^{\infty} N_i(E)(E_{abs})_i \, dE \qquad (7)$$

where E_{abs} is the energy absorbed in rad from type i radiation of initial energy E.

Allowable Dose Rates

One of the most important missions of space dosimetry will be to relate the physical measurement of dose to the effect on an astronaut from exposure in a space-radiation environment. The responses which must be considered are those that jeopardize fulfillment of the space mission, and those that jeopardize the future health of the astronaut.

The heterogeneous aspect of the incident radiation will produce a non-uniform distribution of dosage in depth. Passage of high-energy particles may severely injure small groups of cells while surrounding tissue will remain unscathed. The time pattern of exposure will be unpredictable and irregular. The ultimate biological effect is known to vary with the pattern of exposure, but in what category will the astronaut be placed? Assignment of an individual to either a single dose category or to a continuous exposure will not be valid.

Thus the question of permissible doses in manned space flight has varied answers. The conservative answer (29) is the application of those levels allowed in radiation work on earth; i.e., 0.3 rem/week or 5.0 rem/year plus one emergency dose of 25 rem. The liberal answer (27) is that doses between 51 and 100 rad exposure will cause only trivial and transitory clinical changes, if any at all, and pose no medical problem. By way of comparison, exposure to 100 rem over a long period of time will be expected to shorten the life span in man by

8½ months, and 100 rem in a single exposure will shorten it 3½ years (10).

Figure 6 is a reproduction of part of a graph of the effect upon man of single exposure X or γ radiation. From this figure brief, single-dose, high-intensity exposure to total doses greater than 100 rem can be followed by severe radiation sickness, while exposure of 40r may produce traces of radiation sickness in half of a large crew, with more severe symptoms to 10 to 20 percent of the crew.

For this work a maximum has been chosen not to exceed 100 rem in a three-year mission with a single exposure not to exceed 40 rem.

Methods of Solution

Passive shielding of solar flares has been discussed by many authors. If the effect of secondary radiation produced in stopping protons in a hydrogeneous shield is neglected, the dose absorbed by a space traveller vs. shield thickness for the solar flare of 14 July 1959 is shown in Figure 7. A shield thickness of 37.5 gm/cm^2 reduces the dose due to this flare to 3 rem. For a three-year mission with the probability of encountering 20-23 of these flares, plus 30 rem for cosmic radiation, the astronaut would accumulate 90-99 rem. The water required to shield a 3500-cubic foot sphere would weigh 130,000 lb (9).

For the class 4$^+$ flare of 23 February 1956, it has been

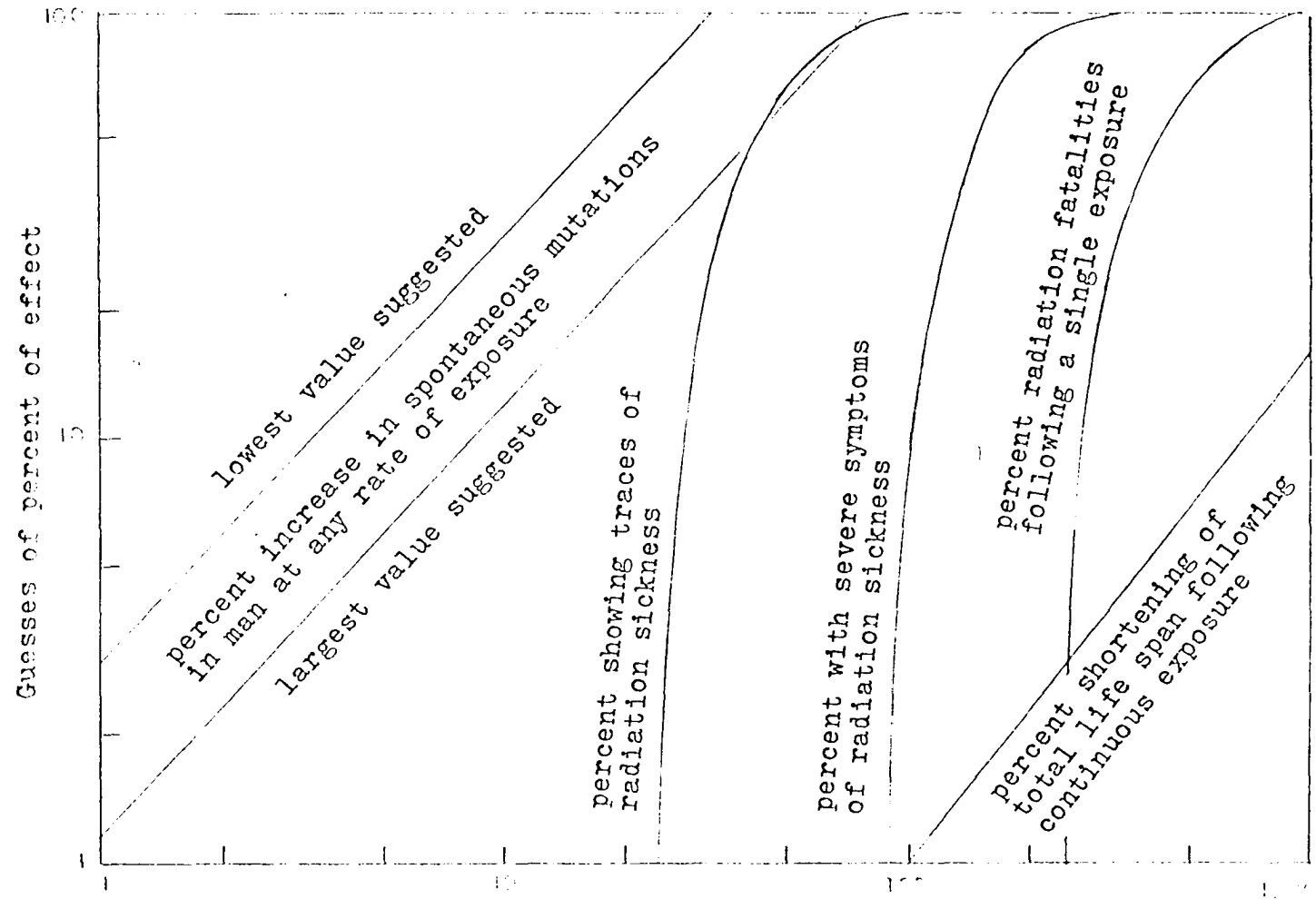

Figure 6. The effect of whole body radiation on man

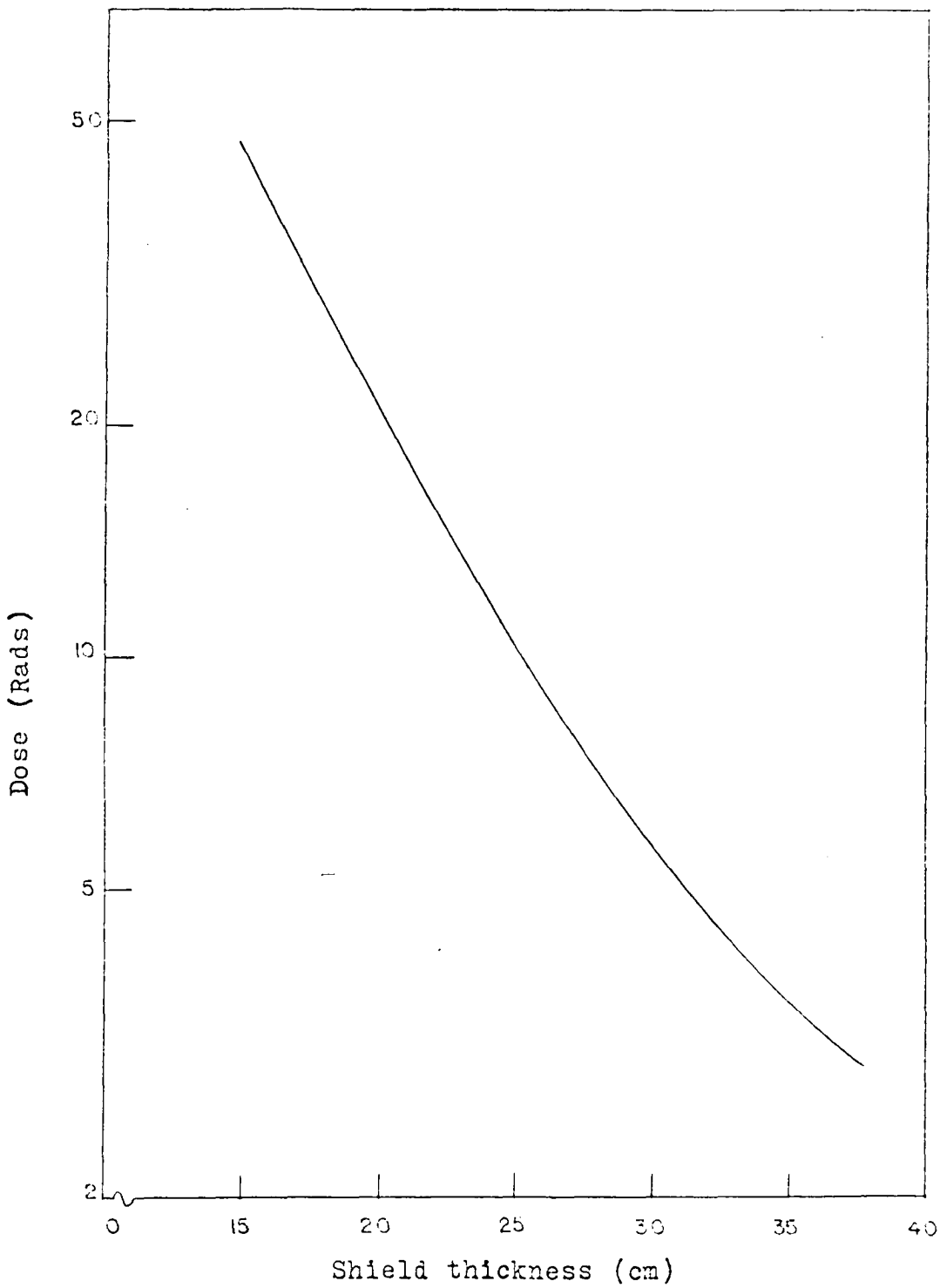

Figure 7. Dose from a class 3^+ solar flare vs. water shield thickness - secondary particle generation neglected

estimated (37) that in order to keep the proton radiation dose below 25 rem, all particles with energy less than 1.44 Bev must be shielded. This requires about 580 g/cm^2 of carbon or a shield 8.5 feet thick. To shield a 110 cubic foot sphere would require 834,000 lb. This does not include the possible dose from secondary radiation.

As exploration extends into outer space, and mission time becomes longer, the probability of encountering one or more class 4 flares will become a certainty. The number of men on the mission and consequently the shielded volume and weight will all increase. Several radically different types of shields have been considered for the solution of this problem (28,29). Two of these methods are electromagnetic and electrostatic shielding. The electrostatic has been discounted since the application of a potential great enough to deflect 1 Bev protons, causes electrons to strike the shield with the same energy, 1 Bev. The subsequent bremsstrahlung will pose a serious shielding problem. In addition the energy required to produce and maintain a potential of 10^9 volts, the potential required to deflect 1 Bev protons, exceeds the capacity of the largest generator constructed on earth.

The second possibility is a magnetic shield. The principle problem in conventional electromagnets is the huge power required to replace the I^2R losses in the field windings and the power required to remove the heat generated. Magnetic

shielding using superconducting field coils appears to offer an attractive shielding method provided only that the engineering problems involved in the construction of the large coils can be solved. The purpose of this thesis is to solve some of these problems.

MAGNETIC SHIELD CONFIGURATION

Shielding Provided by the Magnetic Solenoid

The objective of space shielding is to reduce to an allowable level the radiation dose received by human occupants of a space vehicle from a level which might otherwise be fatal on long unshielded missions. Because the spectra of charged particles in space are very steep (see Figures 1, 2, 3), it is possible to determine a threshold energy level such that all particles having energy less than the threshold will be excluded, and the dose accrued from all particles with energy above the threshold is tolerable.

A passive shield excludes the low-energy particles by stopping them; an active shield excludes the low energy particles by deflecting them so that their path misses the shielded region. A simplified view of the shielding provided by a magnetic shield is shown in Figure 8. Outside the

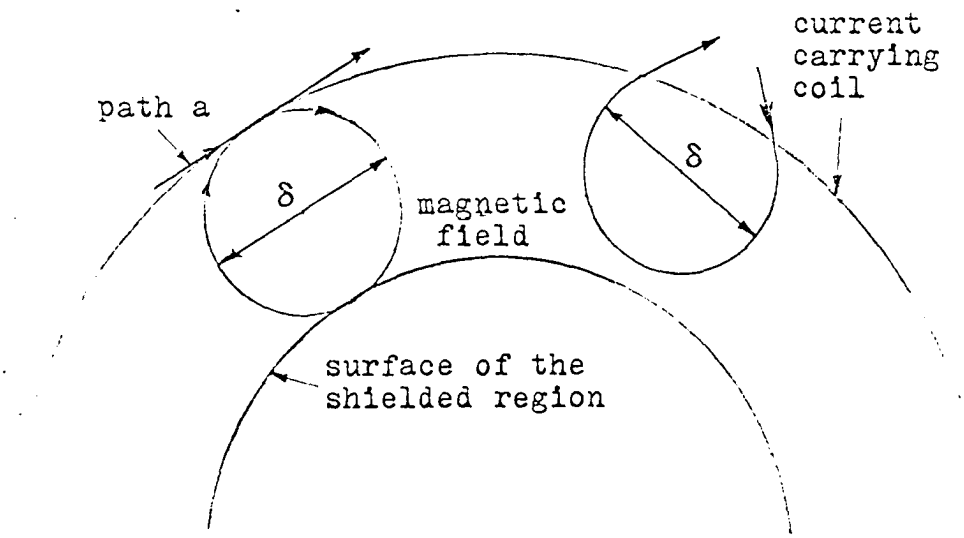

Figure 8. Shielding of charged particles by a magnetic field

surface of a shielded region is a magnetic field of some thickness δ, where δ is twice the equilibrium cyclotron radius of a particle with the threshold energy. δ is determined by

$$\delta = \frac{2m\, v_{\perp}\, c}{eB} \qquad (8)$$

where m is the particle mass in grams

$v_{\perp}$ is the particle velocity perpendicular to the field lines in cm/sec

B is the magnetic field strength in gauss

e is the electronic charge in statcoulombs

c is the velocity of light in cm/sec

and $\delta/2$ is the equilibrium cyclotron radius in cm.

In a field strength of 100,000 gauss, a 1-Bev proton traverses a circle with an 84-cm. diameter.

A simple geometric configuration which provides effective magnetic shielding is the infinite solenoid. The infinite solenoid cannot, of course, be built, but the characteristics of a large diameter toroidal coil are essentially that of the infinite solenoid. The shielding provided by the toroid is that shown in Figure 8. One loop of the coil lies in the plane of the paper and is represented by the external line. The magnetic field is perpendicular to the paper and fills the cross sectional area within the coil; there is no field outside the coil. The threshold energy is that energy for which

a particle moving in a plane perpendicular to the magnetic field lines just grazes the magnetic field (path a), and its path is bent in the magnetic field so that it just touches the edge of the shielded volume. The field will deflect higher energy particles which have an energy component perpendicular to the field which is less than the threshold energy.

The magnetic field in the torus is curved and non-uniform. In the absence of an electric field, the Maxwell equation for the curl of the magnetic field strength is

$$\nabla \times \vec{B} = \frac{4\pi}{c} \vec{j} \qquad (9)$$

where $\vec{j}$ is the current density in the solenoid and $\vec{B}$ is the magnetic field strength. Applying Stokes theorem to the integral of the curl of the magnetic field strength over the magnetic path gives the familiar

$$B = \text{constant}/R \qquad (10)$$

where R is the major torus diameter. Thus, the magnetic field strength is independent of the minor toroid or coil diameter. The constant in Equation 10 is

$$\text{constant} = (4\pi/10)(NI/2\pi) \qquad (11)$$

where B = H has units of gauss

N = the number of turns

I = the current in amperes

and R has units of cm.

The effect of a strong magnetic field on man is unknown; however, electronic equipment, mechanical equipment made with

ferromagnetic material, and many common ferromagnetic implements would be severely affected by strong magnetic fields. Therefore a field-free volume will be provided.

This field-free region can be provided by winding another toroid with the same major diameter, with a minor diameter equal to the diameter of the shielded region shown in Figure 8, placing the smaller toroid within the larger one, using the same number of turns, and sending an equal but oppositely directed current through the two coils. This configuration results in a field-free region surrounded by a strong, though variable, magnetic field of constant thickness.

Mission Volume Requirement

The vehicle mission is conceived as an exploration of the inner planets and possibly colonization. An examination of the Large Orbital Research Laboratory (LORL) (41) was made to determine some of the mission parameters for a large vehicle. LORL is designed for approximately 30 min. It has a total pressurized volume of 80,000 cubic feet. The laboratory and command area require 20,000 cubic feet; thus, 60,000 cubic feet of living, working and storage space is required for a crew of thirty. LORL will be periodically refueled with men and provisions; the exploration vehicle will not be. Consequently, additional crew members and additional space will be needed to provide services and replacement where needed; i.e.,

physician, medical technicians, and replacement personnel.

For this mission the LORL crew size was increased from 30 to 40 men and the living and working volume increased from 60,000 to 80,000 cubic feet to take care of the additional ten men. Since the vehicle will not be refueled in space, a nominal 50 percent increase in volume is required. The laboratory and command area adds 20,000 cubic feet; the resulting vehicle volume is established at 140,000 cubic feet.

Since a prime requisite for a space shield is a minimum launch weight, the lowest possible mass is a goal. A toroid with a fixed volume has a minimum surface to volume ratio if the minor diameter is as large as possible. It is assumed that the vehicle will be lifted into orbit in sections by Saturn-5 vehicles and assembled in space. The maximum diameter of this booster is 33 feet. Thus, 33 feet is the maximum shield diameter.

Superconducting Coil Design

At cryogenic temperatures ($18^{\circ}K$) about half of the metallic elements exhibit the property of superconductivity; that is, at or below a specific temperature called the transition temperature (T_c) the material appears to suddenly lose all of its resistance. This phenomenon is associated with a change in the behavior of the conduction electrons at low temperatures. In addition to the metallic elements, several hundred intermetallic compound conductors have been found to exhibit superconductivity. In this group is Nb-Zr, a superconducting alloy commonly used as coil material. It is a

tough ductile material which is easily fabricated and can be treated, during construction, like any structural material. Westinghouse Research Laboratories have developed a Nb-Zr alloy called HI-120 which has the properties shown in Figure 9 (48).

The resistance of a superconductor can be restored to its value for the normal state by applying a sufficiently large magnetic field. Since a current flowing along a superconductor will generate a tangential field at the surface of the metal, there will also be a critical current which cannot be exceeded without entry to the normal state. The graph in Figure 9 shows the relationship between critical current and critical magnetic field in 10 mil HI-120 wire. For other diameter wire, Silsbee's hypothesis shows

$$\frac{2I_c}{10r} = H_c \qquad (12)$$

where I_c is the critical current (amperes)

H_c is the critical field for I_c (gauss)

r is the radius of the wire (cm).

Consider a shield with a maximum magnetic field strength of 100,000 gauss. The distribution of the magnetic field across the cross section of the toroid will be that shown in Figure 10. If 5 mil HI-120 wire is used, the maximum allowed current is 5 amperes. From Figure 10, the minor diameter of the shielded area is 25 feet, and the major diameter is 122 feet. Using Equation 10 one finds approximately 16,000 turns

Product	Standard	Special
Base wire	.010" diameter ±.0002"	3-mil diameter and larger
Copper plating electrolytically deposited copper	.001" thickness on radius ±.0002"	0.2-mil thickness on radius and larger
Insulation epoxy enamel	.00075" thickness on radius (nominal)	from 0.2 to 0.9-mil thickness on radius
nylon	.....	from 0.2 to 0.9-mil thickness on radius

Lengths: Guaranteed continuous lengths up to 10,000 feet minimum and 15,000 feet average per order will be supplied at standard prices.

	R.T.	233°K	77°K	4.2°K
Tensile strength, 1000 psi:	170	180	240	330
Yield strength, 1000 psi:	152	162	220	310
Reduction in area, %:	35	26	20	14
Modulus of elasticity: 12.2 x 10^6 psi at 20°C				
Coefficient of thermal expansion: 7.15 x 10^{-6} in/in/°C from 0° to −200°C				
Electrical resistivity: 73.2 microhm-cm at 20°C 70.3 microhm-cm at −40°C 63.9 microhm-cm at −196°C				

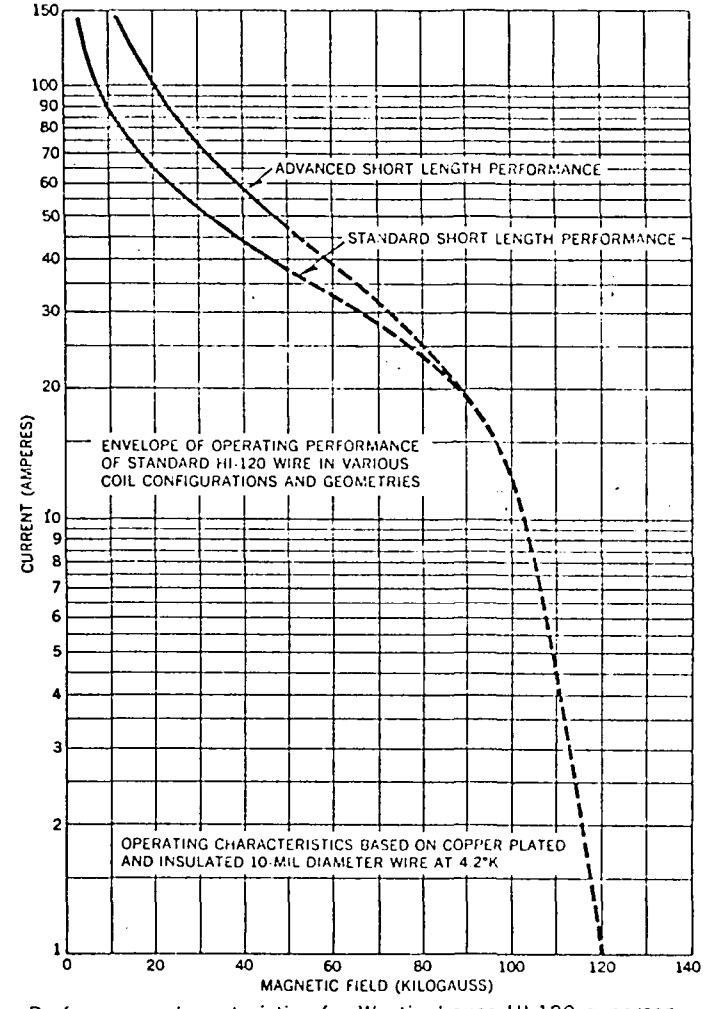

Performance characteristics for Westinghouse HI-120 superconducting wire, both in "short length" and in "coil" geometry.

Figure 9. Properties of Westinghouse HI-120

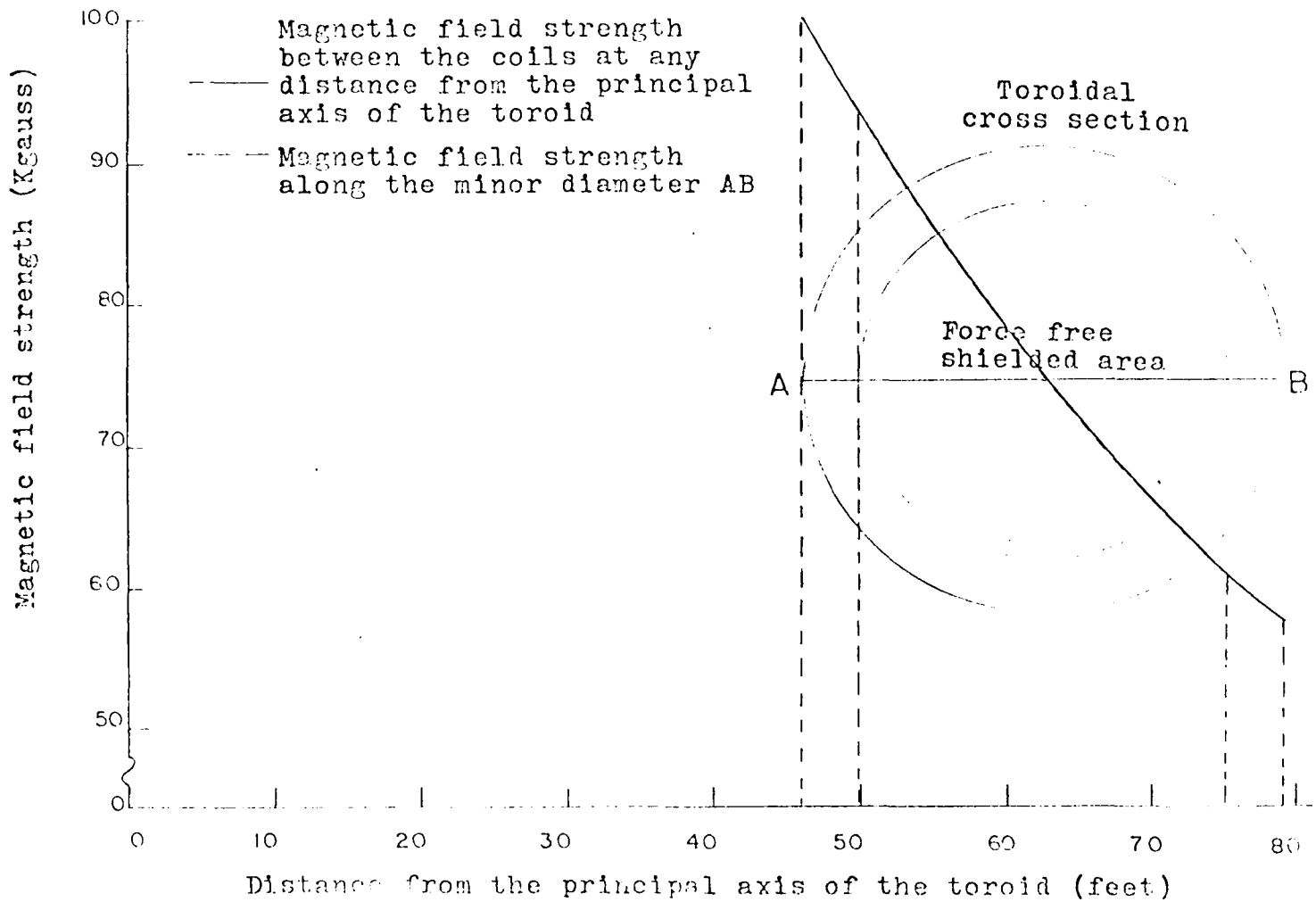

Figure 10. Distribution of the magnetic field in the 100 Kgauss toroid

are required per cm. of toroid length. If the wires are wound in one foot sections and 384 sections are stacked side by side, the coils can be made to form the toroidal shield. Each 1 foot section will require 9450 miles of wire for the external coil and 7150 miles for the internal coil. Winding these coils, inspection, and repair of them in space would provide an extremely difficult engineering problem; therefore, a different type of coil is proposed.

The proposed coil is formed of a thin walled superconducting tube, clad on the outside with 1 mil of copper for insulation, and with an outside diameter of 1 inch. The tube will carry liquid helium to provide the cryogenic environment. In equation 10, N for this coil is one turn per inch, and the critical current density will determine the requisite tube wall thickness.

The critical current density in thin plate was evaluated by Riemersma (35). As a superconducting material reaches its critical state, the magnetic field begins to penetrate the material, thus inducing a current in the superconductor. The induced current opposes the transport current causing the degradation of the field. Just prior to the onset of the induced current, the transport current density has reached its critical value. This maximum current density across a 3-mil plate, wide enough to eliminate edge effects, is shown in Figure 11. This is a calculated curve; Riemersma further states that there is agreement with calculated and measured

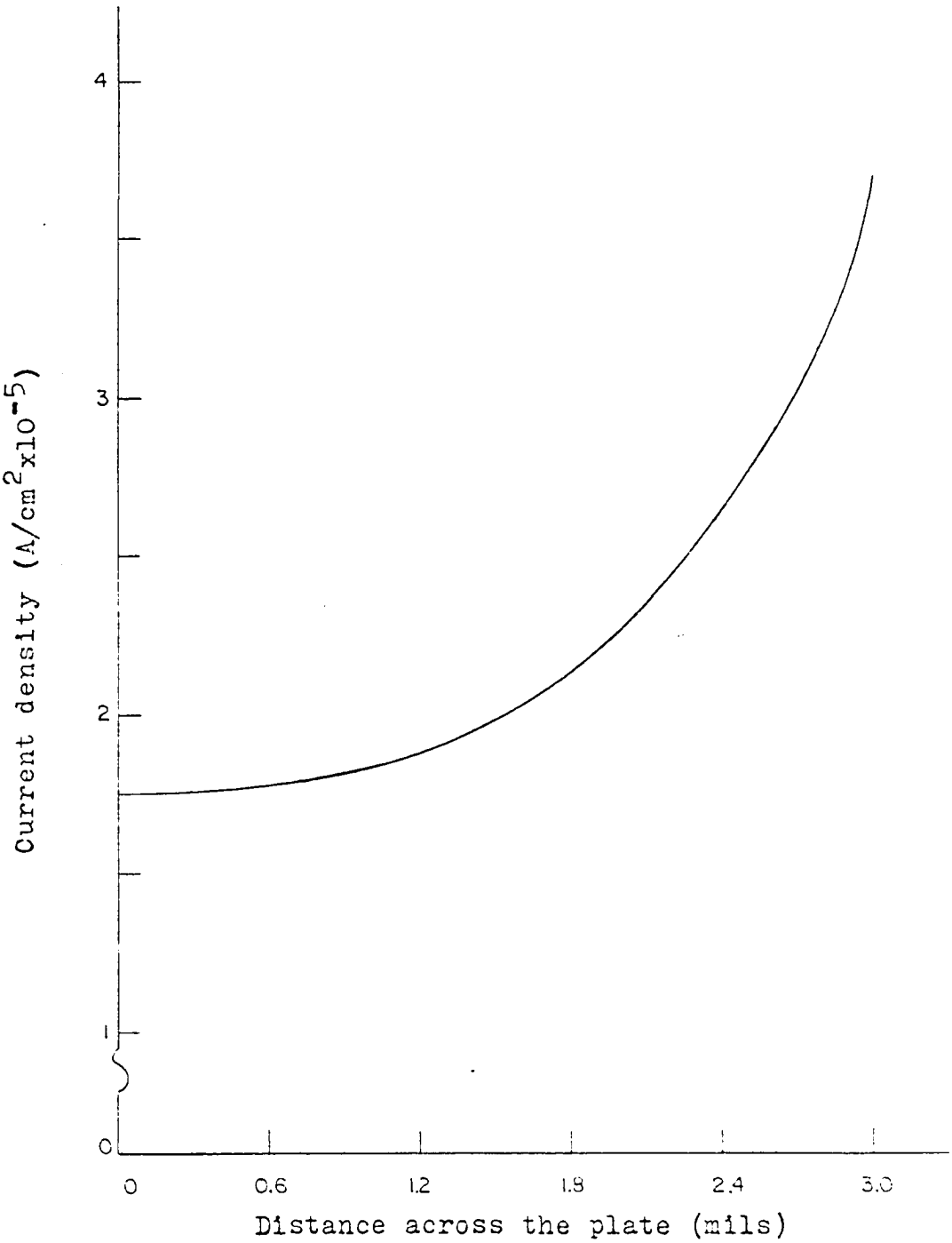

Figure 11. Current distribution in the critical state for 3 mil plate. B = 9.5 Kgauss

magnetization curves, and although the analysis is correct only for flat plates, there is no objection to applying the general conclusions to superconductors of other shapes.

It has been assumed, therefore, that the magnetization curves, generated by Westinghouse for the material HI-120, will have the same shape for plate or for wire. Thus the distribution of critical current vs. critical field strength in Figure 9 was used to construct the distribution in Figure 12 with the normalizing point at 9.5 Kgauss taken from Figure 11.

Consider the shield with a maximum magnetic field strength of 100,000 gauss discussed above. From Figure 11, the allowable current density is 0.31×10^5 Amperes/cm^2; from Equation 10, the required current is 151,200 amperes; therefore, 0.757 sq. in. of tube is required. This area can be provided by a bank of two tubes per inch. If the coils are wound in 10 foot sections, 24,900 ft. of tubes will be required for the external coil. Fabrication of the required length of tubular superconductor will pose a formidable engineering problem, but winding, inspection, and repair in space should not be difficult.

Maxwell Stresses

Superconductors are strongly diamagnetic materials; that is, the magnetic field does not penetrate into the superconductor. Since the mean magnetic field in the medium is the magnetic induction B, throughout a superconductor B = 0.

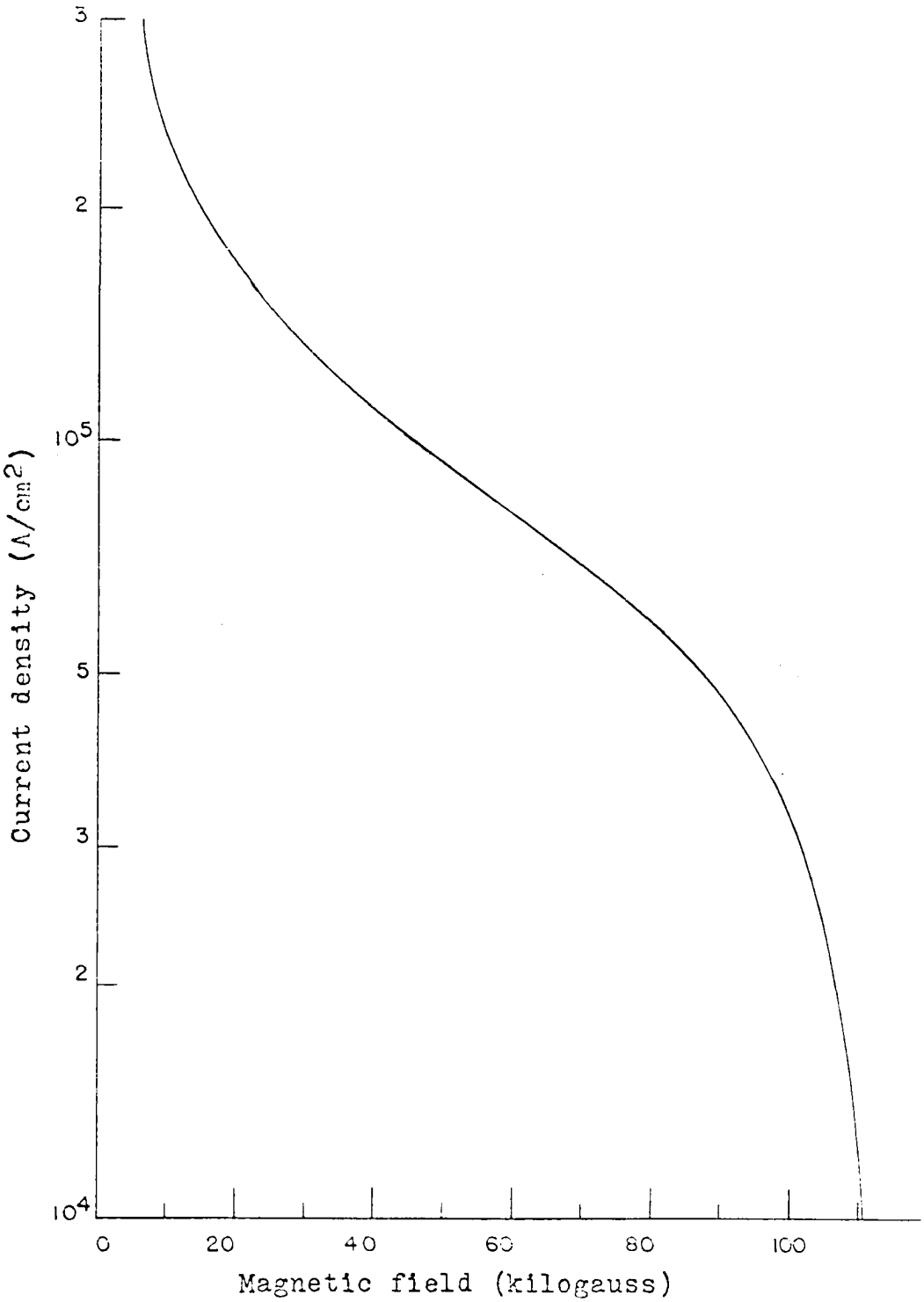

Figure 12. Performance characteristics for Westinghouse HI-120 in the form of 0.003 inch plate

In a thin surface layer B = 0 is not valid; the magnetic field penetrates a superconductor to a depth of the order 10^{-5} cm. The normal component of the induction must be continuous at any boundary between two media; this condition follows from the condition div B = 0. Since B = 0 in a superconductor, the normal component of the external field must be zero on the surface; that is, the field outside of a superconductor must be everywhere tangential to its surface.

For any conductor in a magnetic field, the magnetic forces which act on the solid body of the conductor may be replaced by a system of surface forces which act only on the surface of the body (Figure 13). The stresses, $\vec{T}$, developed

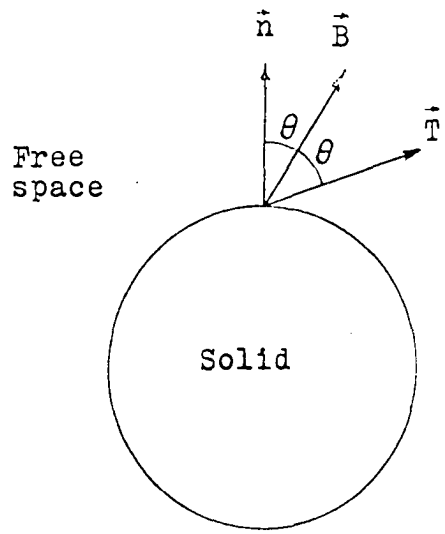

Figure 13. Stresses on a conductor in a magnetic field

are equal to

$$\vec{T} = \frac{1}{4\pi}\left[\vec{B}(\vec{n}\cdot\vec{H}) - \tfrac{1}{2}\vec{n}(\vec{B}\cdot\vec{H})\right] \qquad (13)$$

where $\vec{B}$ and $\vec{H}$ are the values of the field in the external medium, and $\vec{n}$ is the external normal to the surface of the body. Since $\vec{H}$ must be tangential to the surface of a superconductor, $\vec{n}\cdot\vec{H} = 0$; and, since $\vec{B} = \vec{H}$ in free space,

$$\vec{T} = -\frac{1}{8\pi} B^2\vec{n} \; ; \qquad (14)$$

that is, the surface is subjected to a compression, of magnitude equal to the field energy density $B^2/8\pi$ and directed along the outside normal of the superconducting surface.

Since the magnetic forces act normal to the current carrying surfaces, the outer coil will be put in tension and the inner coil will be in compression. The forces involved are quite large. For example in the 100,000 Kgauss shield discussed above, the magnetic forces generate an effective pressure of 3300 psi. The resultant force developed by the pressure on the external coil is 1,310,000 lb, and on the internal coil 1,010,000 lb. The external coil and its support structure can be effectively treated as a thin-walled pressure vessel in tension. The internal coil and its support structure, under uniform compression, can fail by direct compression or by buckling of the wall. The support structure will require stiffening rings to avoid the possibility of buckling. A half section through one side of the torus is shown in Figure 14.

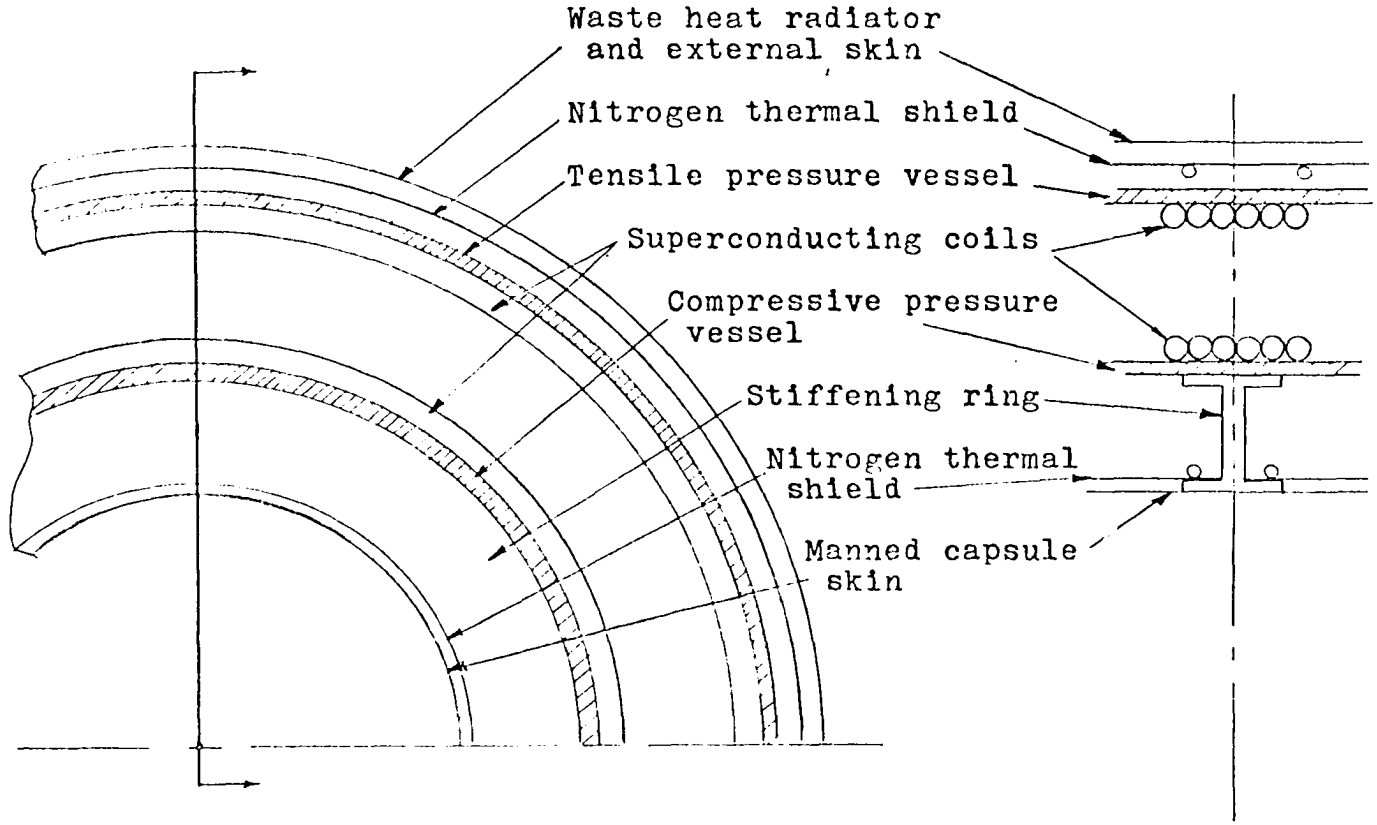

Figure 14. Shield cross section (not to scale)

Cryogenic System

The properties of the superconducting material are illustrated in Figure 9. These properties are established at a temperature of 4.2°K, which is the boiling point of liquid helium at one atmosphere; it is not the transition temperature of HI-120. The transition temperature of the niobium-zirconium system is shown in Figure 15 (49). In the proposed configuration, the Nb-Zr tube is kept superconducting by circulation of liquid helium through the tube coil. The cooling process is analogous to the long-distance, liquid-gas, transfer system discussed by R. B. Jacobs (17).

Figure 16 shows the components of the simplified transfer system, and Figure 17 shows the processes involved in the transfer. The liquid enters the pump container from the coil tube and from a helium liquefier. The helium in the superconducting circuit is diverted through a normal pipe, and is cooled by the liquid in the pump container. It then enters the pump in state r (saturated liquid). The liquid increases in pressure and temperature as it passed through the pump and is discharged at state o. After leaving the pump the liquid is cooled to state i; it then enters the transfer line. In the transfer line, the pressure drops because of friction and the temperature rises due to friction and heat leak. The line is operated so that the liquid becomes saturated as it enters the pump compartment.

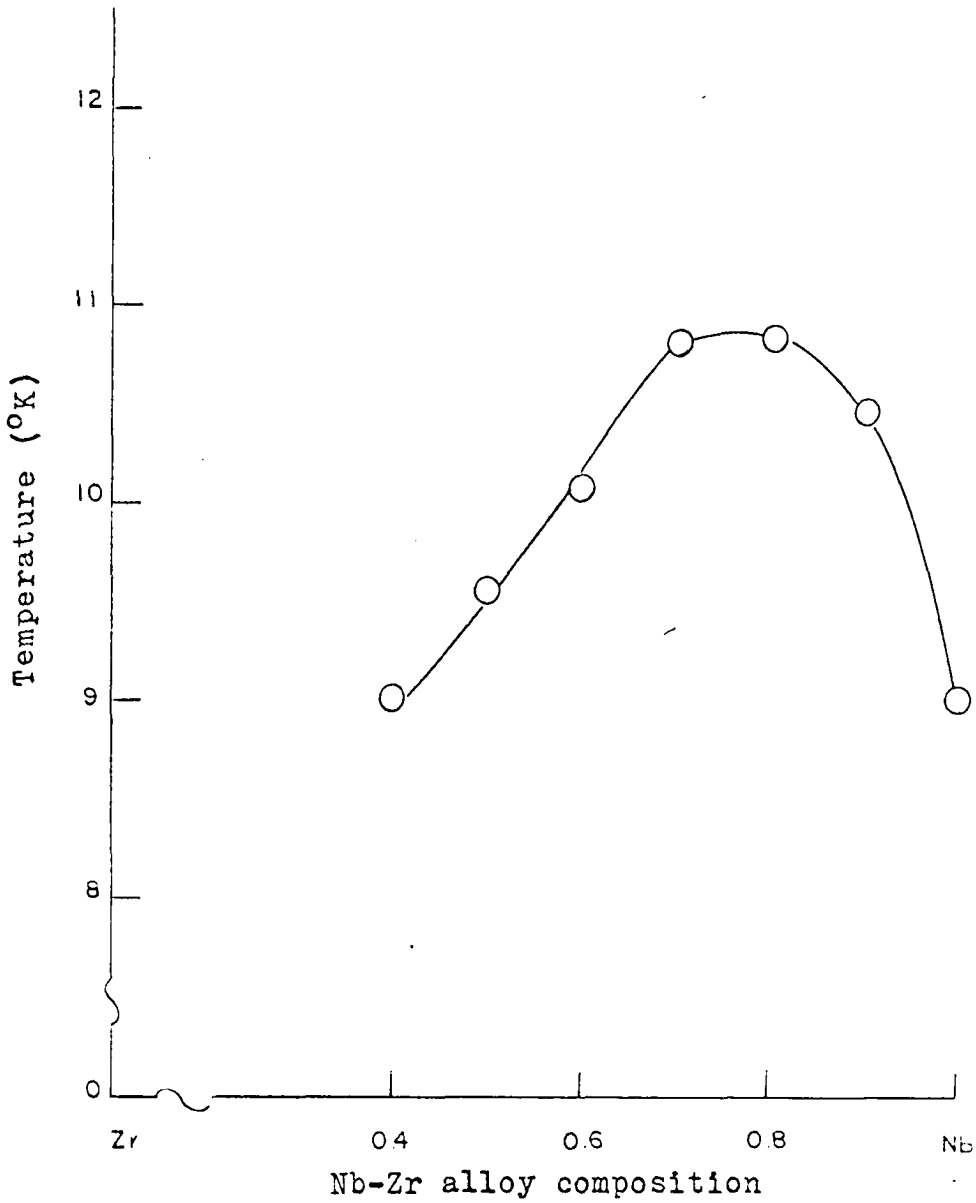

Figure 15. Transition temperature for Nb-Zr system

note: the superconducting circuit, the non-superconducting circuit and the pump comprise the transfer line

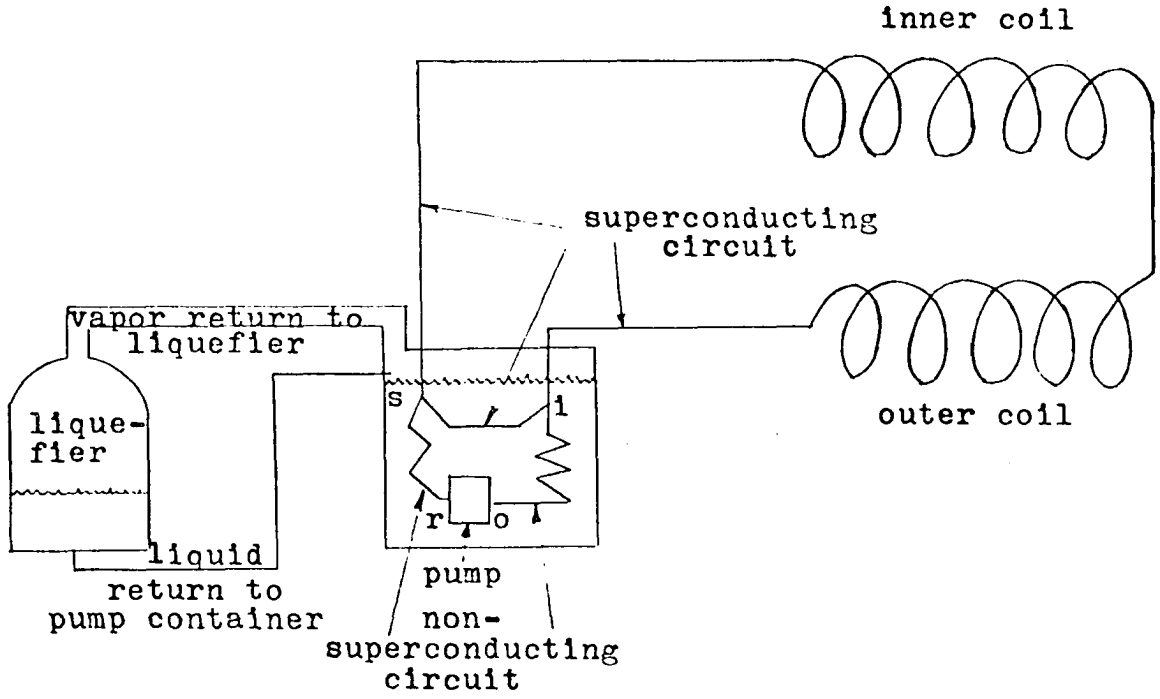

Figure 16. Components in transfer system

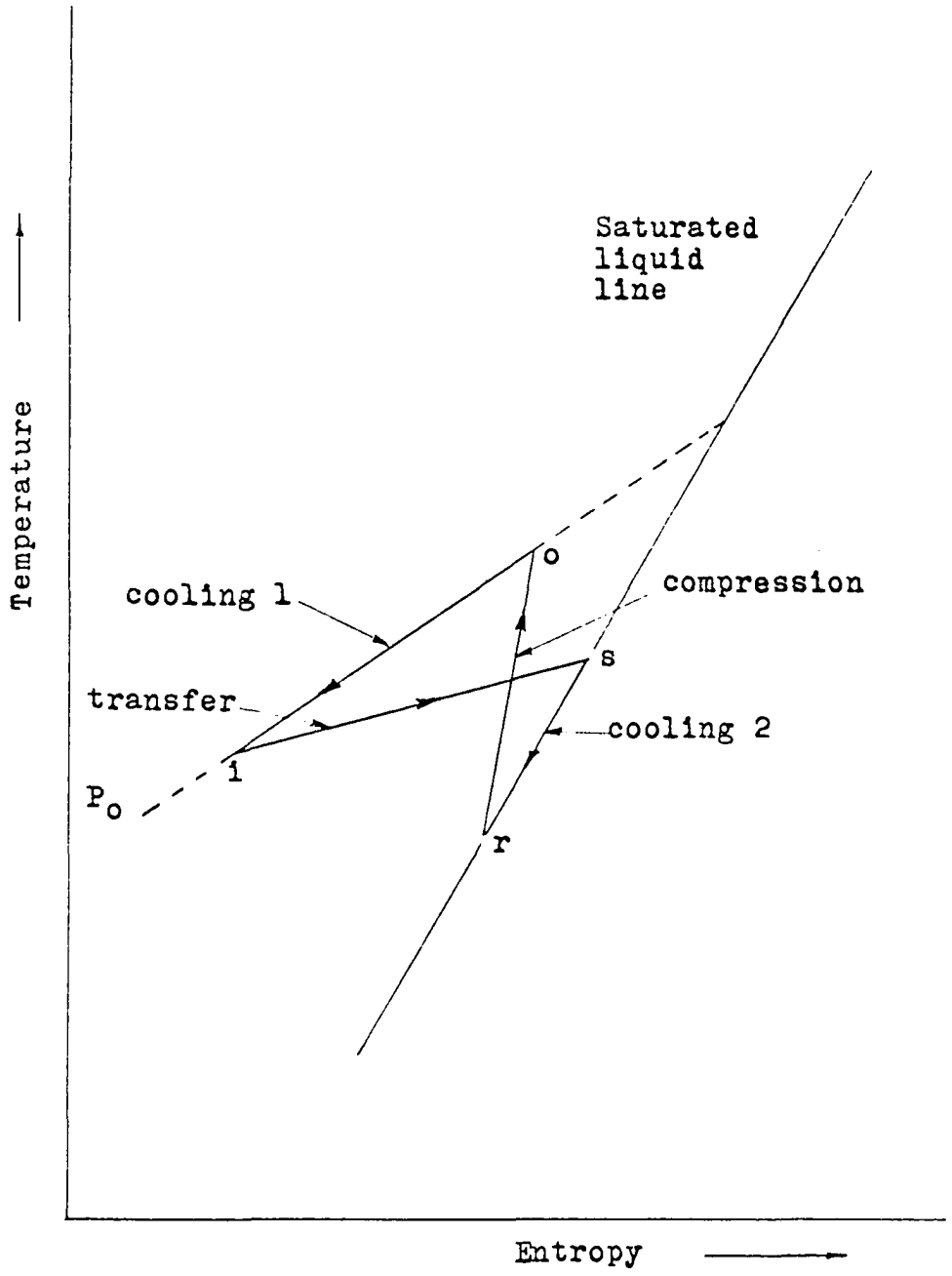

Figure 17. Processes involved in transfer system

The heat leak into the liquid helium from the manned compartment at 297°K and from solar radiation will be large enough to cause vaporization during transfer. Therefore, nitrogen-cooled radiation shields will be placed between the skin of the manned compartment and the inner coil and between the external skin of the vehicle and the external coil.

The mass of liquid vaporized in these two processes necessitates the operation of helium and nitrogen liquefiers. The operation of these liquefiers which includes the removal of the absorbed heat will constitute the principal power drain in the system.

Waste Heat Radiator

Heat generated in the manned vehicle and that absorbed in the cryogenic system must be radiated away from the vehicle. The waste heat radiator installation is incorporated into the external skin of the vehicle. The radiator will be a condensing ammonia tube and fin system, and will probably be segmented. The half of the vehicle in the shade will radiate the waste heat to the space sink. The tubes must be armored to improve the probability of non-failure of the radiator due to meteoroid penetration.

Launch Configuration

The shield and the manned compartment will be assembled in room-sized sections 20 feet long. Each section of the shield will be self contained; that is, each section will have

a self contained cryogenic system including a helium and a nitrogen liquefier, a start-up system exclusive of the power supply, and a waste-heat system.

Seven sections will be mounted end to end on an Apollo Saturn 5 and lifted to a 300-mile orbit. The Saturn 5 can put a payload of 230,000-250,000 lb in low earth orbit (lower weights can be put in higher orbits). The maximum volume of the payload would be 125,000 cu. ft. and the diameter would be about 33 feet although some payload overhang is allowed (25).

The number of Saturn 5's required will be determined by the length of the shield. The payloads will be clustered for orbital storage prior to assembly. If possible some power should be retained in the 3rd stage of the Saturn boost vehicle for orbital rendezvous. The seven sections lifted together will be put into position by simple rotation to form a smooth arc. Assembly will then take place either remotely or else manually; remote assembly is desirable.

Since this system is unpowered, a space tug, employing a SNAP-50 for a power source, will be employed to power the shield, and to take the vehicle on its journey through space. The final configuration is shown in Figure 18.

Figure 18. Manned vehicle configuration. The propulsion unit is a Mars ferry vehicle developed by Hal Brown at Space Power Operations of the General Electric Company

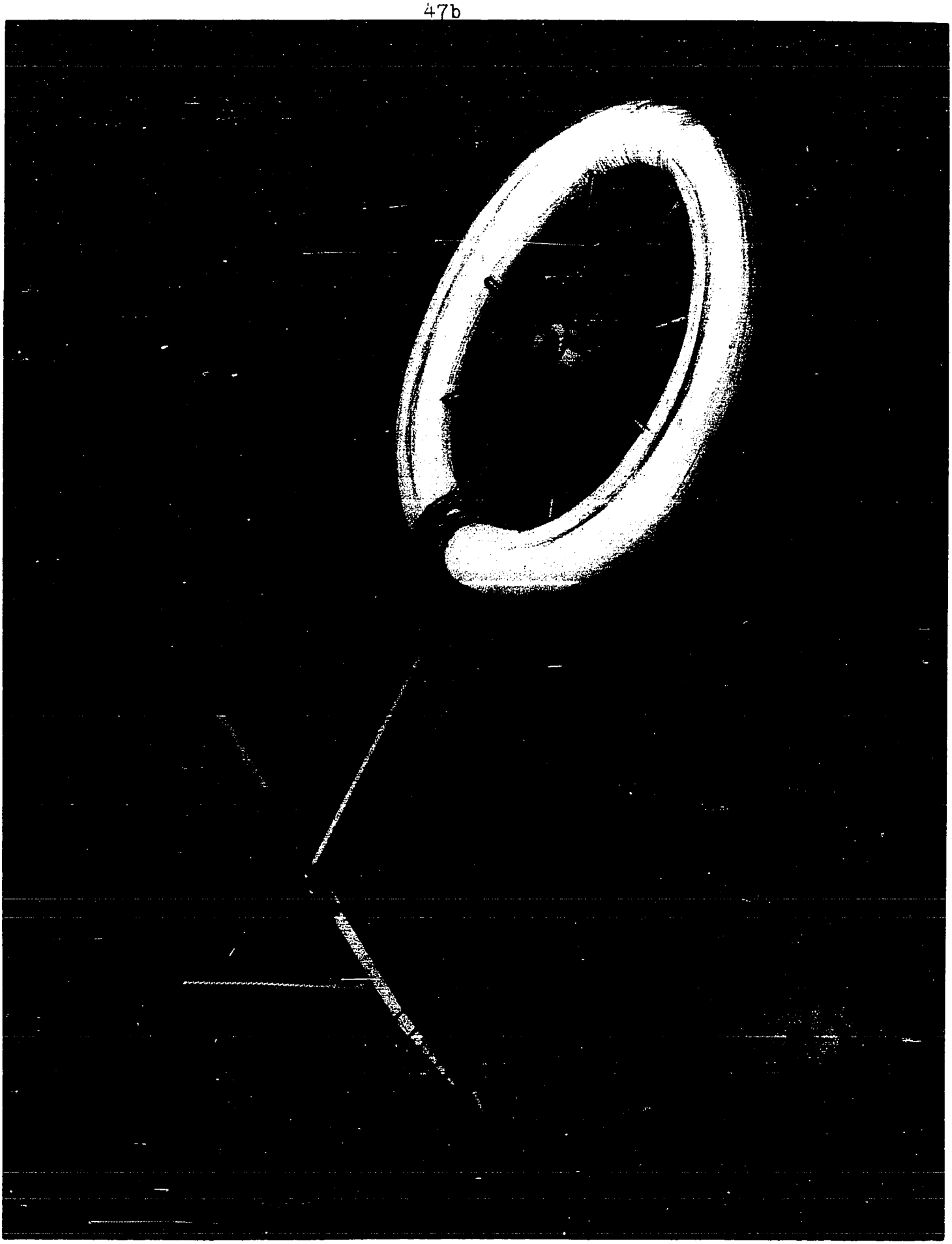

CONFIGURATION OPTIMIZATION

Basic Assumptions

In the 100,000-gauss shield example discussed in The Magnetic Shield Configuration, the resultant force developed by the magnetic pressure on the external coil is 1,310,000 lb. If an alloy having the same strength-to-weight ratio as Nb-Zr is used, the mass of structure required to withstand this stress is 2.73×10^6 lb; 1.62×10^6 lb is required for the internal coil. Thus, the total structural weight is 4.35×10^6 lb.

If the magnetic field strength is decreased, the stresses will decrease, and the required structure thickness will decrease. In order to retain the same shielding capability, the thickness, δ , of the magnetic field region must be increased. Since the external diameter is fixed at 33 ft., an increase in δ results in a decrease in the shielded cross sectional area. To maintain the required shielded volume, the length of the toroid must be increased. Thus the decrease in magnetic field strength will decrease the structural mass due to a reduction in structural wall thickness, but will also result in an increase in weight due to the increase in toroid length. The balance of one effect against the other results in a minimum weight configuration.

A family of vehicle shields in which the maximum magnetic field strength was varied from 100,000 gauss to 25,000 gauss

was investigated to obtain the minimum weight configuration. This design family had the following features, some of which differ from the final design:

1. Because of the complexity of the design of the stiffeners, the compressive structure was designed as a simple compressive member; that is, no buckling was considered.

2. Although the final design makes use of titanium as a structural material, a 20-percent heavier material was used in the optimization study to compensate for the difference in weight made by the addition of the stiffeners to the final design.

3. The material has the properties of HI-120. The specific weight is 374.4 lb/ft^3 and the yield strength at $4.2^{o}K$ is 310,000 psi. A maximum allowable unit stress of 300,000 psi was assumed in the optimization.

4. The position of the internal coil was determined to protect a volume of 200,000 cubic feet. The stiffeners will occupy approximately 30 percent of the cross section, thus a useful volume of 140,000 cubic feet will result.

5. The thickness, δ , of the magnetic field was determined from the average field strength in the shield.

6. The average field strength was also used to determine the surface stresses in the coil.

7. The maximum field strength was used to determine the allowable current density.

8. The tubes in the external toroid will be expected to

carry a part of the tensile load proportional to the tube cross sectional area.

Results of the Optimization

The inputs and numerical results of the configuration study are shown in Table 6. Figure 19 shows the superconducting tube weight versus average field strength in the shield. Figure 20 shows the shield structural weight versus average field strength. Both curves minimize near 30 Kgauss. Figure 21 shows the variation of shield weight vs. toroid length. Figure 21 was included to show the slow variation in shield weight vs. distance near the minimum weight.

The system minimum was established at 1120 ft. One benefit of the long radius for the toroid is the small variation of magnetic field strength throughout the vehicle cross section. The field strength varies from 28.5 Kgauss to 34 Kgauss; thus, the threshold energy varies from 845 Mev to 1210 Mev with an average very close to 1 Bev.

Table 6. Inputs and numerical results of the configuration optimization

	Maximum magnetic field strength (kilogauss)	External toroid diameter (ft)	Internal toroid diameter (ft)	Toroid length (ft)	Average magnetic field strength (kilogauss)	Average magnetic pressure (psi)
1.	100	33	25.4	394	75	3300
2.	80	33	23.9	445	61.9	2250
3.	60	33	21.4	560	49	1410
4.	50	33	19.75	652	42	1040
5.	40	33	17.1	870	35.5	742
Min	34	33	15.0	1120	31	566
6.	30	33	13.0	1510	27.5	444
7.	25	33	9.75	2680	24	339

Table 6. (Continued)

	Circumferential tensile force external toroid (lb)	Required external wall thickness (in)	Weight of external structure (lb)	Circumferential compressive force internal toroid (lb)	Required internal wall thickness (in)	Weight of internal structure (lb)
1.	1,310,000	2.18	2.73×10^6	1,010,000	1.68	1.62×10^6
2.	892,000	1.49	2.11×10^6	645,000	1.075	1.105×10^6
3.	559,000	0.93	1.66×10^6	360,000	0.60	0.695×10^6
4.	411,000	0.685	1.43×10^6	298,000	0.497	0.615×10^6
5.	294,000	0.49	1.36×10^6	152,000	0.254	0.364×10^6
Min	223,000	0.372	1.34×10^6	101,800	0.1698	0.278×10^6
6.	176,000	0.294	1.41×10^6	68,400	0.114	0.216×10^6
7.	134,000	0.224	1.91×10^6	38,600	0.066	0.166×10^6

Table 6. (Continued)

	Vehicle	External toroid			
	Total structural weight (lb)	Allowable current density (amp/cm^2)	Required current (amperes)	Required area (in^2)	Superconductor weight (lb)
1.	4.35×10^6	0.31×10^5	151,200	0.757	950,000
2.	3.215×10^6	0.585×10^5	125,000	0.332	470,000
3.	2.355×10^6	0.80×10^5	99,000	0.192	342,000
4.	1.985×10^6	0.92×10^5	84,000	0.143	298,000
5.	1.724×10^6	1.07×10^5	71,000	0.104	288,000
Min	1.618×10^6	1.18×10^5	62,600	0.0824	296,000
6.	1.626×10^6	1.27×10^5	55,000	0.0678	325,000
7.	2.076×10^6	1.40×10^5	48,500	0.0536	457,000

Table 6. (Continued)

	Internal Toroid			Vehicle	
	Maximum magnetic field strength (kilogauss)	Allowable current density (amp/cm^2)	Required area (in^2)	Superconductor weight (lb)	Total weight of superconductor (lb)
1.	94	0.41×10^5	0.57	550,000	1.5×10^6
2.	75	0.64×10^5	0.303	311,000	0.78×10^6
3.	56.2	0.84×10^5	0.183	212,000	0.554×10^6
4.	47	0.97×10^5	0.134	166,000	0.464×10^6
5.	37.8	1.1×10^5	0.101	145,000	0.433×10^6
Min	32.3	1.2×10^5	0.081	133,000	0.429×10^6
6.	28.5	1.3×10^5	0.0655	124,000	0.450×10^6
7.	24.3	1.43×10^5	0.0525	132,000	0.589×10^6

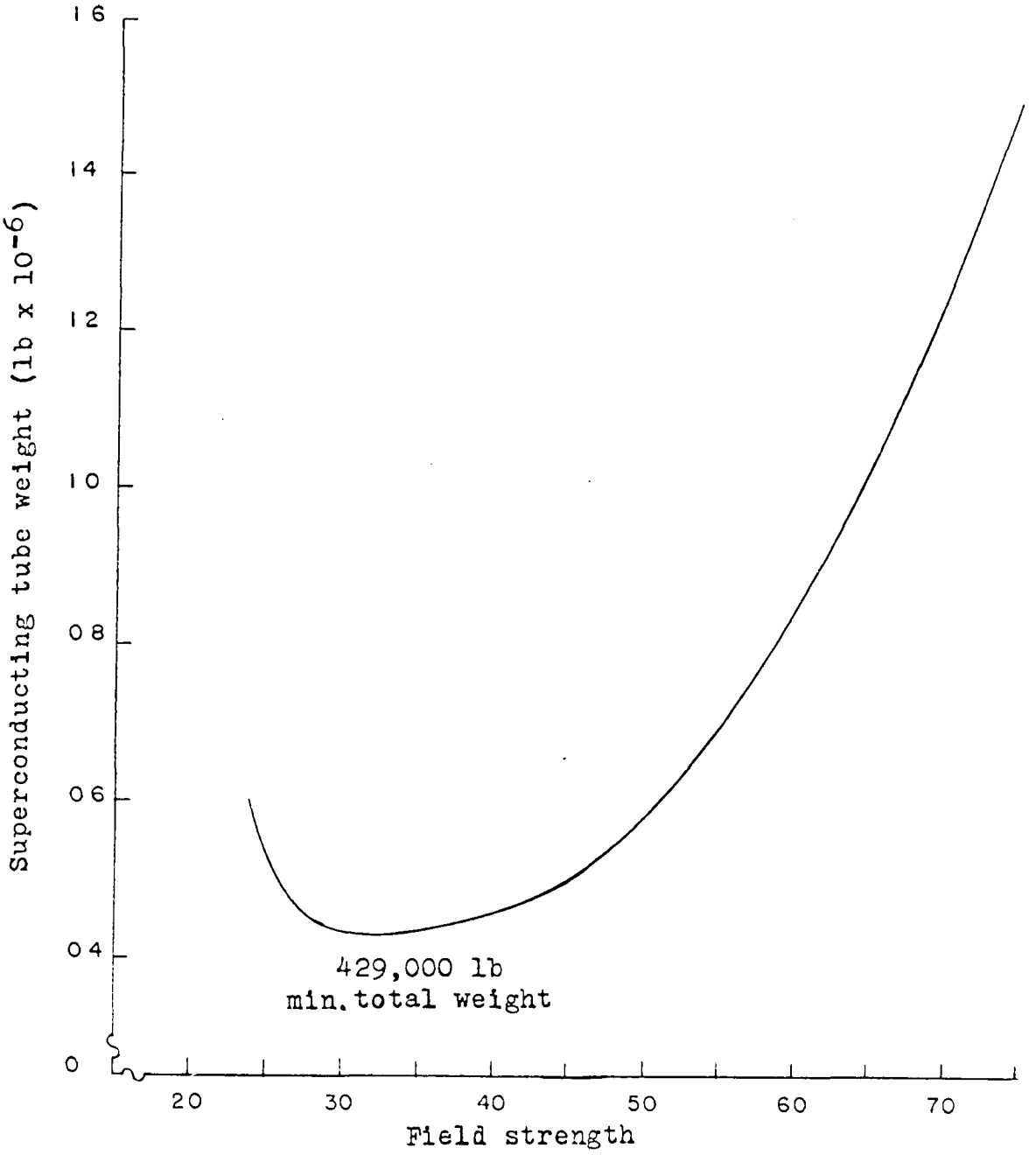

Figure 19. Superconducting tube weight vs. average field strength for a superconducting shield

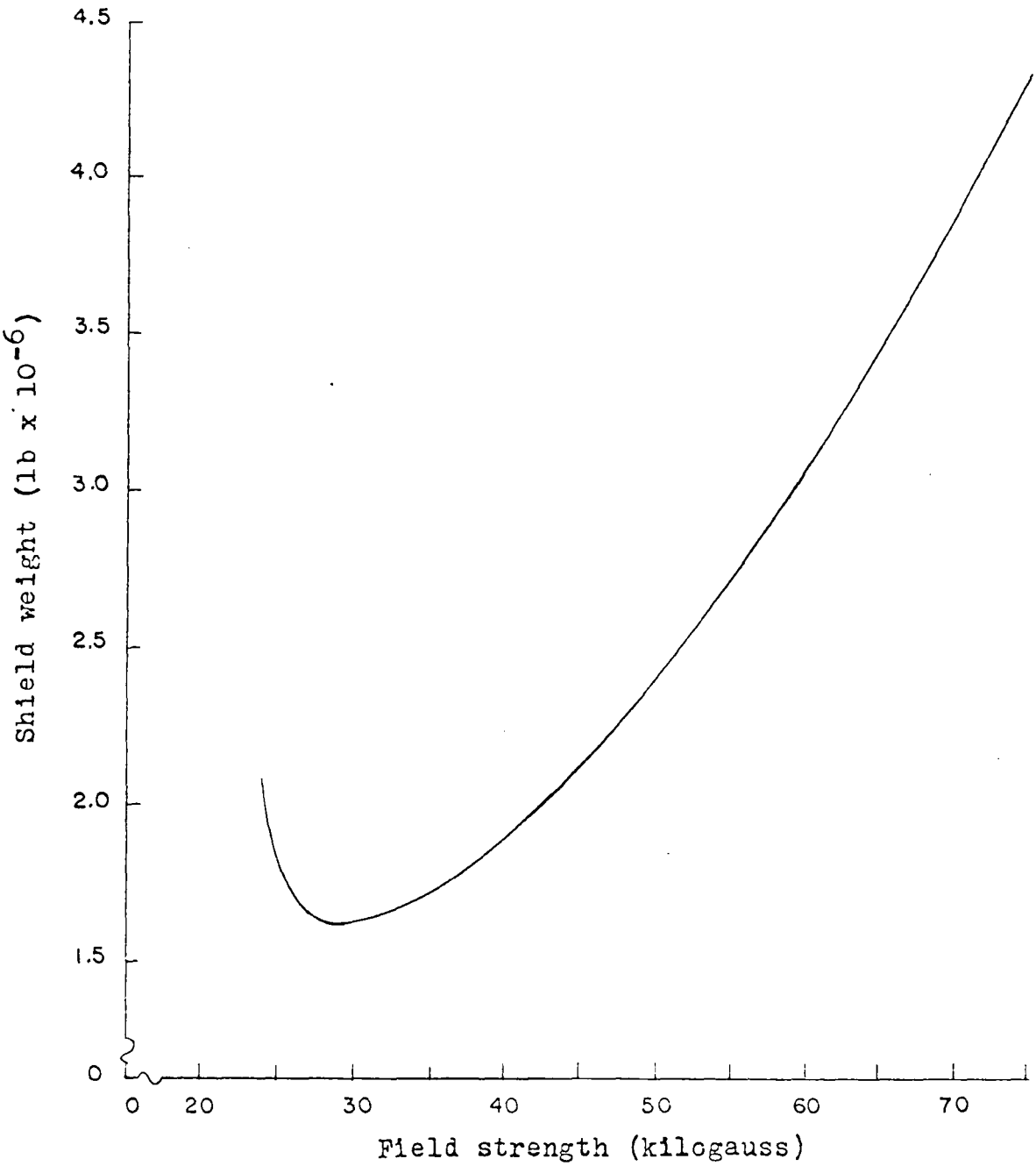

Figure 20. Structural weight vs. average field strength for a superconducting shield

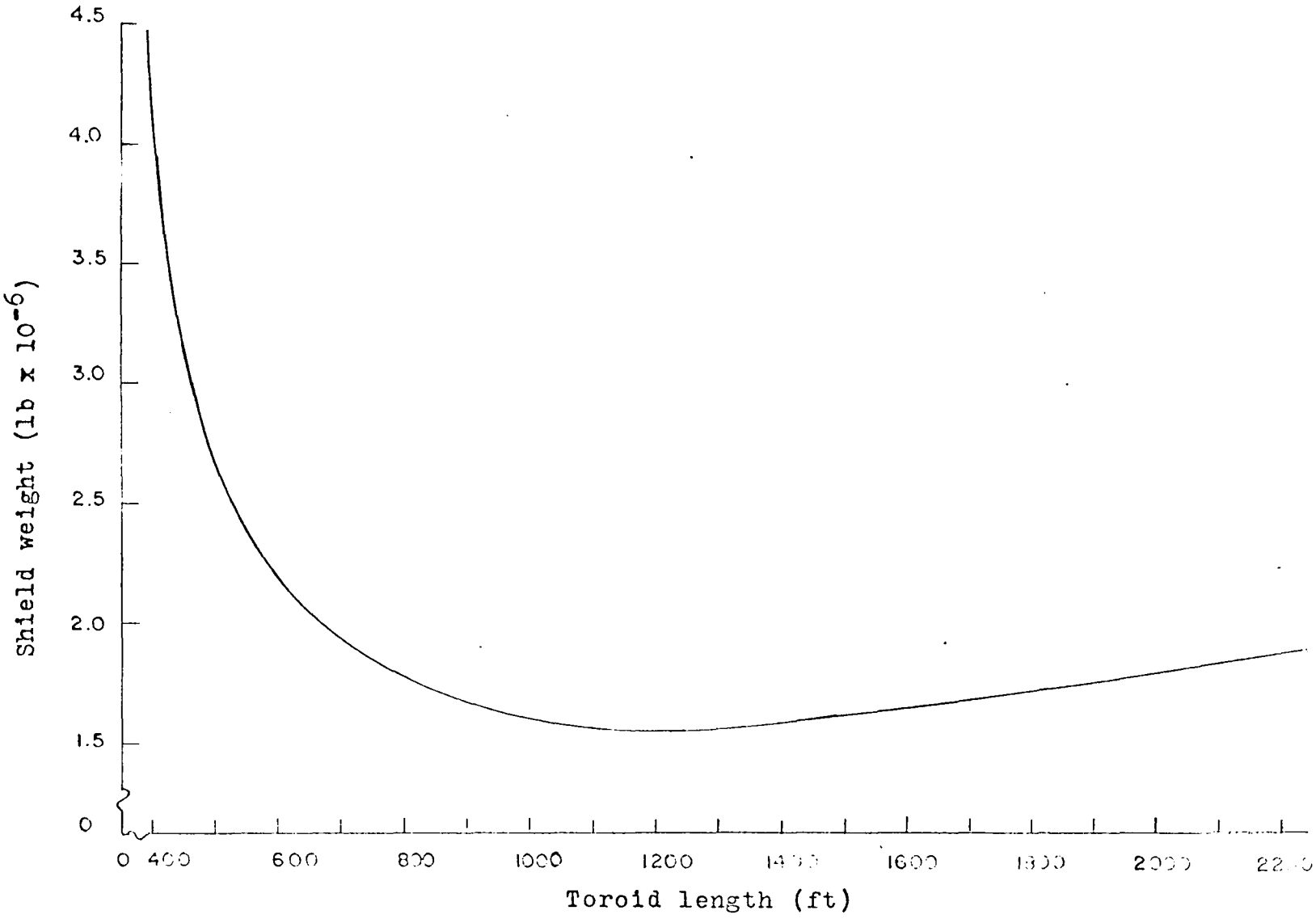

Figure 21. Structural weight vs. toroid length for a superconducting shield

MECHANICAL DESIGN

General Configuration

A minimum weight configuration has been approximated with an 1120-foot long toroid with an internal torus diameter of 15 feet and an external torus diameter of 33 feet. The toroid will be divided into fifty-six 20-foot arcs, and each 20-foot section of shield will be self-contained. Both coils carry 62,600 amperes and generate an average magnetic field strength of 31 kilogauss. The two coils in a section will be connected in series to obtain the opposing magnetic fields in the force free region.

The tubes which connect the coils will distort the magnetic field in a cylindrical field around the crossover pipe. The distortion will take place over a limited area. At the surface of the tube the distortion is approximately 30 percent; at 4 inches the distortion has been reduced to less than 3 percent. The effect of the distortion on the shielding properties can be minimized by connecting the coils with a curved crossover pipe rather than a straight pipe.

Figure 14 shows the general configuration of a cross section (not to scale). It is the purpose of the mechanical design to; (1) design the compressive pressure vessel and stiffening ring; (2) design the tensile pressure vessel; (3) establish the ability of the tubes to withstand the compressive magnetic stress; (4) examine the thermal contraction

problem and the deformation due to stress; and (5) examine the meteoroid penetration problem as it concerns the superconducting coils and the nitrogen tubes in the external thermal shield. The design of a vehicle skin and waste heat radiator is a problem common to every space vehicle and will not be discussed in detail.

The structural properties of some of the materials used in the design are shown in Figures 22 to 26 (31). Some additional properties are discussed in the text of the design as they become pertinent to the design. Figures 22, 23, and 24 show the thermal expansion between $0^{\circ}F$ and $-460^{\circ}F$ for HI-120, C-120-AV titanium, and beryllium respectively. The data for the HI-120 curve was taken from Figure 9 and includes an extrapolation below $-350^{\circ}F$. Figure 25 shows the stress-strain diagram for C-120-AV titanium at and below $68^{\circ}F$. Figure 26 shows the variation of modulus of elasticity at low temperatures for the titanium.

The direction of the magnetic stress has been established to lie along the outside normal to the superconducting surface, but directed into that surface. A toroidal coil confines the magnetic field to lie within the toroid. Thus the magnetic pressure in the shield acts only against the surface of the coil which faces the magnetic field region.

The tensile pressure vessel is placed outside the external coil; the compressive pressure vessel is placed inside the internal coil. In order to transmit the stress to the wall

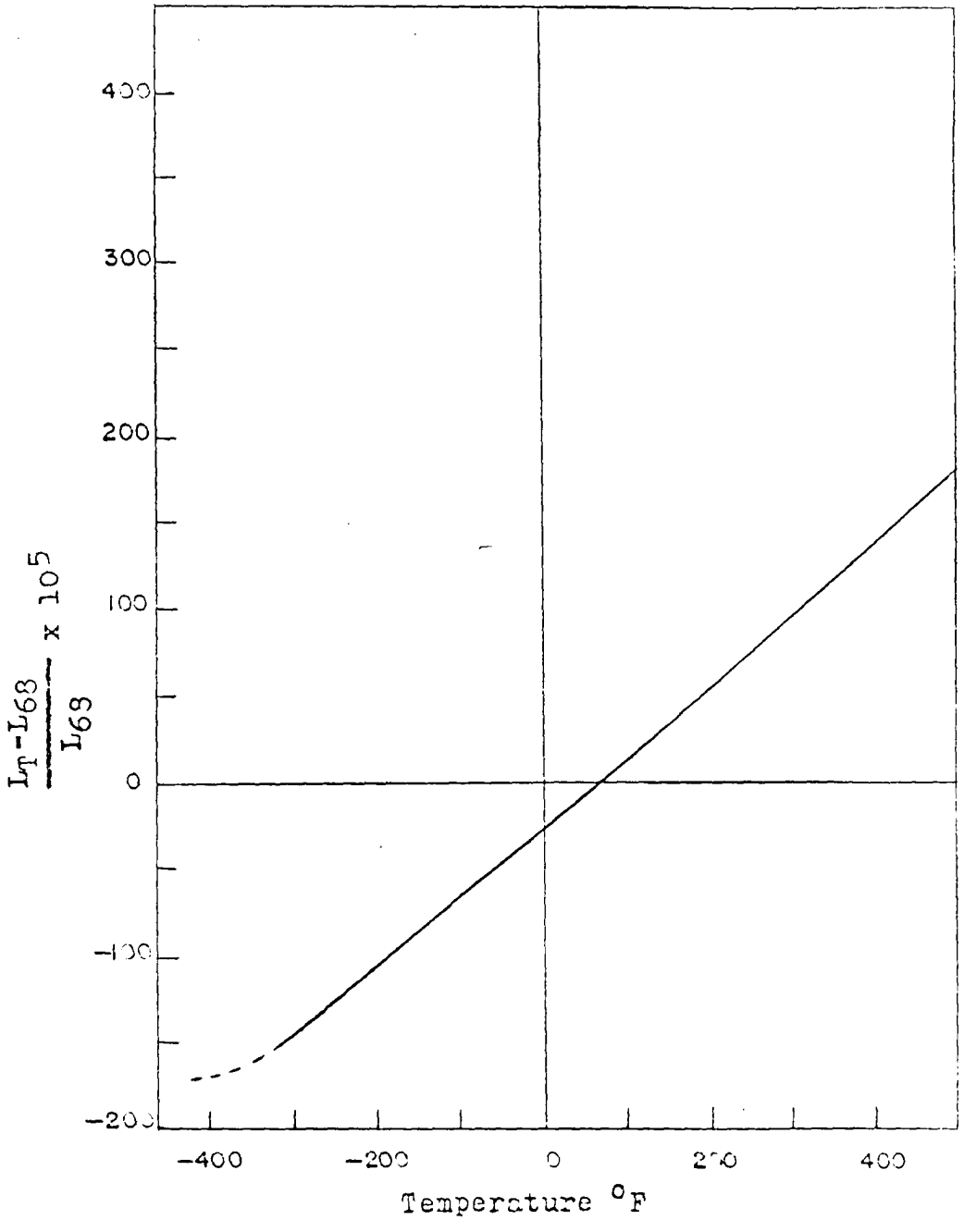

Figure 22. Thermal expansion of HI 120 material

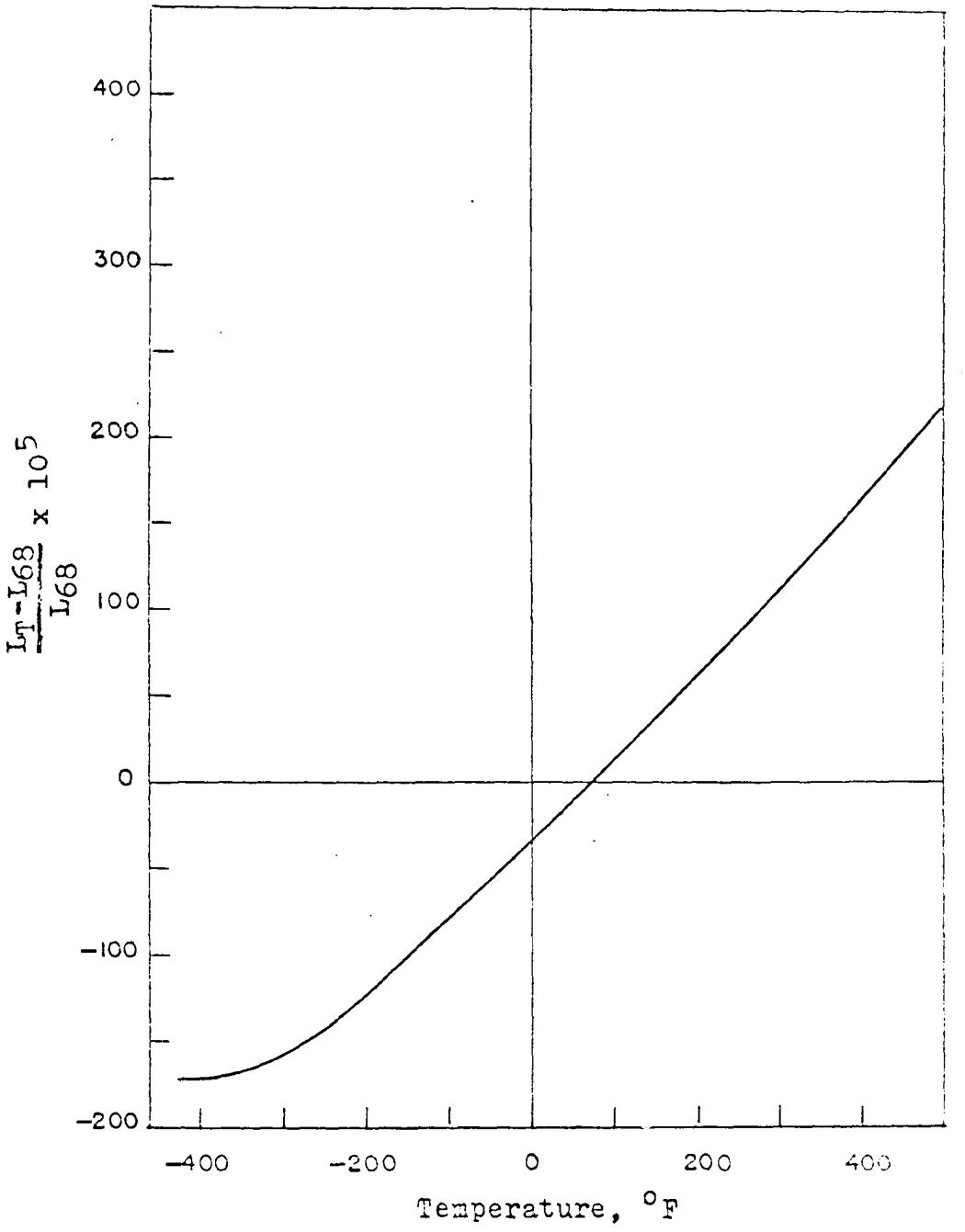

Figure 23. Thermal expansion of C-120-AV titanium

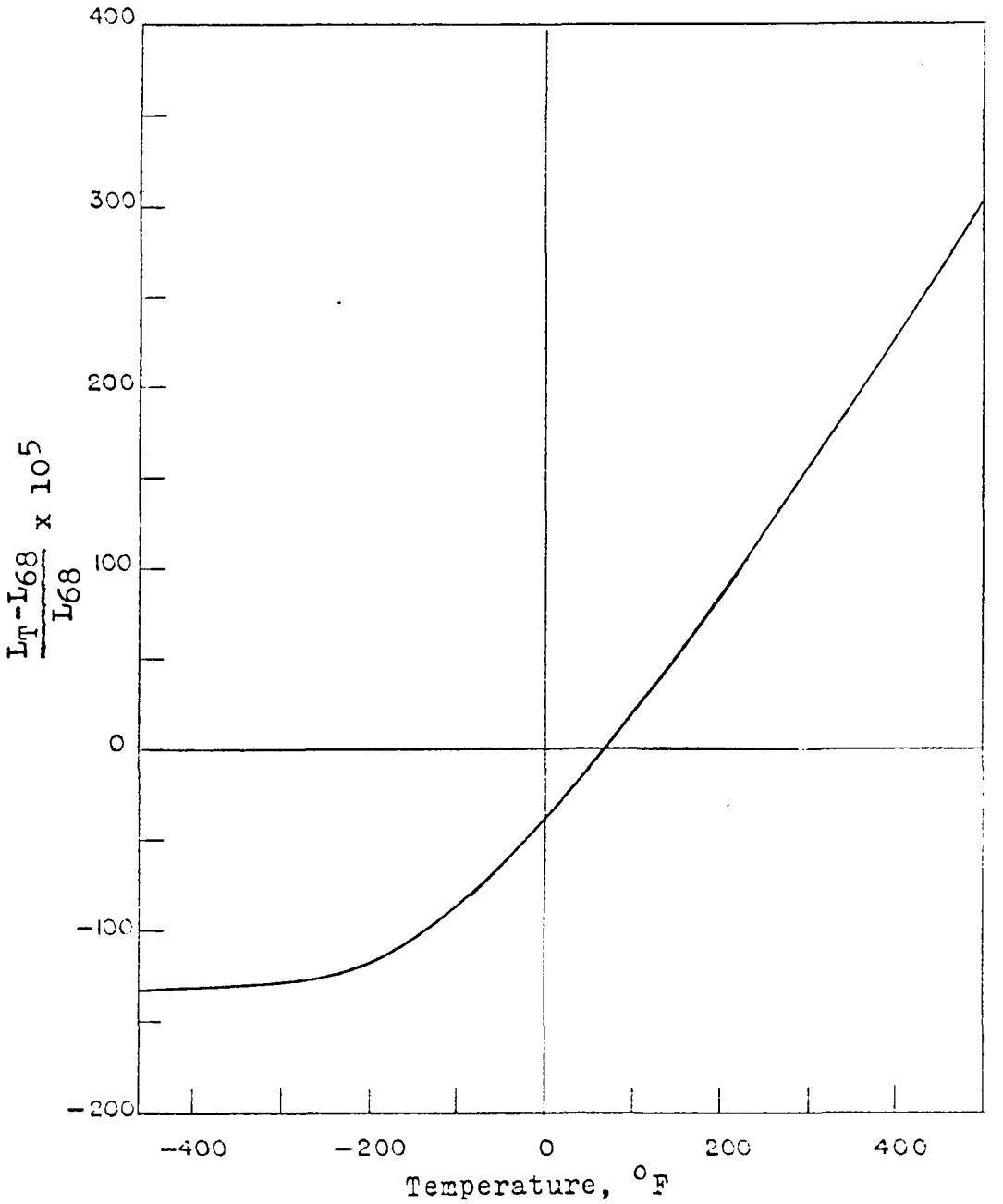

Figure 24. Thermal expansion of beryllium

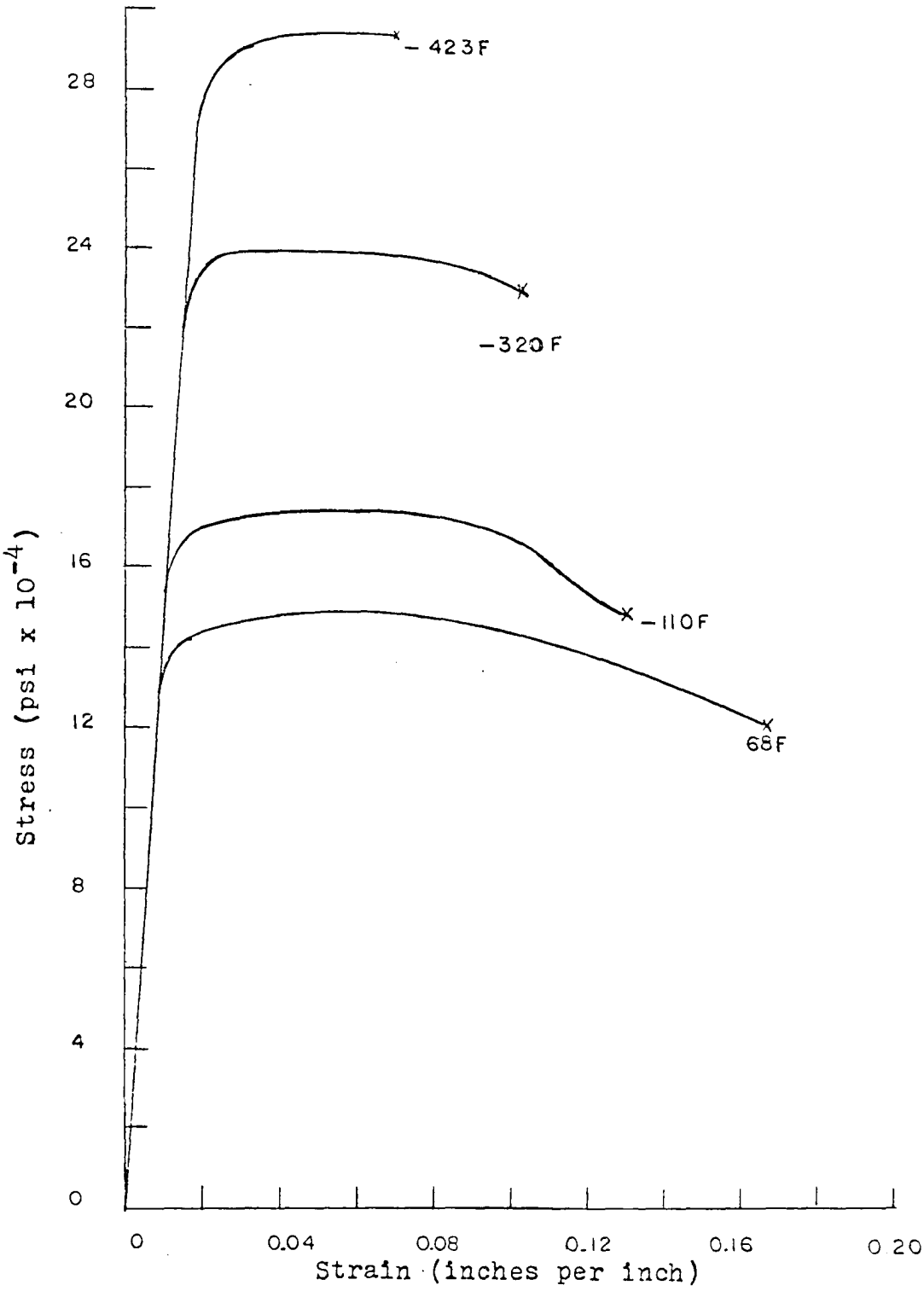

Figure 25. Stress-strain diagram for C-120-AV titanium

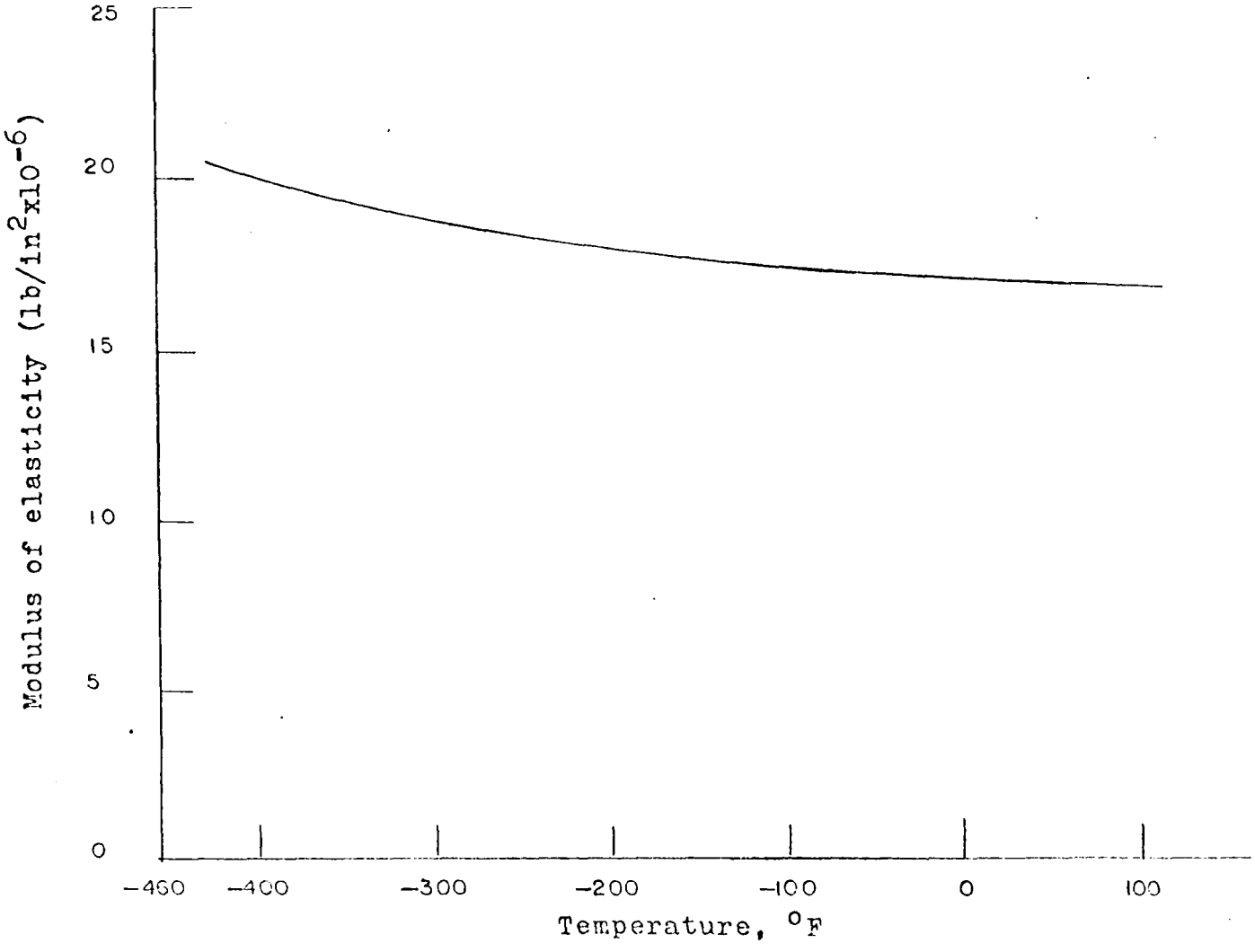

Figure 26. Modulus of elasticity of C-120-AV titanium

uniformly, and to eliminate point stresses on the tubes, a bearing material will be placed on the surface of the tubes which face the pressure vessels, before the pressure vessels are put in place.

Polyethylene is proposed as the bearing material; it has a compressive yield strength of 25,000 psi at $4^{\circ}K$. Although subject to brittle failure, it can stand rough treatment so long as temperature shock is avoided (39). Expansion joints will be provided to take care of coil distortion due to temperature change and coil deformation due to stress. The bearing material will not carry any of the circumferential stress.

Since the compressive pressure vessel and the compressive magnetic stress on the tubes are analogous, the method of solution of this problem is examined first. In an analysis by R. Sturm (44), the critical collapsing external pressure of a thin walled cylinder is

$$W_S = KE \frac{t_s^3}{D^3} \qquad (15)$$

where W_S is the critical pressure (psi)

E is the modulus of elasticity (lb/in^2)

t_S is the wall thickness (inches)

D is the diameter (inches)

and K is a constant which is a function of the dimensionless ratios L/R and D/t

where L is the unsupported length of tube (inches)

R is the tube radius (inches).

The constant K is called a collapse coefficient. A graph of the collapse coefficients is shown in Figure 27. The superconducting tubes can be considered to be long unsupported cylinders. For this condition K = 2.2. From Figure 9, E = 12.2 x 10^6 psi at 20°K; from Table 6, the tube wall is 26.2 mils plus 1 mil clad, thus the collapsing pressure is 536 psi. This is slightly lower than the magnetic pressure existing; however, a half mil increase in tube wall thickness, or an expected increase in modulus of elasticity at low temperatures will put the tubes in the safe range.

Interior Torus

The interior pressure vessel is a circular segment of a toroid 20 feet long. Because of the large radius of curvature (178 ft), the section deviates by six inches in 20 feet from a cylindrical shape, Sturm's analysis is assumed to be applicable to this vessel. In Equation 15 the expression, Et_s^3, is a measure of the structural rigidity of the skin. The material should have a high modulus of elasticity and a low density. The ideal space age material is beryllium (E = 44 x 10^6 psi, specific gravity = 1.85, compressive yield strength = 77,000 psi) (5).

The minimum allowable wall thickness is 0.66 in. to sustain the direct compressive stress. Thus, using Equation 15, the collapse coefficient is determined to be 264. From Figure 27, for K = 264, L/R is 0.54. Thus the maximum unsup-

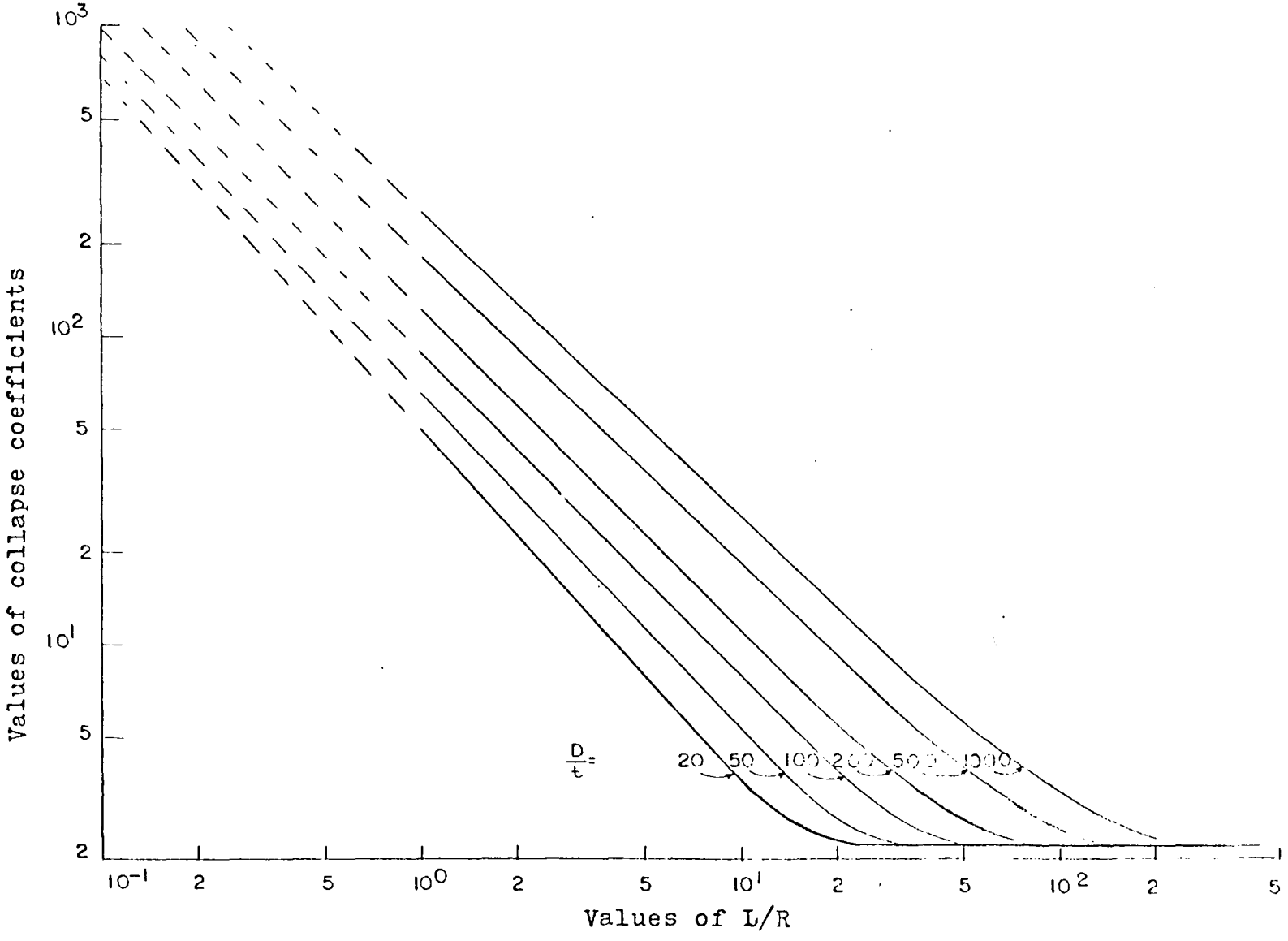

Figure 27. Collapse coefficients for round cylinders in compression

ported length for the cylinder is 4.05 feet. Four feet has been chosen; thus, each 20 foot cylinder will require 6 stiffeners.

The flexural rigidity of a long stiffened cylinder necessary to withstand an external pressure W_S is given by the expression

$$EI_S = \frac{W_S D^3 L_S}{24} \qquad (16)$$

where EI_S is the flexural rigidity of the stiffened section (lb-in.^{2})

I_S is the moment of inertia of the combined stiffener and plate (in.^{4})

D is the diameter of the shell (inches)

L_S is the stiffener spacing (inches).

The required flexural rigidity for the internal vessel is 7350×10^6 lb-in^2. A curved I-beam, with the properties listed below, will be used to provide the necessary moment of inertia.

Nominal size	Depth of section	Area of section	Flange width	Flange thickness	Web thickness
11 x 4½	11.0 in.	7.21 in.^{2}	4.55 in.	0.40 in.	0.35 in.

Fabrication difficulties still exist with beryllium in standard sections; therefore, the I-beams will be fabricated of titanium. Figure 28 shows a scaled drawing of the shield cross section. Section B-B shows a section through the inner pressure vessel.

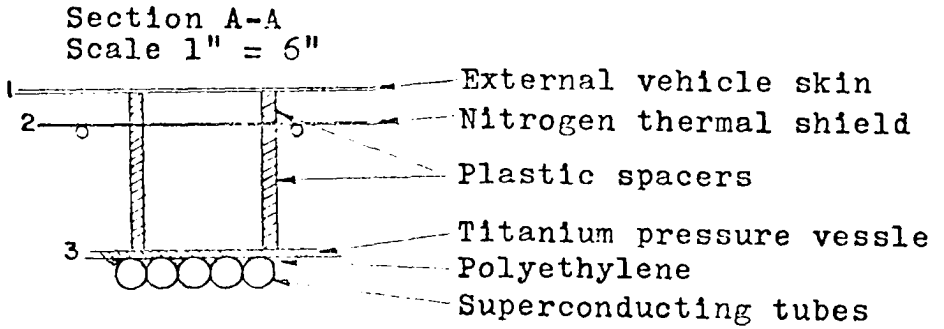

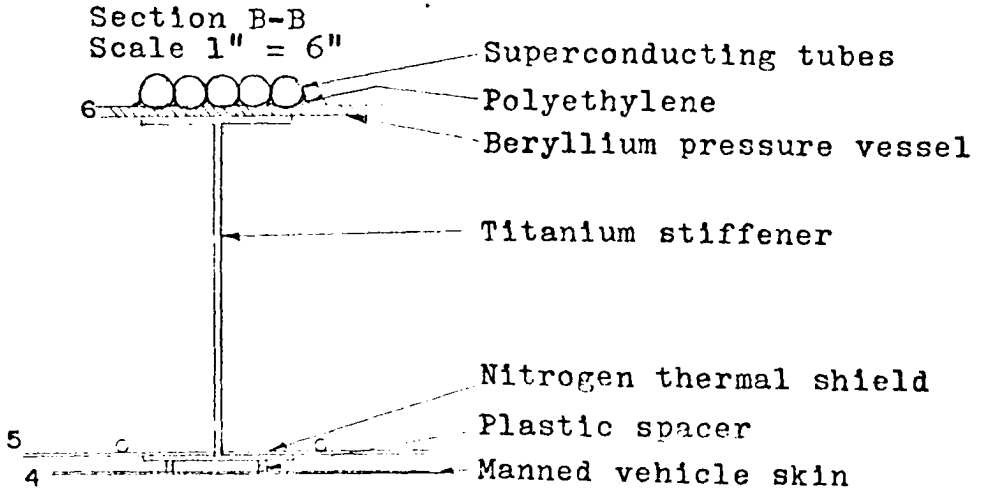

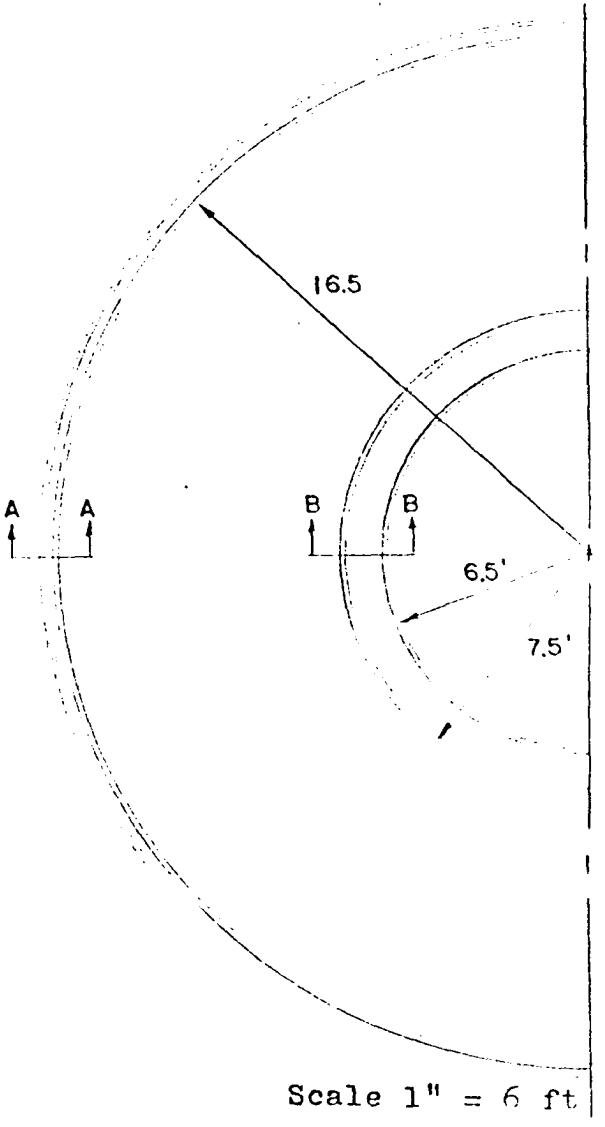

Figure 28. Shield cross-section

Exterior Torus

Section A-A of Figure 28 shows a cross section of the external pressure vessel. After the application of stress, the HI-120 tubes and the titanium skin become a unit, and the tubes can be expected to carry a fraction of the load proportional to the ratio of cross sectional area times allowable stress for HI-120 and titanium. Consider a one inch wide strip of outside wall and tube; the force on this strip is 233,000 lb. The allowable tube stress is 300,000 psi; therefore, the tubes carry 49,500 lb. The allowable stress for titanium is 280,000; therefore the wall must be 0.31 in. thick. Allowable stress is based on yield strength at $4^{\circ}K$ with a margin of safety of approximately ten percent.

Deformations

Consider the diameter (395.38 in.) of the titanium-HI-120 interface. At $-460^{\circ}F$, the inner titanium diameter contracts 0.69 inches. Upon the application of stress, the diameter expands 5.53 inches so that the final diameter is 400.22 in. The initial outside diameter of the HI-120 coil is 393.05 in. At $-460^{\circ}F$, the outer diameter contracts 0.70 inches. Upon the application of stress, the diameter expands 7.87 inches; therefore the tube and wall will act as a unit but will not induce stresses in each other.

There are three interfaces in the inner pressure vessel. During cool down the titanium shrinks more than the beryllium; therefore, a shrink fit is required. However, the difference in diameter at $68^{\circ}F$ is only 0.07 inches for a 180 inch diam-

eter. These diameter differences may be absorbed in construction tolerences; however, the shrink stress is enough to put 6150 psi tension in the beryllium skin and 10,200 psi compression in the titanium flange. The initial inside diameter of the coil is 181.39 inches. At -460°, after contraction, the diameter is 181.07 in., and the beryllium skin and the tubes become a unit. After application of stress there is less than 0.001 in. contraction of the rigid structure.

Consider section A-A of Figure 28. Neither the nitrogen cooled thermal shield nor the external skin will have the flexibility of the tubes or the wall. For these structures the spacers will be designed as spring loaded plastic tubes. Plastic is used for its poor thermal conductivity. The spacers are spring loaded, since the titanium wall and the heat shield will experience a net movement of approximately 2 3/4 inches.

Meteoroid Shielding

The system will be vulnerable to meteoroid penetration. Since meteoroid velocities have not been approached on earth, there are various theories concerning meteoroid penetration. The author had occasion to examine two of these theories in his work at General Electric's Flight Propulsion Laboratory Department (8). The results of the most conservative criteria (Bjork's) and a less conservative criteria (Cornhauser's) is shown in Figure 29. A survival probability of 0.9 is approx-

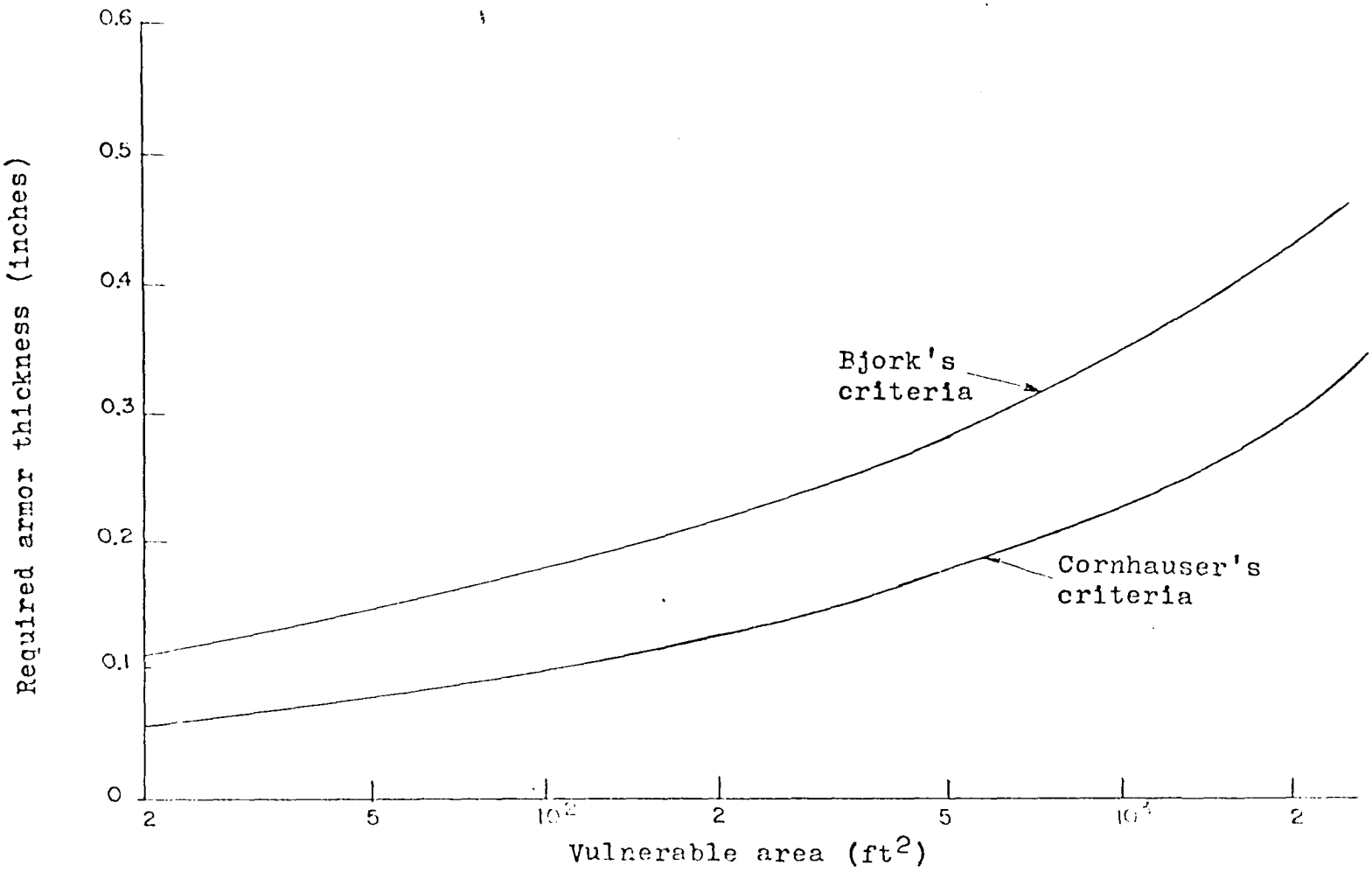

Figure 29. Meteoroid shielding for a one year survival probability of 0.9

imately equal to 0.1 punctures in one year. Since each segment of the shield is self-contained, vulnerable area will be based on a single segment. Only the tubes are vulnerable. The thermal shield is comprised of a system of parallel one quarter inch tubes, 20 feet long, and spaced approximately two feet apart. The tubes are connected by a 0.01 inch 1100F aluminum fin. The vulnerable area is 20 ft^2. The entire surface of the coil is vulnerable, so this amounts to 2100 ft^2. Even using the most conservative criteria, beryllium armor for the thermal shield would weigh only 60 lb. For the main coil, the titanium pressure vessel provides the required armor in Cornhauser's criteria, but falls far short in Bjork's criteria. The effect of the external skin and the thermal shield reduces the required armor thickness by shattering the meteoroids. For this design it has been assumed that the titanium skin aided by the external bumpers will provide the required meteoroid armor. In the event of penetration, repair must be made in space. One object of the tube-coil concept is to facilitate repair in space.

Table 7. Total shield weight

Inside shell		Outside shell	
Beryllium skin	6000 lb	Titanium skin	14400 lb
6 stiffeners	2895	bearing material	624
tubing	2375	tubing	5290
helium	485	helium	1065
bearing material	284	total outside	21379
total inside	12039		
Total weight for each 20 foot section			33,418 lb
Total system weight exclusive of inner and outer thermal shields, meteoritic armor and liquid gas recycle equipment			1,870,000 lb

Launch Stresses

During launch, the system will be subject to accelerations not greater than 7g's. Therefore, to anchor the inner toroid, three titanium cables will connect the titanium skin outside with the titanium stiffener inside. The cables will be spaced 120 degrees apart, and be used on each end of a 20 foot section.

From design studies of the Large Orbital Research Laboratory (41) the manned capsule weight has been estimated at 530,000 lb. If this weight is evenly divided among the 56 shield sections:

Weight of the inside torus	12,039 lb
Weight of manned capsule	9,500
Weight of interior module	21,539 lb.

If the vehicle sustains a maximum of 7g, the load will be 150,500 lb. In the maximum stress situation two cables will carry the load. Thus a titanium cable with a cross section of 0.6 in^2 will be stressed to 125,000 psi and will deform 0.77 in. Allowance for this amount of movement between the two superconducting coils must be made.

CRYOGENIC DESIGN

General Configuration

The cryogenic systems shown in sections A-A and B-B of Figure 28 are analogous to the schematic of a transfer line shown in Figure 30. With high vacuum insulation, the primary mode of heat transfer is radiation. A high vacuum is obtained in space by venting the system to space. The inner line contains the liquid to be transferred. Separated from the liquid line by a high vacuum space is a shield refrigerated by an intermediate temperature liquid. The shielding liquid is insulated from ambient temperature by a high vacuum.

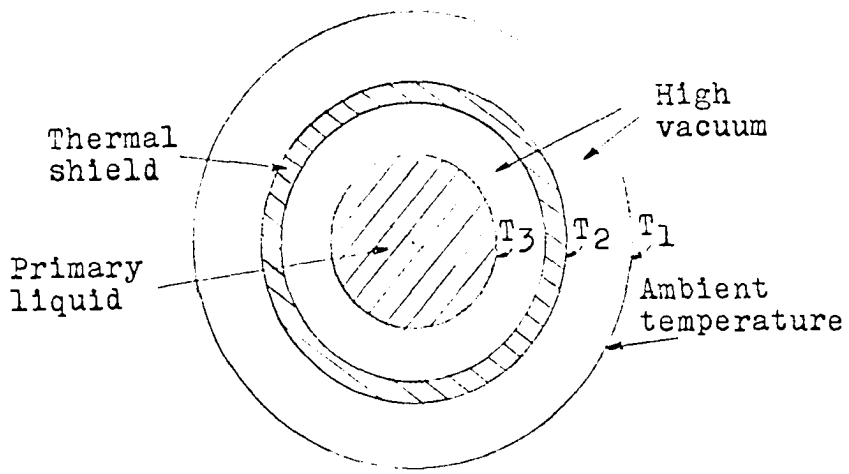

Figure 30. Transfer line schematic

With a thermal shield, the ambient temperature radiation is absorbed by the shielding liquid. Only radiation emitted at the temperature T_2 of the shielding liquid reaches the primary liquid. The thermal shields, shown in Figure 28, are

fin and tube arrangements. All other components are treated like the three concentric pipes shown in the schematic.

The components of both the helium and the nitrogen systems are the same as that shown in Figure 16. The processes which take place in the transfer lines are those shown in Figure 17. It is the purpose of the cryogenic design to: (1) optimize the flow through the helium and nitrogen transfer lines; (2) describe the nitrogen and helium liquefiers; and (3) determine the power used by the refrigeration system.

External Skin Temperatures

The heat balance of a space vehicle is determined by an energy equation accounting for all heat fluxes through the skin of the vehicle and between parts of the vehicle. In the vicinity of the earth, the sources of heat are solar radiation, radiation from the earth's albedo, radiation from other orbiting bodies, and internal heat generation. Figure 31 shows the internal-equilibrium temperatures for a space craft whose interior is insulated from the skin (22). The temperature is plotted versus the ratio of emissivities (ϵ_1/ϵ_2) for various percentages of time in sunlight. All other conditions are for a 300-500 mile orbit. The ratio ϵ_1/ϵ_2 is the ratio of the surface emissivities for solar to infrared radiation. This ratio for Snap 8 is 1.13 (7), and it is assumed that this ratio is possible for this vehicle. A 500-mile equatorial

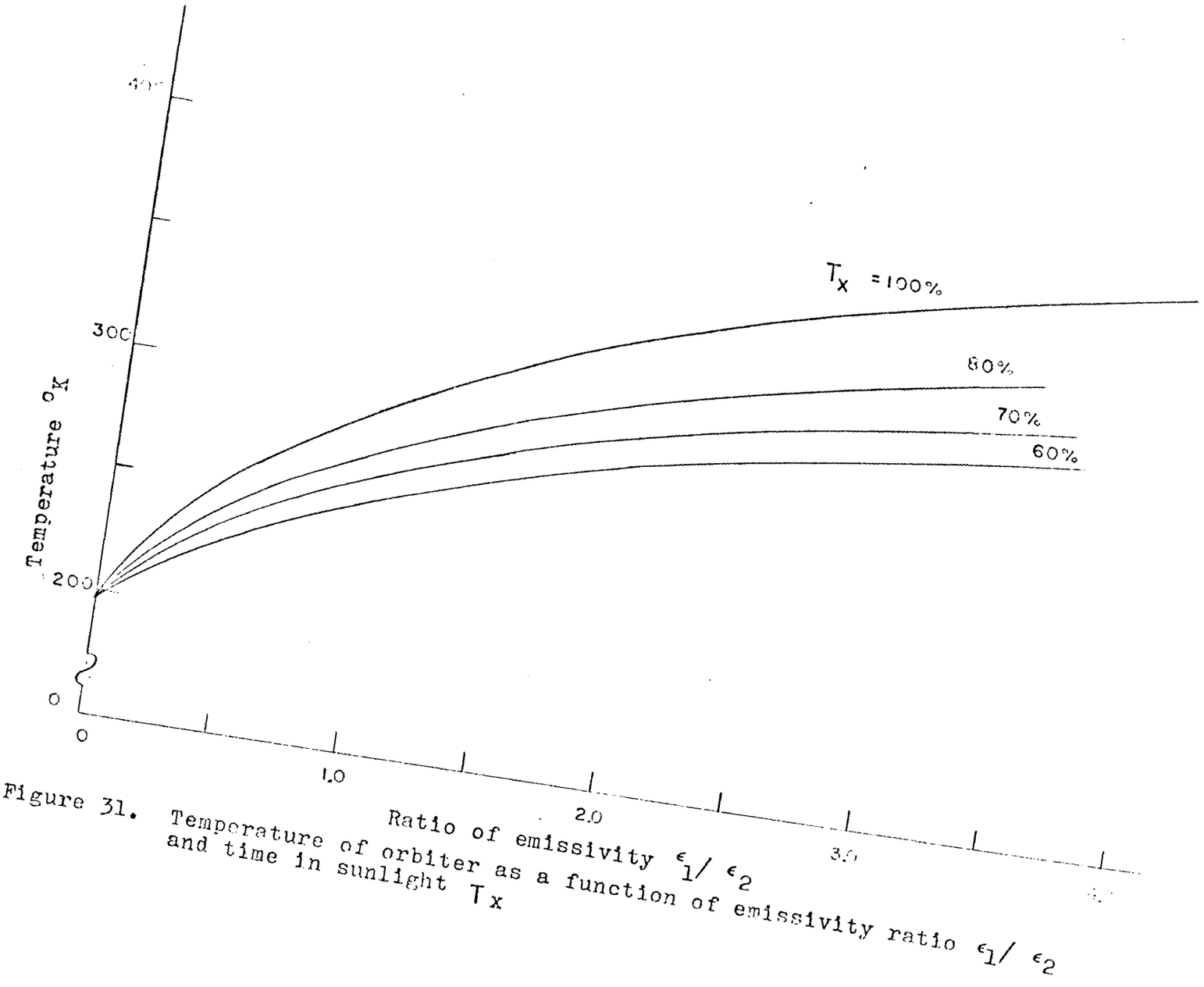

Figure 31. Temperature of orbiter as a function of emissivity ratio ϵ_1/ϵ_2 and time in sunlight T_x

orbit will put a vehicle in sunlight approximately 60 percent of the time, and during startup of the vehicle the equilibrium temperature of the vehicle will be 450°R. For operation away from the earth, the effect of the earth's albedo is much reduced. A conservative estimate of internal temperature at 93 million miles from the sun, will be 540°R. When the vehicle is within the earth's orbit the temperature will be greater; outside of the earth's orbit the temperature will be less. On the manned compartment side of the shield, the temperature will be approximately 540°R.

Net Heat Exchange in the Cryogenic Systems

The rate at which a surface emits radiation is given by the Stefan-Boltzman law:

$$W = \sigma \varepsilon A T^4 \qquad (17)$$

where W is the rate of heat radiation Btu/hr

ε is the total emissivity of the surface

A is the surface area (ft^2)

T is the absolute temperature (degrees Rankine)

and σ is a constant = 0.1714×10^{8} if W, A, and T have the dimensions specified above.

The net exchange of radiant energy between two surfaces is given by the expression,

$$W = \sigma EA(T_2^4 - T_1^4) \qquad (18)$$

where the subscripts 1 and 2 refer to the cold and hot surfaces respectively, and E is a factor involving the emissivities of

the two surfaces. If it is assumed that the toroids are two long coaxial cylinders,

$$E = \frac{\epsilon_1 \epsilon_2}{\epsilon_2 + A_1/A_2(1-\epsilon_2)\epsilon_1} \qquad (19)$$

where the subscript 2 refers to the enclosed surface.

All internal surfaces will be polished. The skin will be assumed to have the same emissivity as titanium $\epsilon_{titanium} = \epsilon_{skin} = 0.04$; $\epsilon_{aluminum} = 0.02$. The radiating surfaces in sections A-A and B-B are numbered so that, $E_{1-2} = E_{2-3} = E_{4-5} = 0.0135$; $E_{5-6} = 0.0123$. Therefore, $(W/A)_{1-2} = (W/A)_{4-5} = 1.98$ Btu/hr-ft^2 falls on each thermal shield. The circumference of shield no. 2 is 103 feet, of shield no. 5 is 47 feet. Tubes carrying liquid nitrogen are spaced 2 feet apart on the circumferences. The tubes are 20 feet long with headers at each end. The headers and connecting pipes will be in a nitrogen temperature area or lower, thus there will be no heat leak and very few other losses in the connections. The tube has a 0.25 in. inside diameter, and is probably armored with approximately 0.1 inch of beryllium or aluminum. The thermal shield is a tube and fin configuration. The fin is 1100F aluminum which is 0.01 inch thick, 1 foot wide, and 20 feet long. A simple heat balance for the fins establishes the temperature

$$T = -\frac{cx^2}{2kt} + \frac{cLx}{kt} + T_o \qquad (20)$$

where c is the heat input by radiation (Btu/hr-ft^2)

k is the thermal conductivity of the fin (Btu/hr-ft ^oF)

t is the fin thickness (ft)

L is the fin width (ft)

x is a distance (ft)

and T is the temperature (^{o}F).

The average thermal shield temperature is 85°K.* Therefore, $(W/A)_{3-2} = 0.0163$ Btu/hr-ft^2 and $(W/A)_{5-6} = 0.0131$ Btu/hr-ft^2.

These inputs were used to establish the pressure and flow required in the helium and nitrogen transfer lines. The heat generated and absorbed in the transfer line is determined by the pressure and flow in the line. The heat absorbed in the line is then transferred to the pump cavity vaporizing part of the fluid in the cavity. The analysis used to determine the amount of liquids vaporized is described in Appendix A.

Nitrogen flow of 0.125 gal/min results in a loss of 0.18 gal/min or 71.1 lb/hour. The operating pressure is 1.4 atmospheres.

Helium flow of 0.5 gal/min results in a loss of 0.088 gal/min or 5.6 lb/hr. The operating pressure is 1.39 atmospheres.

Compensation for these liquid losses requires replacement or storage. The length of operation of a deep space probe precludes storage, therefore a helium and a nitrogen liquefier will be provided for each 20-foot segment.

---

*The investigation of gases that are liquid at cryogenic temperatures has been carried on primarily in the Kelvin scale of temperatures. For temperatures below 100°K, the Kelvin or Centigrade scales will be used; for temperatures above 100°K the Fahrenheit or Rankine scales will be used.

Helium Liquefier

Figure 32 is a schematic diagram of a helium liquefier (39) altered to conform to the shield requirements. Helium is compressed in a four stage compressor with nitrogen intercooling. It exits from heat exchanger 4 at 12 atmospheres and 85°K, and enters the main heat exchanger 5. At 80°K approximately 8 percent of the flow is tapped off and expanded in engine E_1; at 45°K approximately 15 percent of the flow is tapped off and expanded through E_2; at the lower end of the exchanger 52 percent is expanded through E_3 and 25 percent goes through heat exchangers 6 and 7 and through valve B. Each engine expands the high pressure to 1 atmosphere with a corresponding drop in temperature; from E_1, 80°K to 45°K; from E_2, 45°K to 25°K; from E_3, 15°K to 9°K. The expanded helium joins the low pressure stream. Liquid helium forming at valve B drops into the bottom of the Dewar vessel in which the system is encased. Helium then flows to the pump container to maintain the liquid level in the pump container.

In Figure 18, the transfer line from the superconducting coil passes through the helium in the pump container. The fluid in the superconducting line is diverted through a normal connection into a heat exchanger where the heat absorbed during passage through the coil is transferred to the helium in the pump container. The helium in the pump container is vaporized. This vapor plus that accumulating through the valve B will recharge the system. In the helium

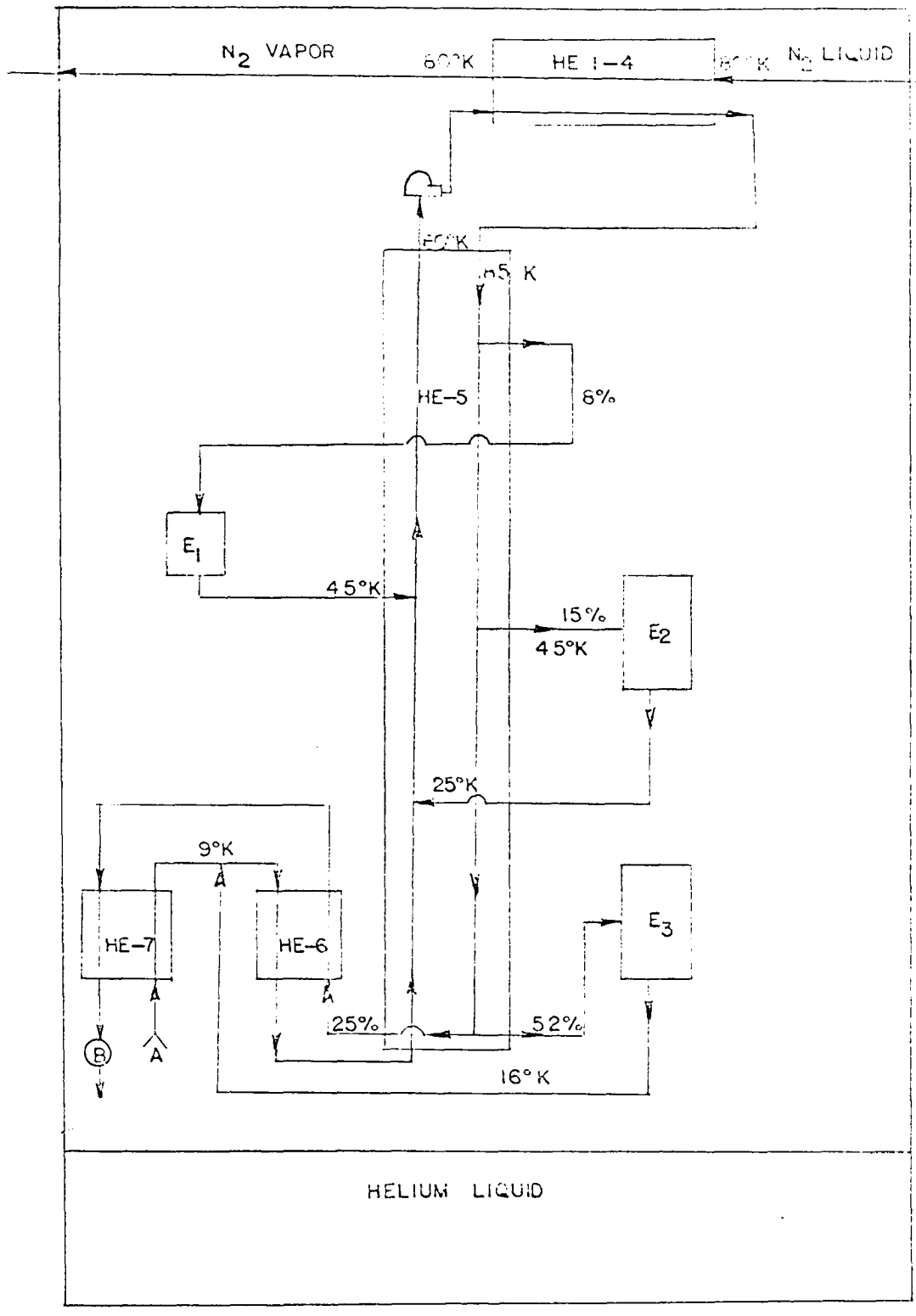

Figure 32. Helium liquefier schematic

liquefier 13.1 percent of the flow is liquefied. Therefore the required flow in the liquefier is:

$$\text{Required flow} = \frac{0.088 \text{ gal/min}}{0.131} = 0.68 \text{ gal/min.}$$

The four stage compressor will be intercooled by the vaporization of nitrogen at 80°K. In each stage the temperature rises from 80° to 100°K and the enthalpy rises 25 cal/gm. The heat of vaporization of nitrogen is 48 cal/gm. Therefore 88.7 lb of nitrogen per hour will be required for the helium liquefier. To this must be added 71.1 lb per hour from the thermal shield. Therefore, 159.8 lb of nitrogen per hour is required from the nitrogen liquefier.

Nitrogen Liquefier

The nitrogen cycle is shown in schematic in Figure 33. This cycle is an altered Keesom cascade (21) composed of four cycles: ammonia, ethylene, methane, and nitrogen. Ammonia is liquefied at 77°F and 10.2 atmospheres, and the liquid is expanded to produce liquid ammonia at -29°F and one atmosphere. Ethylene is liquefied at 19 atmospheres in the liquid ammonia; methane is liquefied at 41 atmospheres in the liquid ethylene; and finally nitrogen is liquefied at 18.6 atmospheres in liquid methane. The results of the analysis of the nitrogen cascade are also shown in Figure 33.

In a three-stage compressor, 2.06 lb of nitrogen vapor is compressed at 18.6 atmospheres; intercooling is provided by passing nitrogen at 4.3 atmospheres back through the liquid

Figure 33. Nitrogen cascade liquefier

	Weight	No	Pressure atmos	Temp	Quality	Enthalpy Btu/lb
NH_3	0.233 lb	A	10.2	77	---	128
		B	1.0	-29	0.197	128
		C	1.0	-29	1.000	602
		D	1.0	62	---	649
C_2H_4	0.66 lb	E	19.0	77	---	270
		F	19.0	25	---	250
		G	19.0	-24	0.000	84
		H	1.0	-155	0.595	84
		I	1.0	-155	1.000	208
		J	1.0	62	---	286
CH_4	0.586	K	41	77	---	392
	0.894	L	41	77	---	392
	0.586	M	41	-58	---	304
	0.894	N	41	-122	0.00	166
	1.48	O	41	-122	0.00	166
		P	1.0	-258	0.679	166
		Q	1.0	-258	1.000	235
		R	1.0	-210	---	263
		S	1.0	62	---	400
N_2	2.08	T	18.6	-208	---	109.2
		U	18.6	-253	---	90.0
		V	18.6	-253	0.00	38.6
		W	1.0	-321	0.455	38.6
	1.00	X	1.0	-321	0.000	0
	2.08	Y	1.0	-321	1.000	84.5

note: only phase change takes place in the external skin circuit

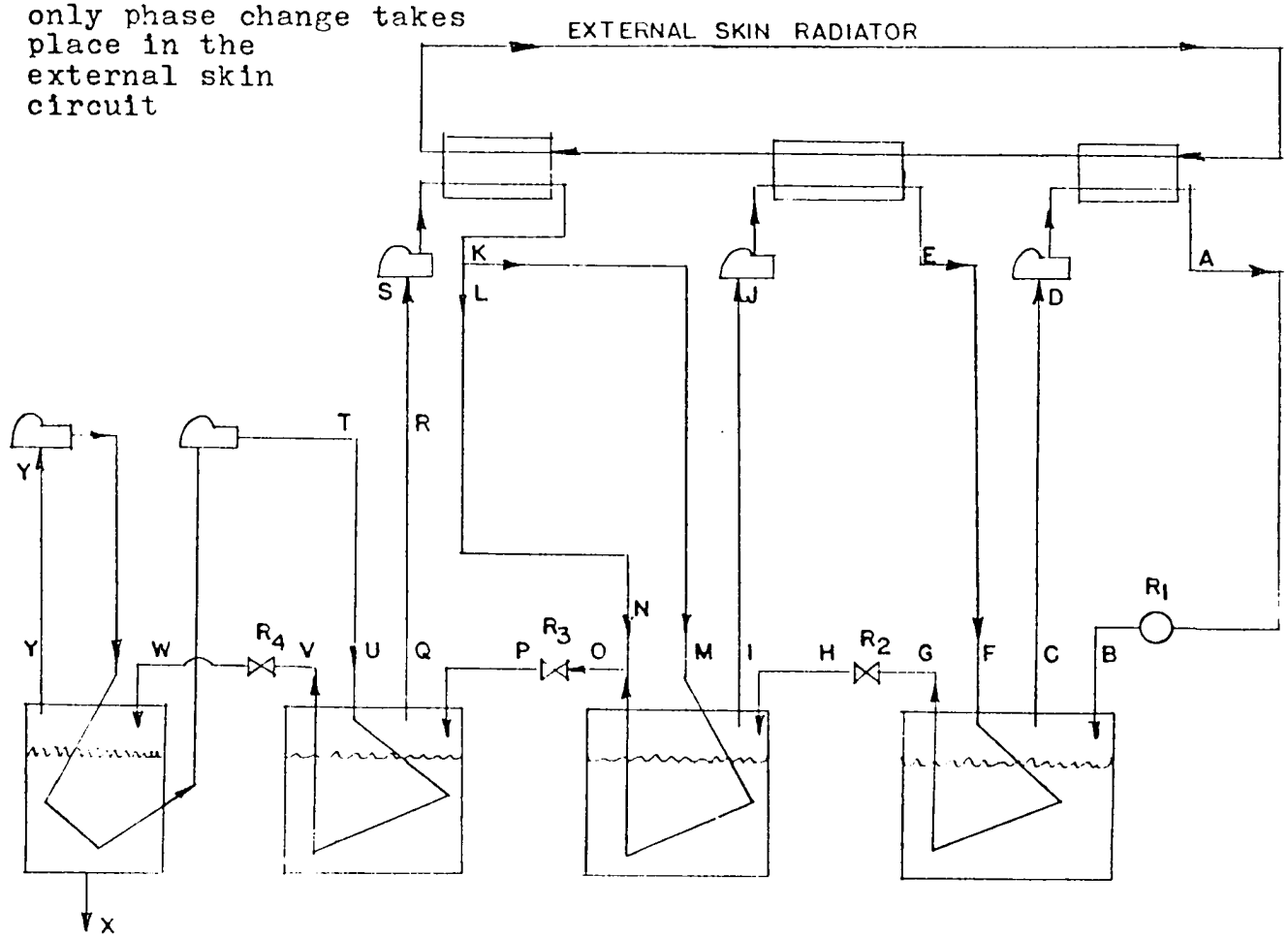

nitrogen. In this pass 0.31 lb of nitrogen is vaporized. Expansion through R_4 provides 1.31 lb of liquid nitrogen. Therefore 1 lb of usable nitrogen at 77°K and one atmosphere is provided.

Refrigerator Power Requirement

In the analysis of a Keesom cascade, it has been shown that, within the limits of calculation, the work needed to operate the system is equal to the work of the compressors in the system (21).

Table 8. Work required per pound of nitrogen

Compressor	Hp-hr
N_2	0.102
CH_4	0.148
C_2H_4	0.032
NH_3	0.015
	0.297

If a compressor efficiency of 75 percent is assumed, the work required to liquefy 160 lb/hr (of nitrogen) is 47.5 kw/section.

The four stage compressor in the liquid-helium cycle will use 0.31 hp-hr per lb of helium. If this is considered as the principle area in which work is done, the power requirement is 13.1 kw/section.

For the entire shield the total power consumption is 3.4 electrical megawatts. If a SNAP-50 is used for the mission power source, and it is 16 percent efficient, more than 4 electrical megawatts will be available for the operation of the mission. (SNAP-50 generates 50 thermal megawatts).

Surface Radiator Capability and Requirement

At 540°R, the surface of the vehicle can radiate 3.6 x 10^6 Btu/hr. However, only half of this area can radiate to the space sink at one time. The skin must radiate most of the heat generated in the manned compartment and all of the heat involved in the cryogenic system.

The heat generated in the compression of CH_4, C_2H_4, and NH_3 will be transferred to the surface radiator. Heat generated in a Keesom cascade is shown in Table 9.

Table 9. Heat generated in compression of Keesom cascade gases

Gas	Enthalpy (Btu/lb)	Weight (lb)	Heat (Btu)
CH_4	280	1.48	415
C_2H_4	130	0.66	85.6
NH_3	612	0.233	142.5
			643.1 Btu/lb of N_2

In one 20-foot section 1.03 x 10^5 Btu/hr will be dumped into the surface radiator. This is less than four percent of the capacity of the radiator.

Electrical Startup Circuit (23)

The startup circuit is featured by a switching element which permits operation of the coil either from an external source or on the permanent current basis. This switch element is kept at liquid helium temperature since it must be either resistive or superconducting. The normal to superconducting transition is affected by changing temperature; that is by heating the gate wire electrically.

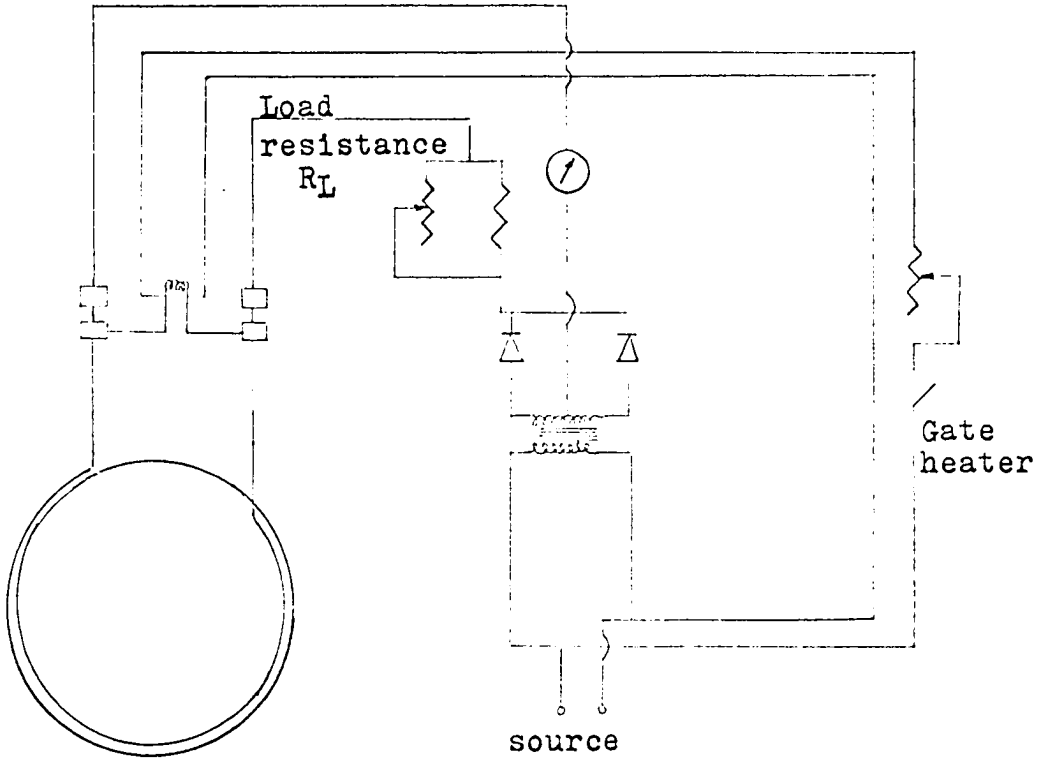

Figure 34. Superconducting startup circuit

At startup the high current in the gate switch circuit keeps the switch normal with resistance R_S. By varying the load resistance, R_L, the current in the circuit is set at the operating current. Then the gate heater current is reduced so the switch becomes superconducting and the current is restrained to the superconducting circuit.

APPLICATION

Direct Dose from a Solar Flare

The class-4 solar flare is the principal hazard of space missions longer than three months. The integral proton spectrum at the peak intensity of the class-4 solar flare of 23 February 1956 is shown in Figure 2. The shield has been designed to reduce the dose incurred from this flare to 40 rem.

All charged particles of energy less than one Bev are excluded from the shielded area (see Appendix B). Higher energy particles are excluded if their path through the magnetic field misses the manned compartment. The threshold energy varies for different angles of incidence to the surface of the vehicle. The paths of the threshold energy particles in a plane perpendicular to the magnetic field are shown in Figure 35. The threshold energies are indicated on their respective paths. From this figure, it can be seen that all particles of energies less than 10 Bev impinging on the vehicle from the second quadrant are excluded.

On planes inclined to the plane of Figure 35, a particle can enter the shielded region if it has a component of velocity $v_\perp$ perpendicular to the magnetic field of such magnitude so that $\frac{1}{2}mv_\perp^2$ for the proton is greater than the threshold energies shown on the particle paths. The threshold energies at various angular orientations are given in Table 10. The angle θ designates an angle in the plane of Figure 35; the

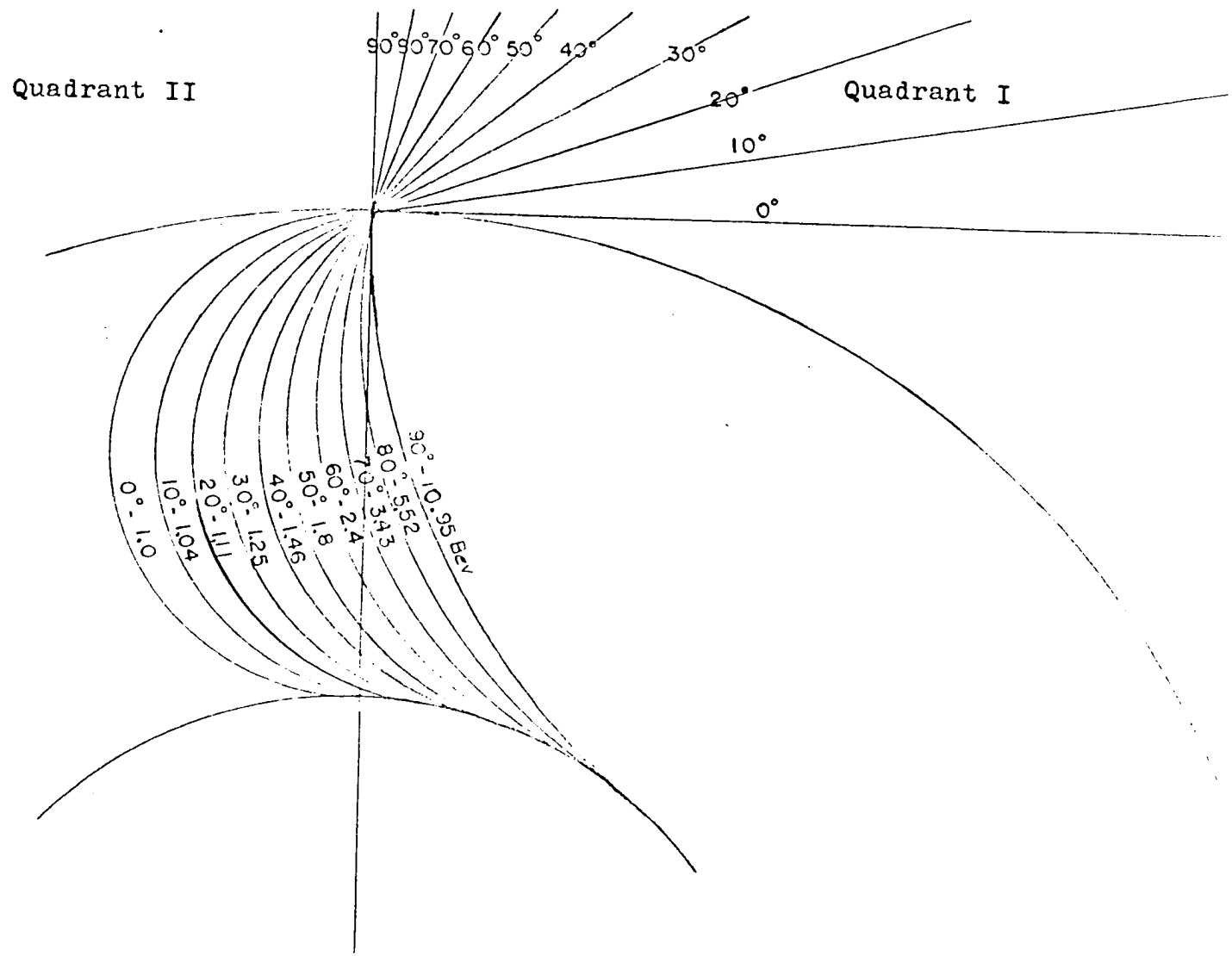

Figure 35. Paths of threshold energy particles

Table 10. Threshold energies at several angular orientations

θ =		0°	10°	20°	30°	40°	50°	60°	70°	80°	90°
Θ =	0°	E=1.0Bev	1.04	1.11	1.25	1.46	1.8	2.4	3.43	5.52	10.95
	10°	1.018	1.06	1.13	1.27	1.49	1.83	2.44	3.49	5.61	11.14
	20°	1.07	1.11	1.19	1.34	1.56	1.92	2.56	3.66	5.9	11.7
	30°	1.155	1.20	1.28	1.44	1.69	2.08	2.78	3.96	6.35	12.6
	40°	1.305	1.35	1.45	1.63	1.90	2.35	3.12	4.45	7.2	14.3
	50°	1.555	1.61	1.72	1.94	2.27	2.8	3.72	5.3	8.6	17.0
	60°	2.0	2.08	2.22	2.50	2.92	3.6	4.8	6.86	11.4	21.9
	70°	2.91	3.02	3.22	3.64	4.25	5.25	6.98	10.0	16.0	31.8
	80°	5.75	5.96	6.4	7.2	8.4	10.4	13.8	19.7	31.8	63
	85°	11.48	11.9	12.7	14.3	16.7	20.6	27.4	39.2	61.1	125
	90°										

the angle ϕ indicates the angle made by the inclined planes.

The energy transfer rate by absorption for protons given in Table 4 was plotted on Figure 36. The RBE for these high energy protons was assumed to be equal to one (40).

The technique for determining the direct dose is straightforward. Select the angle ϕ. For each value of θ there is a threshold energy and an angular proton flux impinging on the shield at an angle θ. Since the energy transfer rate varies with energy, a stepwise integration process was carried out to determine the total energy absorbed in the shielded vehicle by particles entering within the ten degree increments in Table 10. These values were plotted vs. θ from 0 to 2π, and an integrated absorbed energy for each ϕ-plane was determined. These integrated energies were plotted vs. sin ϕ, and again integrated to determine the absorbed dose for an octant. Only the two octants associated with quadrant I of Figure 35 contribute a measurable dose to the manned compartment. It has been estimated that the dose accumulated during the onset and decay of the flare is 1.7 times the dose accumulated during a one hour exposure to the peak activity (9). The total dose for the direct proton component is 24.2 rads. A sample calculation is included in Appendix B.

Secondary Particle Generation

In addition to the direct proton dose, there is also a secondary dose due to the cascade and evaporation neutrons.

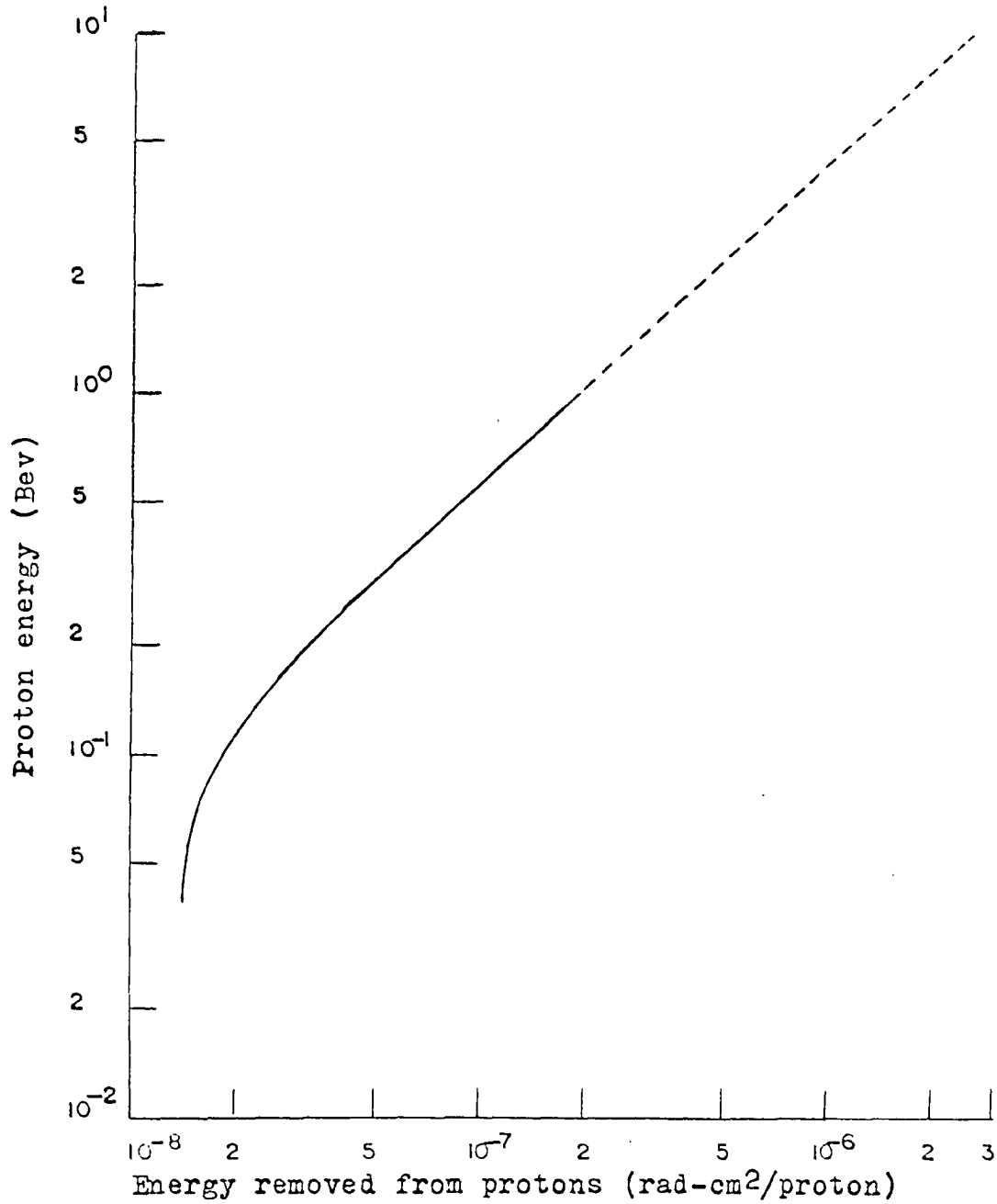

Figure 36. Energy absorbed from protons by tissue by absorption

The cross section for the proton reaction which initiates the cascade is given by Equation 5. The following assumptions apply to the secondary dose.

1. Since the proton flux penetrating the manned compartment is low, only cascade and evaporation neutrons originating in the external structure will contribute to the secondary dose.

2. Titanium (atomic weight, 47.9) makes up 80 percent of the structure and will be considered to be the principal source of secondaries.

3. Half of the angular proton flux is directed away from the vehicle and has no reaction in the vehicle.

4. Charged secondary particles will not contribute to the total dose.

5. Approximately sixty percent of the neutrons will be directed into the manned compartment (3).

6. The energy of the secondary neutrons will be estimated from Figure 37 (3).

7. The number of secondary neutrons per reaction will be estimated from Figure 38 (3).

8. The titanium cross section is 3.7×10^{-2} barns and remains constant for all energies greater than 25 Mev.

9. The neutron and proton cross sections for complex nuclei are approximately equal at energies where the coulomb barrier does not influence the cross section. Therefore, the value of the energy lost by protons by absorption can be used

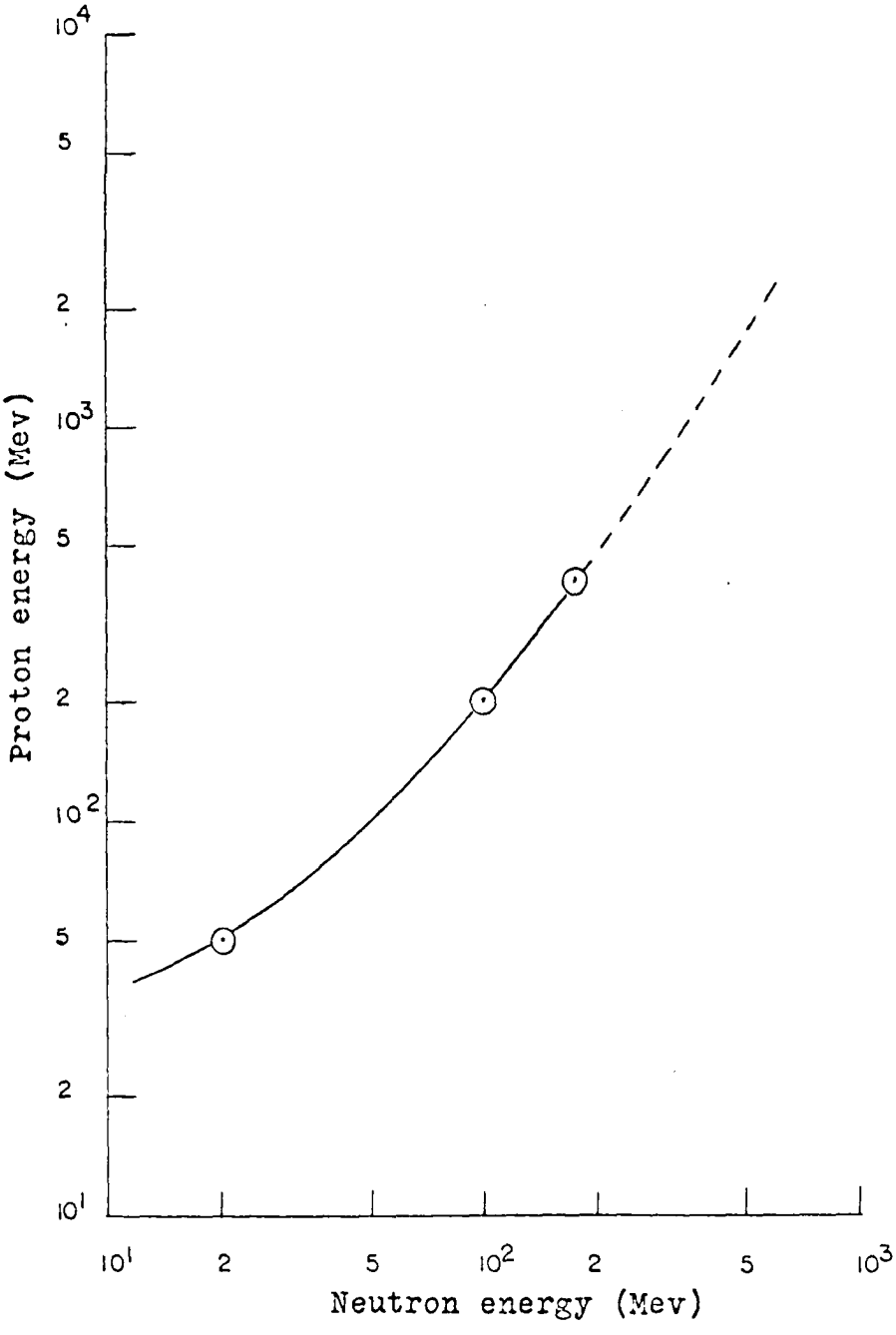

Figure 37. Average energy of secondary neutrons emitted in the foreward direction in the 0^{o} to 30^{o} cone

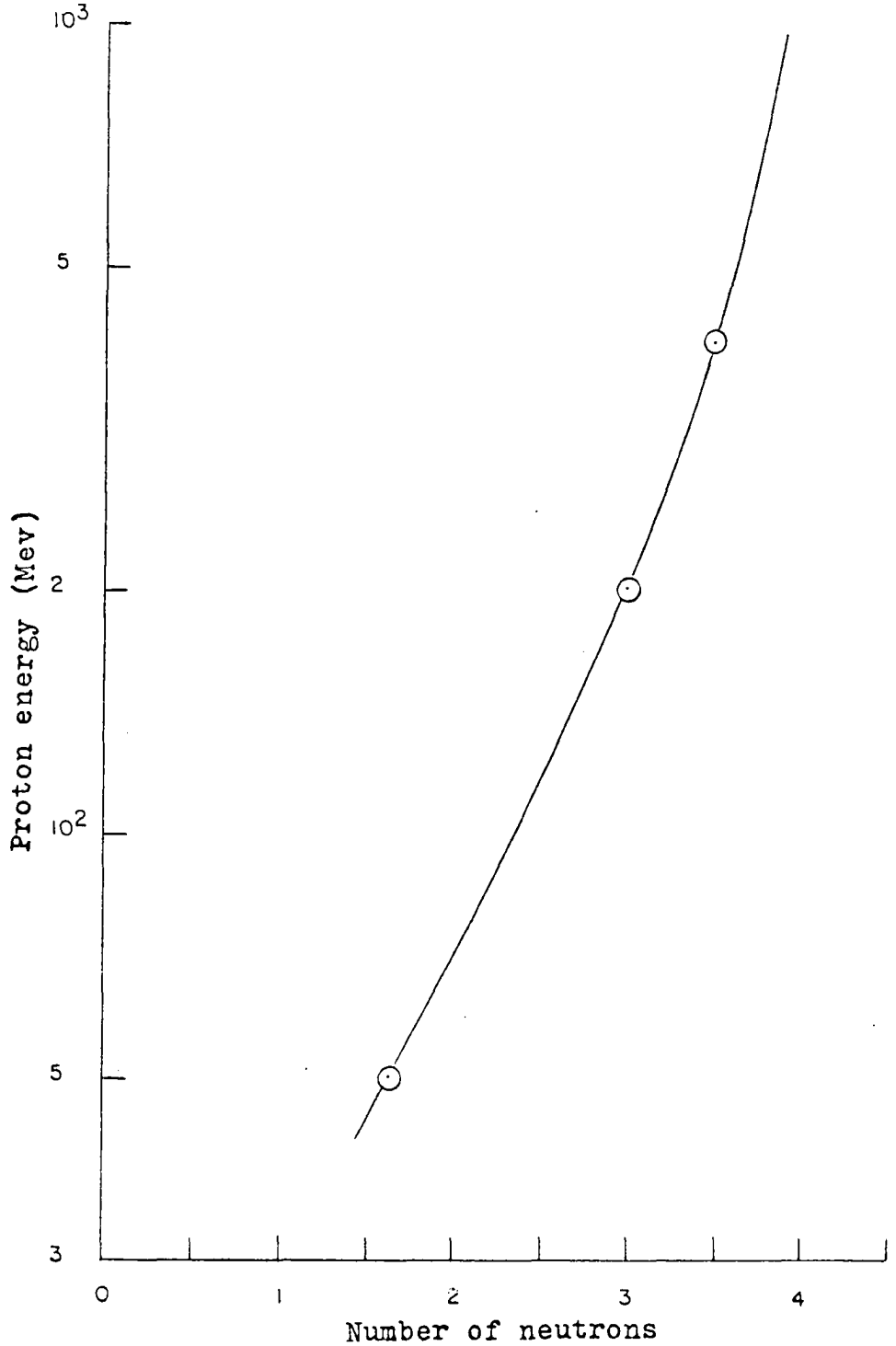

Figure 38. Average number of neutrons per reaction

as the energy lost by a neutron of equal incident energy by absorption. These values are shown in Figure 36.

10. The RBE for high energy neutrons is equal to one (40).

The secondary neutron dose is 13.5 rads. A sample calculation is included in Appendix B.

The total dose accumulated during the most energetic solar flare on record is approximately 38 rad. This dose is within the design requirements; that is, any single event dose shall not exceed 40 rad.

CONCLUSION

Magnetic radiation-shielding appears to be feasible. The engineering problems related to the design construction and operation of a magnetic radiation-shield in space are amenable to solution. The principal difficulties envisioned will be (1) procuring a sufficient amount of superconducting material to construct the coils, and (2) launching and assembling this massive system in space. In the launch configuration, the manned vehicle and shield will weigh approximately 2.5×10^6 pounds.

The walls of a passive-graphite shield must be 8.5 feet thick, if the dose accrued behind it is to be kept comparable to that accumulated within the magnetic shield (37)*. A graphite shield used to protect a volume large enough for forty men to wait out a solar storm (1200 cubic feet) would weigh 2.75×10^6 pounds. The magnetic shield which protects the entire manned vehicle (140,000 cubic feet) would weigh 1.9×10^6 pounds.

The magnetic shield will provide continuous protection for the man in space from solar flares and from the lower energy components of the cosmic rays. The crew will not be forced to abandon experiments and vehicle operation during the flares. The principal disadvantages of the active shield are (1) the substantial power used to maintain the cryogenic temperatures, and (2) the probability of mechanical failure.

*Secondary particle generation was not considered in this calculation.

For both systems, the shielding weights are high. However, in the absence of an entirely new scheme of radiation shielding, shield weights of this magnitude will have to be considered in any long term exploration-colonization mission to the planets.

BIBLIOGRAPHY

1. American Society of Refrigerating Engineers. Air conditioning refrigerating data book. Tenth edition. Design volume. Menasha, Wisconsin, Author. 1957.

2. Bean, C. P. and Schmitt, R. W. The physics of high field superconductors. Science 140: 26-35. 5 April 1963.

3. Bertini, H. W. Monte Carlo calculations for intranuclear cascades. Symposium on protection against radiation hazards in space, Gatlinburg, Tenn., November 1962. Proceedings of the symposium, Book 2: 794-807. 1963.

4. Block, F. and Rorschack, H. E. Energetic stability of persistent currents in a long hollow cylinder. Phys. Rev. 128: 1697-1714. 15 November 1962.

5. Darwin, G. E. and Buddery, J. H. Beryllium. New York, N. Y., Academic Press Inc. 1960.

6. Douglas, D., Jr. and Schmitt, R. W., editors. International conference on the science of superconductivity. Rev. Mod. Phys. 36: 1-331. January 1964.

7. Elliot, R. D. and Baugn, J. W. SNAP 2/10A reactor temperatures during the orbital decay period. Unpublished paper distributed as an internal document. Ozalid. Los Angeles, California, Atomics International, Dept. 727, Group no. 070. 1962.

8. Englesson, G. A. Meteoroid shielding. Unpublished paper distributed as an internal document. (Multilithed.) Cincinnati, Ohio, General Electric Company, Flight Propulsion Laboratory Department, Space Power Operation. 1962.

9. Englesson, G. A. Radiation scattering in space vehicles. Unpublished paper distributed as an internal document. (Multilithed.) Cincinnati, Ohio, General Electric Company, Flight Propulsion Laboratory Department, Space Power Operation. 1962.

10. Etherington, H. Nuclear Engineering Handbook. First edition. New York, N. Y., McGraw-Hill Book Company, Inc. 1958.

11. Evans, R. D. The Atomic Nucleus. New York, N. Y., McGraw-Hill Book Company, Inc. 1955.

12. Fox, D. K. and Reichenecker, W. J. New data on superconducting alloys. Materials in Design Engineering 57: 92-3. April 1963.

13. Glasstone, S. Principles of nuclear reactor engineering. First edition. Princeton, N. J., D. Van Nostrand Company, Inc. 1955.

14. Hallen, E. Electromagnetic theory. New York, N. Y., John Wiley and Sons Inc. 1962.

15. Hulm, J. K., Chandrasekhar, B. S. and Riemersma, H. High field superconducting magnets. Advanced Cryogenic Engineering 8: 17-29. 1963.

16. Hulm, J. K., Chandrasekhar, B. S. and Riemersma, H. Superconducting magnets. Technical information reprint 6169. Pittsburgh, Pennsylvania, Westinghouse Electric Corporation. 1963.

17. Jacobs, R. B. Single-phase transfer of liquified gases. National Bureau of Standards circular 596. Washington, D. C., U. S. Government Printing Office. 1958.

18. Jones, W. H., Milford, F. J., and Fawcett, S. I. Status of superconductivity. Battelle Technical Review 11: No. 9, 2-11. September 1962.

19. Kash, S. W. and Trooper, R. F. Active shielding for manned spacecraft. Astronautics 7: 68-75. September 1962.

20. Kelly, R. N. Beryllium structures. Space/Aeronautics 42, No. 1: 64-73. July 1964.

21. Keesom, W. H. Sur l'economie du procede a cascade pour la liquefaction des gaz. Leiden Communications, Supplement No. 76a. 1933.

22. Koelle, H. H., editor. Handbook of astronautical engineering. First edition. New York, N. Y., McGraw-Hill Book Company. 1961.

23. Kolm, H., Lax, B., Bitter, F., and Mills, R., editors. High magnetic fields. Proceedings of the international conference on high magnetic fields. Cambridge, Massachusetts, The Massachusetts Institute of Technology Press. 1962.

24. Kovit, B. Manned Mars missions. Space/Aeronautics 40, No. 6: 65-71. November 1963.

25. Kovit, B. The Saturns. Space/Aeronautics 42, No. 2: 40-52. August 1964.

26. Landau, L. C. and Lifshitz, E. M. Electrodynamics of continuous media. Reading, Massachusetts, Addison-Wesley Publishing Company, Inc. 1960.

27. LeGalley, D. P. and Rosen, A., editors. Space Physics. New York, N. Y., John Wiley and Sons, Inc. 1964.

28. Levy, R. H. The prospects for active shielding. Symposium on protection against radiation hazards in space, Gattlinburg, Tenn., November 1962. Proceedings of the symposium, Book 2: 794-807. 1963.

29. Levy, R. H. Radiation shielding of space vehicles by means of superconducting coils. Research report 106. Everett, Massachusetts, Avco Everett Research Laboratory. 1961.

30. Levy, R. H. and Stekly, Z. J. J. Superconducting coils. Astronaut. Aeronaut 2, No. 2: 30-38. February 1964.

31. Martin Company. Cryogenic materials data handbook, Eighth quarterly report. Washington, D. C., Office of Technical Services, U. S. Department of Commerce. 1963.

32. Mendelssohn, K. Cryophysics. New York, N. Y., Interscience Publishers, Inc. 1960.

33. Murphy, G. Advanced Mechanics of Materials. New York, N. Y., McGraw-Hill Book Company, Inc. 1946.

34. Redmond, R. F. Space radiation and its effect on materials. REIC memorandum 21. Columbus, Ohio, Radiation Effects Information Center. 1961.

35. Riemersma, H. Calculation of the current and field distribution and the magnetization curves for high-field superconducting materials in the form of sheet. Journal of Applied Physics 35, No. 6: 1802-1806. June 1964.

36. Riemersma, H., Hulm, J. K., Venturino, A. J. and Chandrasekhar, B. S. A variable composition, high field superconducting solenoid. Journal of Applied Physics 33, No. 12: 3499-3504. December 1962.

37. Robey, D. H. Radiation shield requirements for two large solar flares. Astronautica Acta VI, Fac. 4: 206-224. 1960.

38. Ruhemann, M. The separation of gases. Second edition. London, Oxford University Press. 1949.

39. Scott, R. B. Cryogenic Engineering. Princeton, New Jersey, D. Van Nostrand Company, Inc. 1959.

40. Shaefer, H. J. LET spectrum and RBE of high energy protons. Symposium on protection against radiation hazards in space, Gatlinburg, Tenn., November 1962. Proceedings of the symposium, Book 1: 393-401. 1963.

41. Space/Aeronautics staff report. MOL and beyond. Space/Aeronautics 41, No. 6: 52-75. June 1964.

42. Stekly, Z. J. J. The feasibility of large superconducting coils. Research report 160. Everett, Massachusetts, Avco Everett Research Laboratory. 1963.

43. Stekly, Z. J. J. Magnetic energy storage using superconducting coils. Washington, D. C., Institute for defense analysis report No. 1412, Vol. 1: 53-75. 1963.

44. Sturm, R. G. A study of the collapsing pressure of thin walled cylinders. University of Illinois Engr. Expt. Sta. Bul. 329. November 1961.

45. Vance, R. W., editor. Cryogenic technology. New York, N. Y., John Wiley and Sons, Inc. 1963.

46. Vance, R. W. and Duke, W. M., editors. Applied cryogenic engineering. New York, N. Y., John Wiley and Sons, Inc. 1962.

47. Walsh, J. B. Electromagnetic theory and engineering applications. New York, N. Y., The Ronald Press Company. 1960.

48. Westinghouse Electric Corporation. Product specification brochure B-8964. Pittsburgh, Pa. Westinghouse Electric Corporation, Superconducting Materials Department. ca. 1964.

49. Westinghouse Electric Corporation. Product specification brochure 53-161. Pittsburgh, Pa. Westinghouse Electric Corporation, Superconducting Materials Department. May 1963.

50. Wilson, R. The nucleon-nucleon interaction. New York, N. Y., Interscience Publishers. 1963.

ACKNOWLEDGEMENTS

The author would like to acknowledge the direction and the gentle, though sometimes not too gentle, prods of his Major Professor, Dr. Glenn Murphy. Discussions with Dr. A. Rana and with Michael A. McCoy were extremely helpful. Excellent proofreading by Robert Carr added some measure of polish to the dissertation.

The research was supported by the Atomic Energy Commission through its Special Fellowship Program in Nuclear Science and Engineering, which is administered by the Oak Ridge Institute of Nuclear Studies. The research was directed by a committee appointed by Dean J. B. Page of the Iowa State University Graduate School which was composed of Dr. Glenn Murphy, Dr. Abdul Rana, Dr. Adolf F. Voigt, Dr. Donald F Young, and Dr. Agust Valfells.

APPENDIX A

In the analysis of Single-Phase Transfer of Liquefied Gases (17), R. B. Jacobs derives the flow equation for the transfer system shown in Figure 16 involving the processes in Figure 17. The flow equation is written in the dimensionless form

$$\pi = \pi_f + \pi_t \tag{21}$$

where $$\pi = P_i/P_r \tag{22}$$

$$\pi_f = 4\frac{\tau}{P_r}\frac{L}{D} \tag{23}$$

$$\pi_t = \exp\left(\frac{\lambda}{RT_r}\left[1 - \frac{1}{\frac{T_i}{T_r} + \frac{qL}{WC_pT_r}}\right]\right) \tag{24}$$

and P_i = pressure of fluid state at the entrance to the transfer line

P_r = pressure at reference state (usually 1 atmosphere)

τ = shearing stress exerted by the pipe wall on the liquid

L = length of the transfer line

D = inside diameter of pipe

λ = latent heat of vaporization

R = gas constant

T_r = temperature at reference state (saturated liquid at one atmosphere)

T_i = temperature at entrance to the transfer line

q = heat leak per unit time per unit length

W = mass rate of flow

C_p = isobaric specific heat

$T_i = T_r$

The dimensionless frictional parameter, π_f, can be written

$$\pi_f = 3.266\ (L/D^3)\ D^2 \tag{25}$$

where L is in feet, D is in inches and $D^2\tau$ is in pounds. An expression for the drag force $D^2\tau$ is given as

$$D^2\tau = C_1(Q/D)^2 + C_2(Q/D)^{1.68} \tag{26}$$

where C_1 and C_2 are functions of the fluid properties and Q is the flow rate in gallons per minute. This expression as a function of Q/D is plotted in Figure 39 for helium and for nitrogen. Once $D^2\tau$ has been determined, π_f can be found from Figure 40 a graph of $D^2\tau$ vs. π_f.

The dimensionless thermal parameter is written:

$$\pi_t = \exp \frac{C_3}{1 + C_4 \frac{Q}{qL}} \tag{27}$$

C_3 and C_4 are properties of the fluid only, and π_t is a function of the heat leak parameter Q/qL only. For helium, C_3 = 2.32 and C_4 = 575; for nitrogen C_3 = 7.65 and $C_4 = 2.33 \times 10^4$.

Once the pressure ratio, π, has been determined, the loss at the pump can be found using Figure 41, a graph of the loss at the pump for nitrogen and helium versus pressure in atmospheres for various pump efficiencies. The pressure ratio is also used to determine the loss by vaporization due to the pressure in the liquid line from Figure 42. The loss by

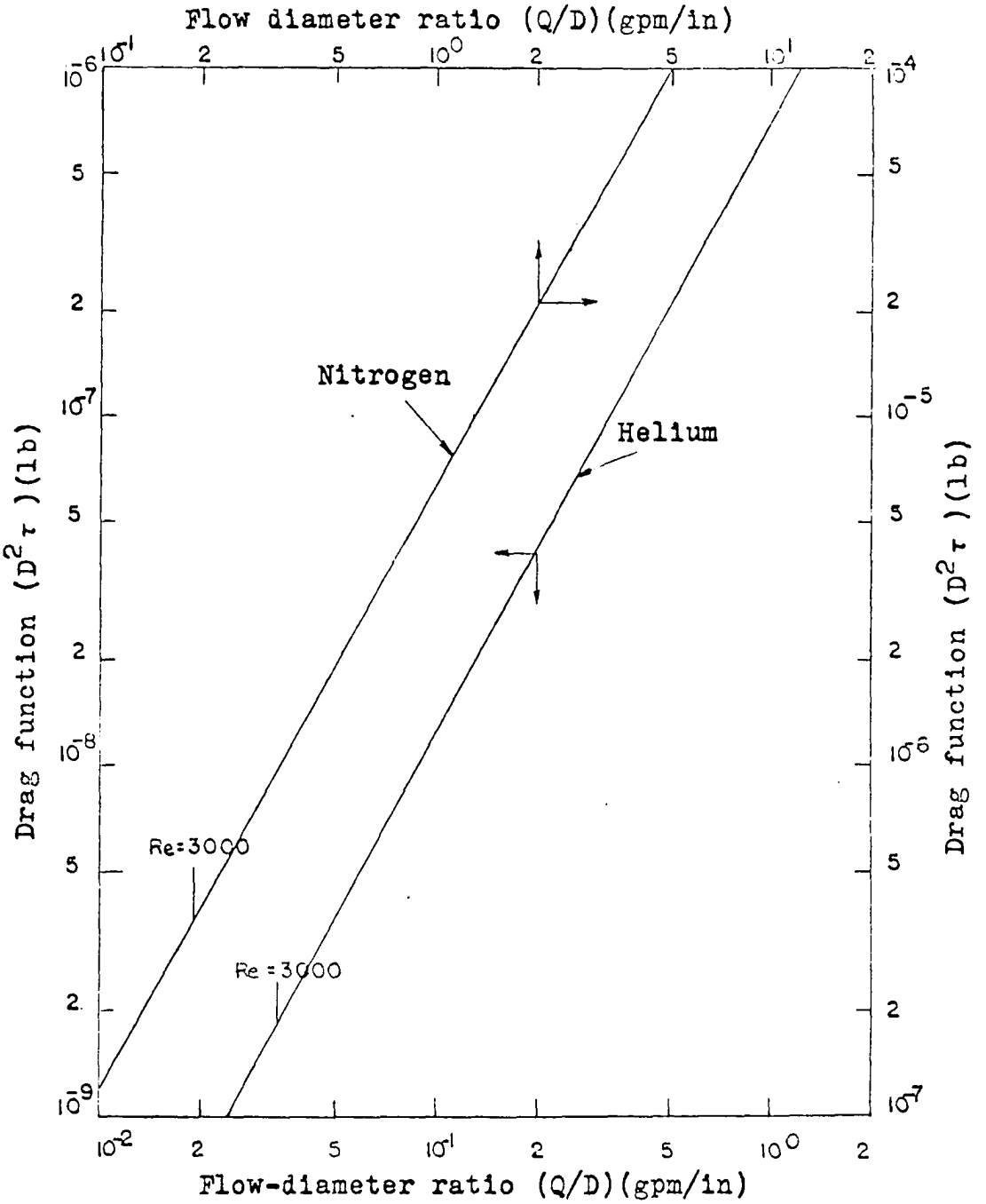

Figure 39. Drag function

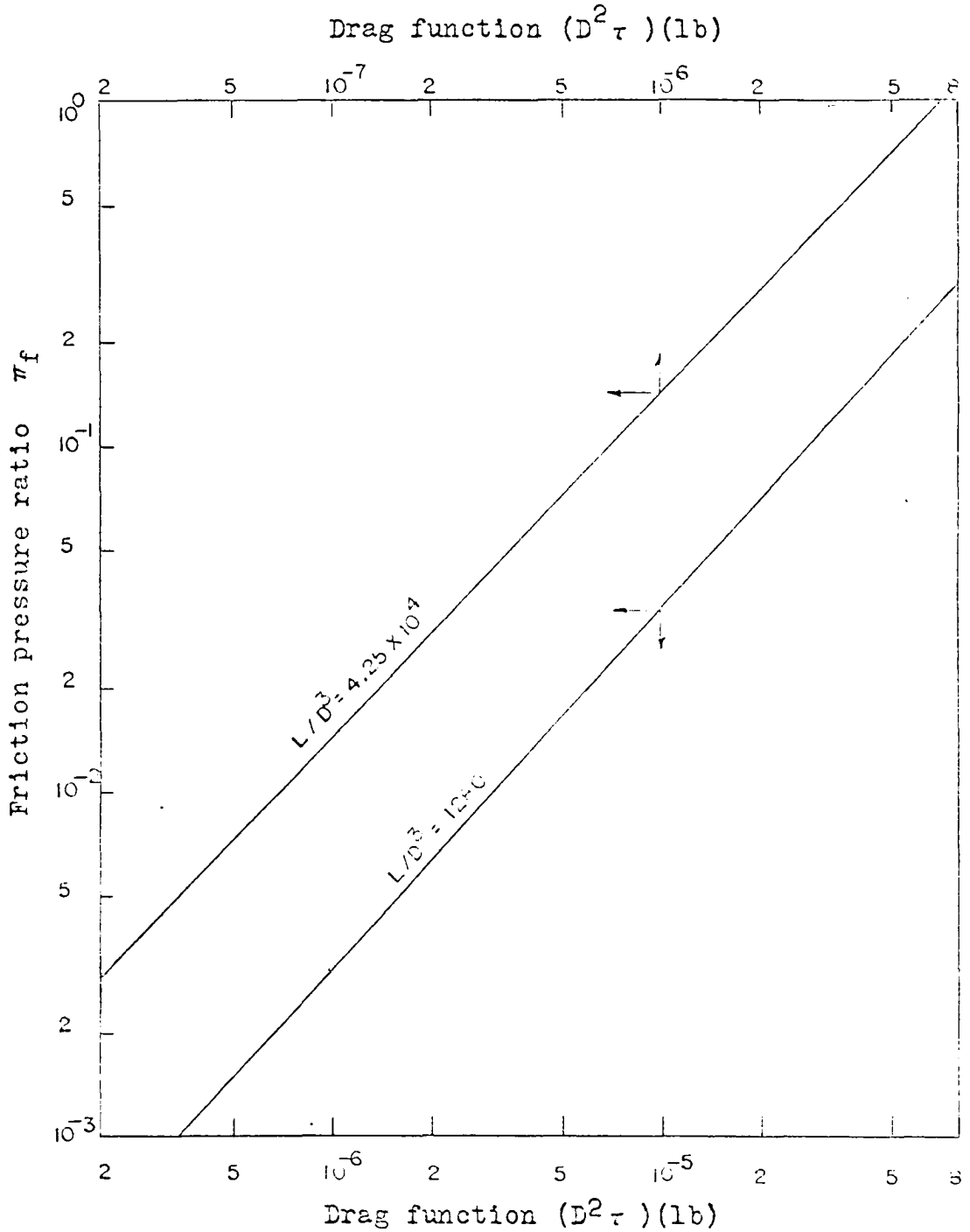

Figure 40. Friction pressure ratio

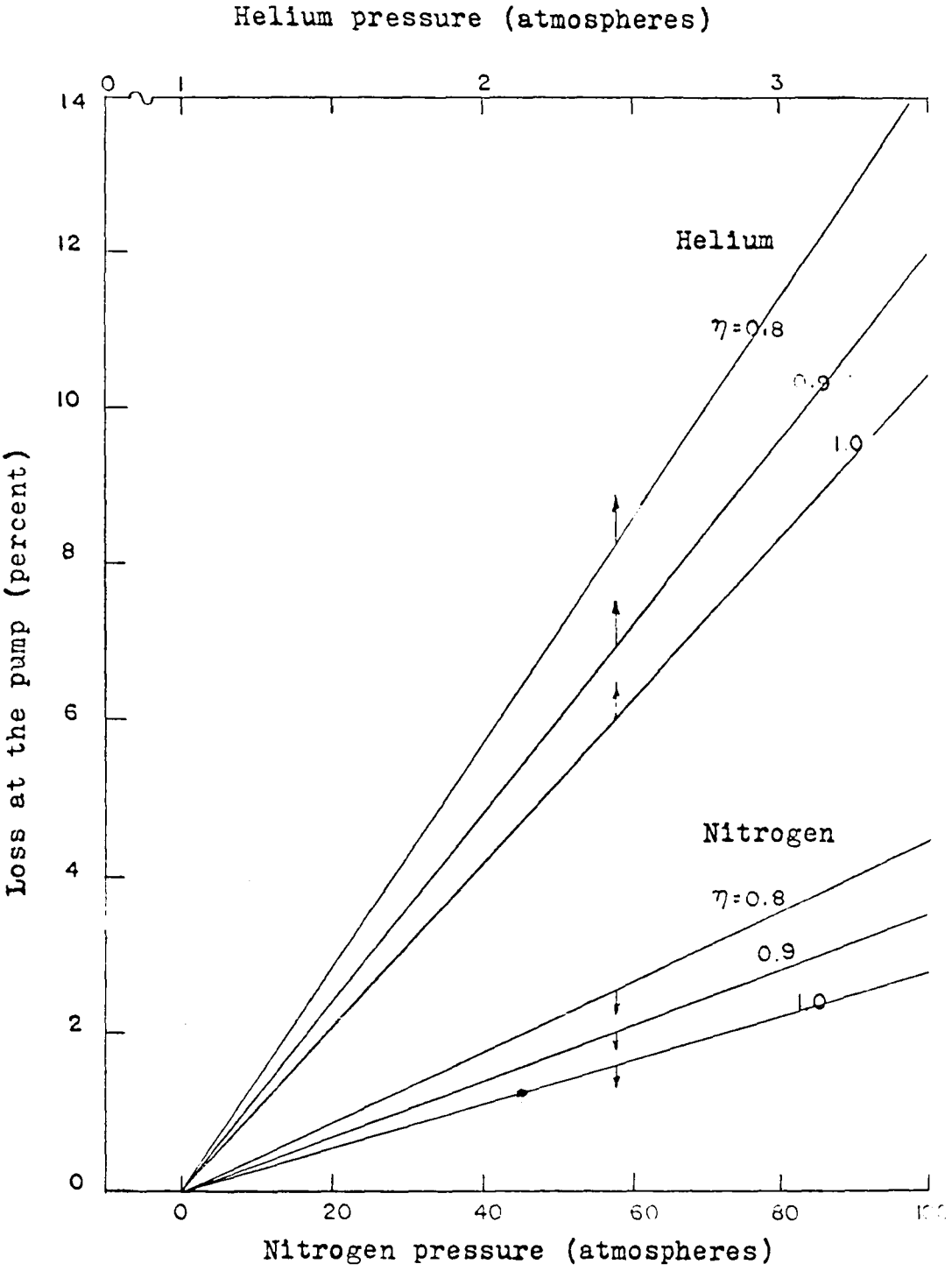

Figure 41. Liquid vaporized due to pump work

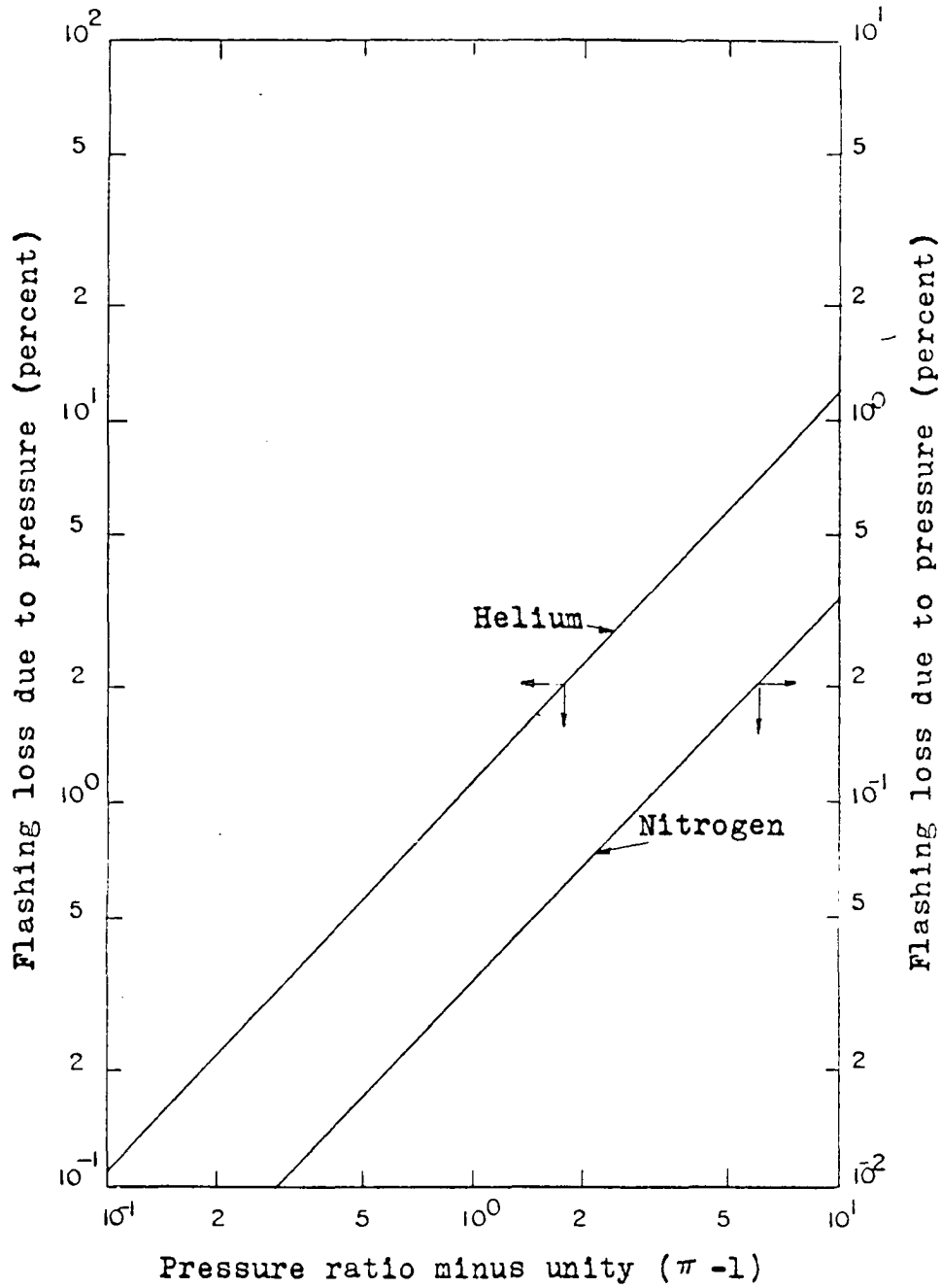

Figure 42. Liquid vaporized due to pressure in the line

vaporization due to heat leak is found from Figure 43, a graph of flashing loss due to heat leak vs. the heat leak parameter, qL/Q.

The optimum nitrogen flow rate is 0.125 gal/min. The liquid losses are determined for the following parameters:

$L = 20$ ft $\qquad \eta = 0.90$

$D = 0.25$ in

$q = 3.96$ Btu/hr-ft of tube

Q	Q/D	$D^2\tau$	π_f	Q/qL	π_t	π	qL/Q
$\frac{gal}{min}$	$\frac{gal}{min\text{-}in}$	(lb)	--	$\frac{g/m}{Btu/hr}$	--	--	$\frac{Btu/hr}{g/m}$
0.125	0.50	1.9×10^{-6}	0.006	0.0016	1.4	1.41	625

Flashing losses in percent				Flashing loss
Pump	Heat	Pressure	Total	gal/min
0.0009	0.0175	0.0008	0.019	0.0024

This loss rate is equivalent to 71.1 lb/hour.

The optimum helium flow rate is 0.5 gal/min. The liquid losses are determined for the following parameters:

$L_{inside} = 11320$ feet $\qquad \eta = 0.90$

$L_{outside} = 24900$ feet

$D = 0.948$ in.

$q_{inside} = 1.09\times10^{-3}$ Btu/hr-ft of tube

$q_{outside} = 1.36\times10^{-3}$ Btu/hr-ft of tube

$qL = (qL)_{inside} + (qL)_{outside} = 46.2$ Btu/hr

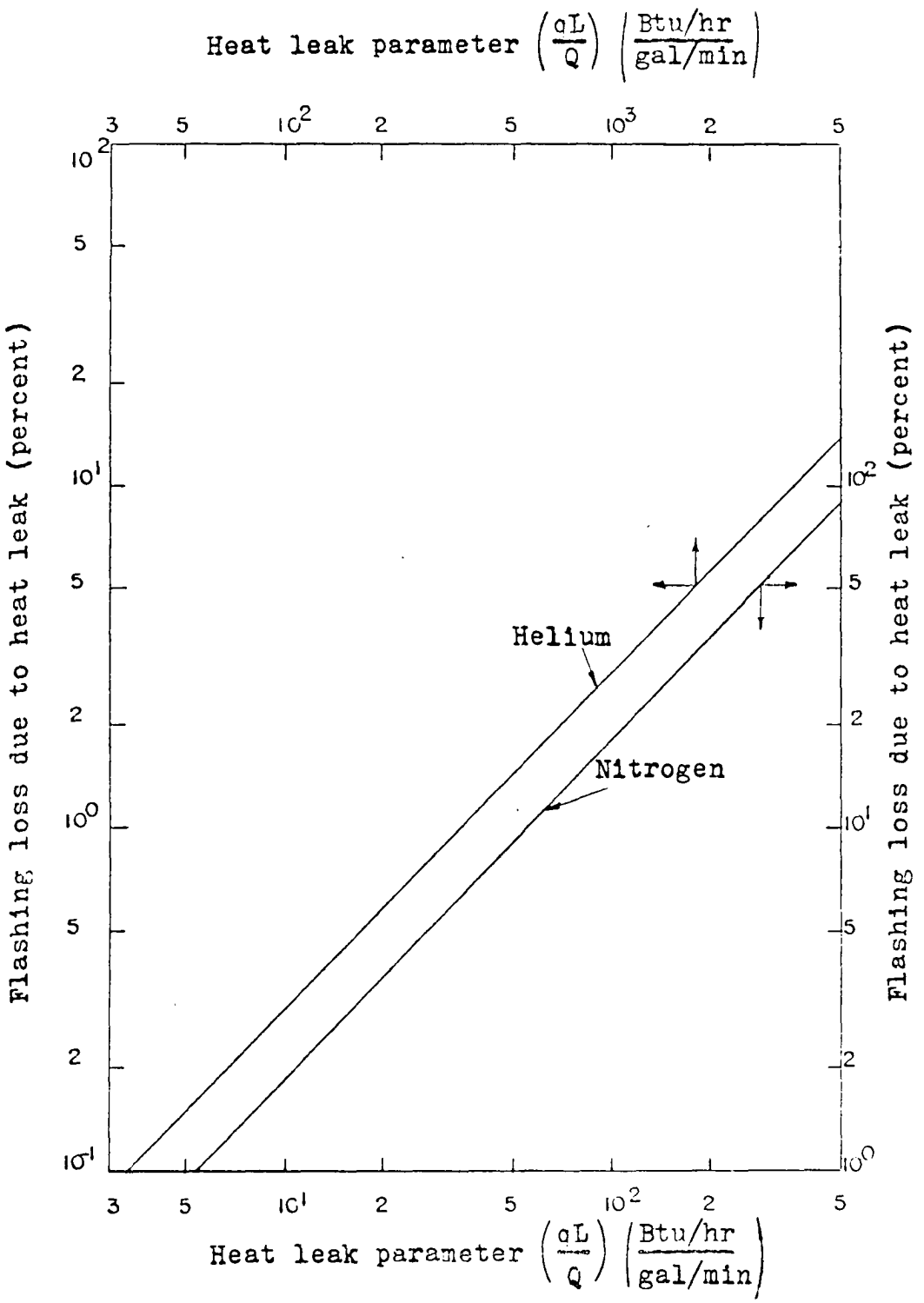

Figure 43. Liquid vaporized due to heat leak

Q	Q/D	$D^2\tau$	π_f	Q/qL	π_t	π	qL/Q
$\frac{gal}{min}$	$\frac{gal}{min\text{-}in}$	(lb)		$\frac{g/min}{Btu/hr}$	--	--	$\frac{Btu/hr}{g/min}$
0.5	0.530	1.85×10^{-7}	0.026	1.08×10^{-2}	1.368	1.394	92.6

Flashing losses in percent				Flashing loss
Pump	Heat	Pressure	Total	gal/min
0.170	0.0042	0.019	0.193	0.088

This loss rate is equivalent to 5.6 lb/hr.

APPENDIX B

The proton dose is determined from a stepwise integration process. Energy intervals are chosen to correspond to the threshold energies along each of the angles θ shown in Figure 35. The proton flux in each interval is multiplied by the energy absorbed in tissue by protons with an average energy corresponding to the energy of the protons in the chosen interval. This calculation, made for each 10 degree interval from 0^{o} to 180^{o} in the $\phi = 0$ plane is shown in Table 11. At angles of incidence greater than 90^{o}, the angular proton flux is too low to make a significant contribution to the dose. The doses listed in column 7 for each angle, θ, are the accumulated doses for all energies greater than the threshold energy at the angle θ. This accumulated dose (column 7) is plotted vs. θ from 0 to 2π, and an integrated average determined for each ϕ plane. The plot of the calculation for the $\phi = 0$ plane is shown in Figure 44. The averages for the ϕ planes are plotted versus sin ϕ in Figure 45, and an integrated dose for one fourth of the sphere is determined. The total proton dose is equal to:

$$19730 \times 10^{-7} \frac{\text{rad}}{\text{sec-sphere segment}} \times 3.6 \times 10^{3} \frac{\text{sec}}{\text{hr}} \times 1.7 \frac{\text{hr}}{\text{flare}}$$

$\times$ 2 sphere segments = 24.2 rads per flare.

The secondary neutron dose is determined using the input values given in Table 12 and the expression

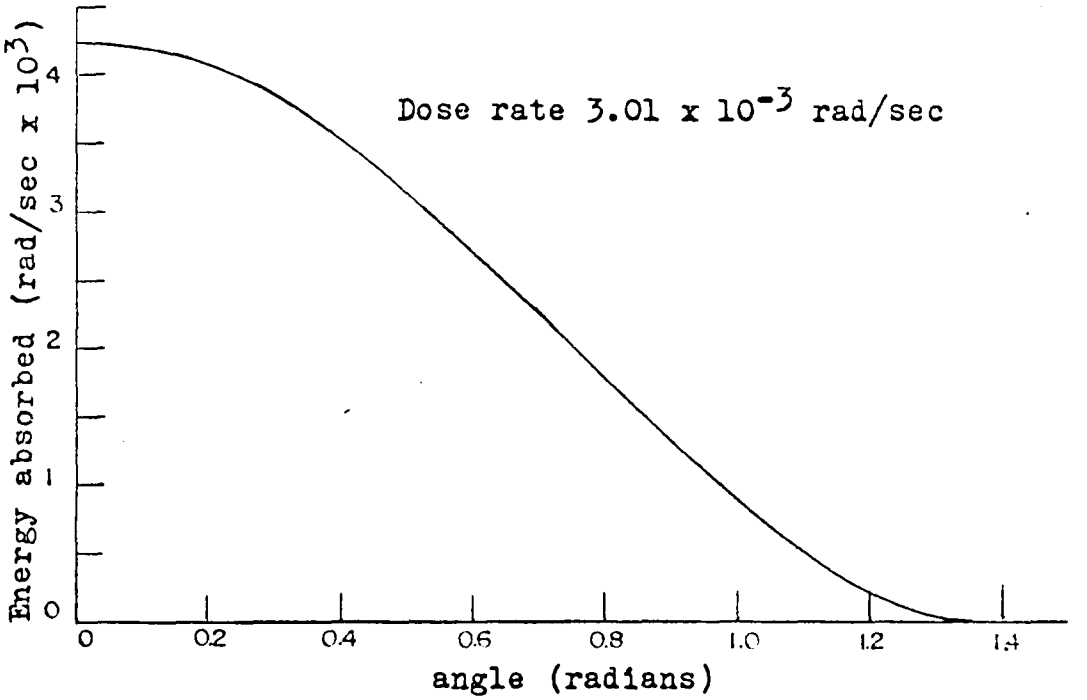

Figure 44. Integrated dose for the ϕ = 0 plane

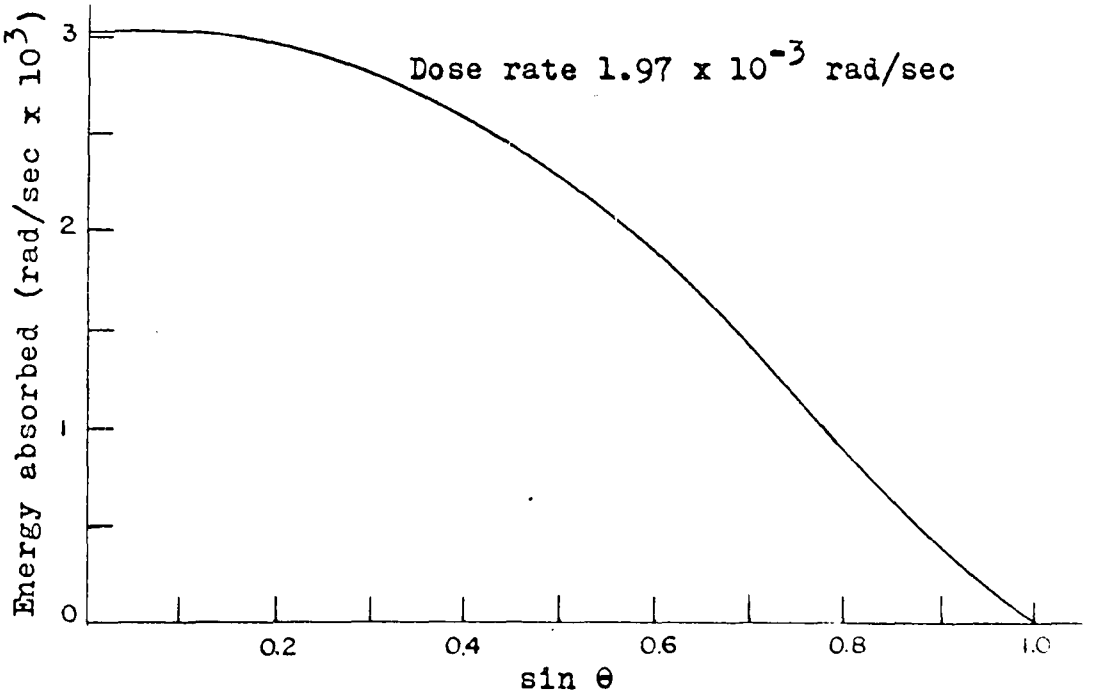

Figure 45. Integrated dose for 1/8 of a sphere

Table 11. Calculations for the dose accrued in the $\phi = 0$ plane

Plane $\phi = 0$	Angle θ	Energy interval Mev	Angular proton flux protons/cm^2-sec-ster	Number N(E) protons/cm^2-sec	Energy absorbed per particle $\frac{\text{rad-cm}^2}{\text{proton}}$	Energy absorbed per interval rad/sec	Energy absorbed per plane rad/sec
	0	1.0 -1.04	1.33×10^4	750	2×10^{-7}	1500×10^{-7}	42283×10^{-7}
	10	1.04-1.11	1.25×10^4	1750	2.1	3675	40783
	20	1.11-1.25	1.07×10^4	2750	2.4	6600	37108
	30	1.25-1.46	8.0×10^3	2700	3	8100	30508
	40	1.46-1.80	5.2×10^3	2800	3.4	8840	22408
	50	1.8 - 2.4	2.6×10^3	1810	4.6	8300	13568
	60	2.4 -3.43	7.9×10^2	660	6	3960	5268
	70	3.43-5.52	1.3×10^2	123	10	1225	1308
	80	5.52-10.95	7.6	7.6	10.75	82	83.5
	90	> 10.95	0.06	0.06	25	1.5	1.5

Table 12. Input values for secondary neutron dose

Proton energy interval (Mev)	Proton flux per energy interval (P/cm^2-sec)	Neutrons per reaction --	Energy of secondary neutron (Mev)	Nvt for a surface dose of 1 Rad neutrons/cm^2
25-50	6×10^5	1.2	10	1.52×10^8
50-100	8.5×10^5	2.2	30	0.78×10^8
100-200	9×10^5	2.8	70	0.68×10^8
200-400	6.5×10^5	3.3	140	0.44×10^8
400-600	2.35×10^5	3.7	210	0.31×10^8
600-1000	2.1×10^5	4.0	275	0.23×10^8
>1000	1.5×10^5	4.1	325	0.2×10^8

$$\text{Dose} = \frac{\text{proton flux}}{2} \times \text{cross section} \times \text{thickness}$$

$$\times \frac{\text{no of neutrons}}{\text{reaction}} \times \text{probability of neutrons entering the manned compartment}$$

$$\times \frac{\text{seconds}}{\text{flare}} \times \frac{\text{rads}}{\text{neutrons/cm}^2} .$$

The secondary dose obtained from protons in the interval from 25 to 50 Mev is

$$\frac{\frac{6\times10^5}{2}\ \frac{\text{protons}}{\text{cm}^2\text{-sec}}\ (3.7\times10^{-2}\text{cm}^{-1})(1\text{ cm})\ 1.2\ \frac{\text{neutron}}{\text{reaction}}\ (0.6)}{1.52\times10^8\ \frac{\text{neutron}}{\text{cm}^2\text{-rad}}}$$

$$\frac{6.11\times10^3\ \frac{\text{sec}}{\text{flare}}}{} = 0.32 \text{ rad.}$$

The total secondary neutron dose is 13.5 rads.

The proton dose calculation is made under the assumption that the magnetic field strength is uniform and the paths are circular. In reality the field strength is inversely proportional to the distance from an axis through the geometric center of the vehicle. A conservative estimate of the energy of the particle turned was graphically determined by considering the field to be made of layers of constant magnetic field strength. The estimate was made at three points and graphed in Figure 46. The average particle energy is 996 Mev. Therefore the 1 Bev threshold is considered valid.

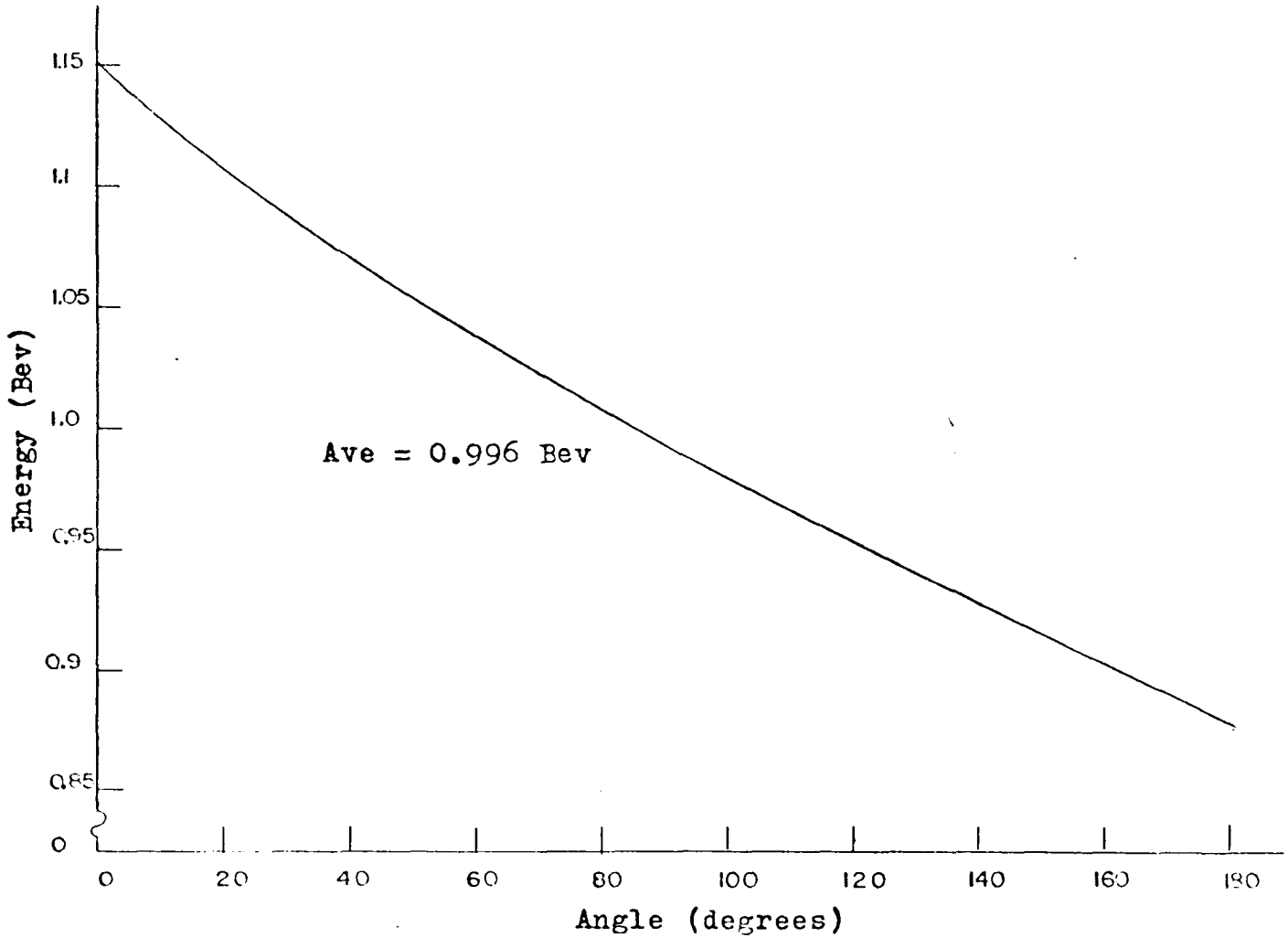

Figure 46. Threshold energies around a circumference of the coil